

# Remote Cardiac Monitoring Using Radar

by

Jonathan S. Burnham

S.B., E.E., M.I.T., 2008

Submitted to the Department of Electrical Engineering and Computer Science

in Partial Fulfillment of the Requirements for the Degree of

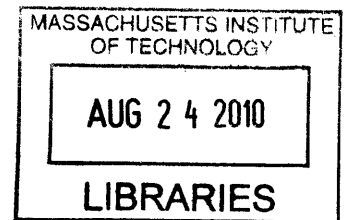
Master of Engineering in Electrical Engineering and Computer Science

at the Massachusetts Institute of Technology

June, 2009

©2009 Massachusetts Institute of Technology  
All rights reserved.

**ARCHIVES**



Author ..... *Jonathan S. Burnham* .....  
Department of Electrical Engineering and Computer Science  
May 21, 2009

Certified by ..... *[Signature]* .....  
Michael Matranga  
Embedded Systems Group Leader  
VI-A Company Thesis Supervisor

Certified by ..... *[Signature]* .....  
Julie E. Greenberg  
Principal Research Scientist, Division of Health Sciences and Technology  
M.I.T. Thesis Supervisor

Accepted by ..... *[Signature]* .....  
Arthur C. Smith  
Professor of Electrical Engineering  
Chairman, Department Committee on Graduate Theses



# **Remote Cardiac Monitoring Using Radar**

by

Jonathan S. Burnham

Submitted to the  
Department of Electrical Engineering and Computer Science

May 21, 2009

In Partial Fulfillment of the Requirements for the Degree of  
Master of Engineering in Electrical Engineering and Computer Science

## **Abstract**

Recording a patient's vital signs without physical contact is a challenging research problem with applications in medicine, search and rescue, and security. In order to study this problem, an ultra wide band (UWB) pulse radar and a fixed-frequency amplitude based radar were constructed and evaluated. The UWB radar was not reliable and did not produce repeatable results, but the fixed-frequency radar successfully recorded heartbeat signatures from twelve human subjects at a distance of 0.5 - 3 meters. The effects of several variables on the results were analyzed. Two experiments conducted to determine the physiological source of the radar amplitude modulations suggest that the modulation is from chest movement, not electrically induced impedance changes.

Thesis Supervisor: Michael Matranga  
Title: Embedded Systems Group Leader

Thesis Supervisor: Julie E. Greenberg  
Title: Principal Research Scientist, Division of Health Sciences and Technology





## Acknowledgments

This thesis would never have started without the support and encouragement of Mike Matranga. I'd like to thank him not only for giving me this chance to conduct interesting research, but for the two years of guidance and experience I received while working under him before this project even began. The invaluable lessons I have learned while working with Mike have helped prepare me for life after graduation more than any class or problem set ever could.

I'd also like to thank Dr. Julie Greenberg for investing so much time into overseeing this thesis and offering guidance and advice. Dr. Greenberg is what every VI-A student hopes for in an MIT advisor, and I benefited greatly from her in depth reviews and expert advice when conducting this research.

There are many people at Draper that supported this project and without whom it would never have been completed. I'd like to thank Dr. Domhnall Granquist-Fraser for spending his time and expertise advising me. His mentorship and advice saved valuable time from being wasted and showed me how good research should be conducted. I'd also like to thank Reed Irion who donated his time to help with this project. His wealth of experience enabled the radar systems to be built in a fraction of the time they would otherwise have been constructed. I learned many invaluable nuggets of wisdom from my time working with Don and Reed that I will always be grateful for.

I'd like to thank William Coskren for funding and supporting this research. I'd like to thank Erick Maxwell, Ryan Freedman, Craig McCubbin, and many others who patiently listened to questions and gave helpful advice. I'd also like to thank all the Draper test subjects who gave of their time to support this project.

Finally, I'd like to thank my beautiful wife who endured many late nights and lonely evenings while this research was conducted and this thesis written. I wouldn't be here today without her loving support.

This thesis was prepared at The Charles Stark Draper Laboratory, Inc., under contract number CON01671-1.

Publication of this thesis does not constitute approval by Draper or the sponsoring agency of the findings or conclusions contained herein. It is published for the exchange and stimulation of ideas.



  
(Author)



THIS PAGE INTENTIONALLY LEFT BLANK



# Contents

<b>1</b>	<b>Introduction</b>	<b>15</b>
1.1	Motivation . . . . .	15
1.2	Thesis Goals and Overview . . . . .	16
<b>2</b>	<b>Previous Work</b>	<b>19</b>
2.1	1960 - 1993 . . . . .	19
2.2	1993 - Present . . . . .	21
2.3	Scope of Current Research . . . . .	23
<b>3</b>	<b>Theoretical Background</b>	<b>25</b>
3.1	Radar . . . . .	25
3.1.1	Amplitude Changes . . . . .	25
3.1.2	Phase Changes . . . . .	26
3.1.3	Time Difference of Arrival . . . . .	27
3.1.4	Types of Radar - UWB versus Fixed-Frequency . . . . .	27
3.2	Heartbeats and Effects Observable with Radar . . . . .	29
3.2.1	Heartbeat . . . . .	29
3.2.2	Observable Effects of the Heartbeat with Radar . . . . .	31
<b>4</b>	<b>Methods</b>	<b>35</b>
4.1	Ultra-Wideband Radar System . . . . .	35
4.1.1	UWB Radar Hardware . . . . .	36
4.1.2	Safety Considerations . . . . .	37
4.1.3	UWB Radar Signal Processing . . . . .	39
4.2	Fixed Frequency Radar Setup . . . . .	47
4.2.1	Fixed Frequency Hardware . . . . .	48
4.2.2	Safety Considerations . . . . .	52
4.2.3	Frequency Sweep Experiment . . . . .	53
4.2.4	Fixed Frequency Radar Signal Processing . . . . .	55
4.3	Other Devices . . . . .	60
4.3.1	ECG Monitor . . . . .	60
4.3.2	Accelerometer . . . . .	61
4.4	Radar Modulation Experimental Methods . . . . .	62
4.4.1	Cardiac Electrical Analog . . . . .	62
4.4.2	Chest Accelerometer Experiment . . . . .	63
4.5	Subject Testing Protocol . . . . .	64

<b>5</b>	<b>Results</b>	<b>67</b>
5.1	UWB Radar Results . . . . .	67
5.2	Fixed Frequency Radar Results . . . . .	69
5.2.1	Movement vs. Impedance Results . . . . .	70
5.2.2	Human Subject Testing Results . . . . .	73
<b>6</b>	<b>Conclusions</b>	<b>87</b>
6.1	Summary of Results . . . . .	87
6.2	Possible Improvements and Further Research . . . . .	89
<b>A</b>	<b>Code Listing</b>	<b>91</b>
<b>B</b>	<b>COUHES Protocol</b>	<b>109</b>
	<b>References</b>	<b>118</b>

# List of Figures

2-1	Experimental setup of respiratory sensing systems . . . . .	20
2-2	Experimental setup of MIR remote sensing system . . . . .	22
3-1	Differences between fixed-frequency and UWB signals . . . . .	28
3-2	Diagram of heart . . . . .	30
3-3	Normal ECG waveform with notable signatures labeled . . . . .	31
4-1	Hardware for UWB Radar . . . . .	37
4-2	UWB Radar System . . . . .	39
4-3	Waveform A - 60 ps pulse from pulse generator . . . . .	41
4-4	Waveform A - Frequency spectrum of 60 ps pulse . . . . .	41
4-5	Waveform B - Received pulse transmitted line of sight . . . . .	42
4-6	Waveform B - Frequency spectrum of pulse transmitted line of sight . . . . .	42
4-7	Waveform D - Average of pulse returns from empty room . . . . .	44
4-8	Waveform C - Average of pulses reflected off of human subject . . . . .	44
4-9	Waveform E - Subtraction of empty room pulses . . . . .	45
4-10	Waveform F - RMS values of averaged pulse returns . . . . .	46
4-11	Waveform G - RMS values low pass filtered . . . . .	46
4-12	Fixed frequency radar setup by McGrath . . . . .	47
4-13	Fixed Frequency Radar System . . . . .	49
4-14	More accurate representation of spectrum analyzer . . . . .	50
4-15	Results of amplitude modulating the 18 GHz signal . . . . .	54
4-16	Frequency spectrum of results from Figure 4-15 . . . . .	54
4-17	Block diagram of the FM demodulator . . . . .	56
4-18	Phase output before line subtraction . . . . .	59
4-19	Phase output after line subtraction . . . . .	59
4-20	Recommended application circuit for accelerometer . . . . .	62
4-21	Physiological analog experiment . . . . .	63
4-22	Test setup showing all connections between equipment . . . . .	65
5-1	UWB radar amplitude with 30 Hz lowpass filter . . . . .	68
5-2	UWB radar amplitude with 3 Hz lowpass filter . . . . .	68
5-3	ECG and radar amplitude highpass filtered without delay . . . . .	70
5-4	ECG and radar amplitude highpass filtered and delayed 110 ms . . . . .	71
5-5	Comparison of accelerometer data and radar amplitude . . . . .	72
5-6	Example of category 1 data set . . . . .	75
5-7	Example of category 2 data set . . . . .	75
5-8	Example of category 3 data set . . . . .	76

5-9 Breathing as recorded by radar . . . . .	79
5-10 Breathing filtered out to reveal heartbeat signatures . . . . .	79
5-11 Subject 0014, data set #3 . . . . .	82
5-12 Subject 0003, data set #4 . . . . .	82
5-13 Subject 0006, data set #3 . . . . .	83
5-14 Subject 0012, data set #4 . . . . .	83
5-15 Heartbeat signatures from 0.5 meters . . . . .	85
5-16 Heartbeat signatures from 3 meters . . . . .	85



# List of Tables

5.1	Variables for each data set . . . . .	73
5.2	Data set category matrix . . . . .	77



# Chapter 1

## Introduction

There are many ways to monitor different aspects of cardiac function such as the heart rate, electrical activity, and mechanical function of the heart. These methods can be as simple as taking a pulse by hand or as complex as a 3-D echocardiogram. While these and many other techniques all provide useful diagnostic information, they almost all rely on some form of direct contact with the patient. In a hospital setting this is often not an issue, but there are many situations where being able to monitor a subject's cardiac activity from a distance would be very useful. The research described in this thesis investigates a non-contacting method of measuring cardiac function through the use of radar.

### 1.1 Motivation

There are many possible applications of non-contacting radar monitoring of cardiac function. Three major areas of interest are: biomedical monitoring, search and rescue, and security [1]. Biomedical monitoring in a hospital or clinic can often be done with contacting equipment such as an electrocardiogram (ECG); however, there are certain scenarios where continuous, non-contacting methods would prove more beneficial. Critical care patients in hospitals are often wakened every hour in order to collect vital signs data [2]. This constant interruption of sleep hurts the patient by slowing recovery [3, 4]. Burn victims who have no skin to safely attach ECG electrodes would also benefit from the use of a non-contacting heart rate monitor [5, 6]. Remote monitoring could also be used as a warning system for sudden infant death syndrome or sleep apnea [4, 7]. One of the original motivations for remote vital sign

monitoring was to develop a device for combat medics to assess casualties on the battlefield before exposing the medics to harm [5].

One benefit of radar based monitoring systems is their ability to penetrate different materials depending on the RF spectrum used. This makes radar based systems particularly useful for any number of search and rescue type scenarios, including monitoring and locating victims located under piles of rubble from a building collapse or under mounds of snow after an avalanche [1]. Because radar based systems can often penetrate walls, there are many applications for law enforcement and special operations including locating and monitoring subjects in a hostage rescue situation [1, 8].

Finally, radar based monitoring systems have many security applications. Hidden radar devices for intrusion detection in museums or in border control situations have been developed [7]. Other applications include detection of hidden humans at entry and exit points and using biometrics collected by the radar for identification and access control [5, 9].

These and even more possible applications of remote vital sign monitoring using radar make this topic a very interesting and exciting field of study. It is hoped that the results obtained in this research will further the implementation of practical systems.

## 1.2 Thesis Goals and Overview

The purpose of this research is to investigate the use of radar for remotely sensing heartbeats. One topic of particular interest is determining whether or not radar systems can measure the electrical activity of the heart similar to an ECG. Data was collected using two radar systems developed for these investigations. Several experiments were conducted to determine whether radar can record cardiac electrical activity, and data was collected on multiple human subjects in order to characterize the ability of the systems to remotely sense heartbeats in general.

The results of the research are detailed in the following chapters beginning in chapter 2 with an overview of previous work in remote vital sign monitoring and its implications for the research described in this thesis. Chapter 3 discusses relevant scientific principles and chapter 4 describes the radar setups and the methods used to collect data from human subjects. Finally, chapter 5 presents the results of all the experiments conducted, and

chapter 6 summarizes the conclusions and gives recommendations for further research.



## Chapter 2

# Previous Work

Using radar to remotely sense vital signs is not a novel concept. Work in this area was begun as early as the 1960s and is still an active area of research today. Previous work in this field can be divided into two periods: work prior to 1993, which used mostly Doppler radar systems, and work after 1993, when Lawrence Livermore National Laboratory published results for their Micropower Impulse Radar, spawning interest in medical applications of ultra-wide band radar.

### 2.1 1960 - 1993

Some of the first investigations for using microwave radiation to measure physiological changes were begun in the late 1950s with the work of Y.E. Moskalenko [10]. He demonstrated the use of microwaves to measure volume changes in different biological materials [11, 12]. In 1972, Johnson and Guy recorded volume changes of the heart by measuring changes in the transmission loss of 915 MHz radiation as it traveled through the human chest [13]. Other early remote sensing systems, of which little is known, are described in [14] and [15]. All of these systems provided a basis for further research in remote monitoring of vital signs.

Most of these systems measured transmission changes of the microwave signal as it passed through the thorax. Radar, however, measures the reflections returned from the objects it encounters. One of the first times radar was used for remote vital signs monitoring was in 1975 by Prof. James Lin of Wayne State University. He constructed a radar system

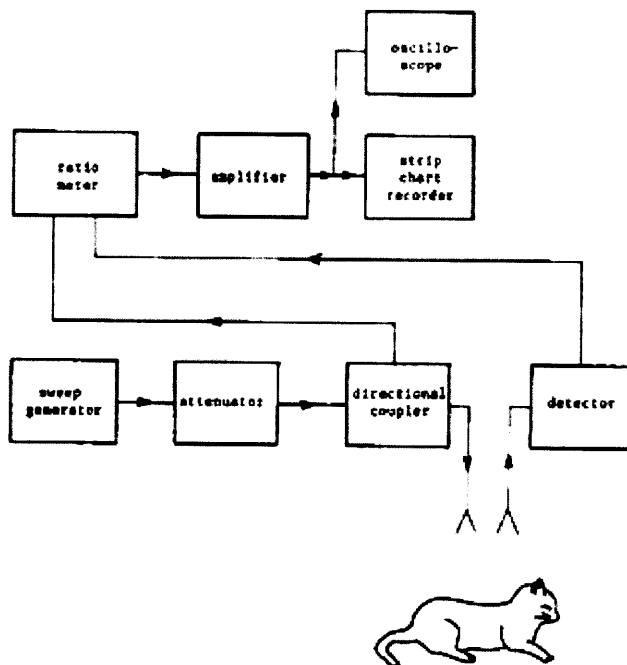


Figure 2-1: Experimental setup of respiratory sensing systems, Lin, 1975 [16]

operating at 10 GHz which looked at the ratio between the transmitted and received power. The radar was pointed at animal and human subjects, and Lin saw that as the chest wall moved due to respiration, it modulated the amplitude of the microwave signal. This change in amplitude was detected by the receiver, providing accurate plots of respiration from 30 cm away [16]. A diagram of the setup from the original paper is shown in Figure 2-1.

After Lin’s research was published, interest in remote monitoring of vital signs grew, and many more groups began their own investigations. Most microwave remote sensing systems began using Doppler based radar to pick up phase shifts, instead of amplitude changes, caused by moving tissues such as the chest wall, since phase shifts give a better signal-to-noise ratio than amplitude based changes [17]. A variety of theoretical and prototype applications of this technology were developed.

One of the more prolific of the early contributors to microwave remote sensing was a group from Georgia Tech Research Institute. They developed a system using Doppler radar called the Remote Vital Signs Monitor (RVSM) [18]. This system went through several iterations and was modified for many different applications. The first RVSM system was sponsored by the Department of Defense in the mid 1980’s and designed to monitor wounded soldiers on the battlefield to determine which had vital signs and which did not.



The system recorded the vital signs of targets up to 100 meters away; however, noise caused by moving grass and leaves severely affected performance at such a distance [5]. This system was patented in 1990 [19]. Another interesting application of RVSM was monitoring the heartbeats of competitors in the riflery competition in the 1996 Olympic Games in order to show TV audiences how competitors timed their shots to their heartbeats. The system was prototyped and worked well, but a lack of TV coverage for riflery prevented the system from being used in the actual Olympics [5].

The RVSM system has demonstrated many possible applications of remote vital sign sensing using Doppler based radar and is still an active area of research today [5, 9, 18]. A more detailed history and a list of notable publications can be found in Lin's 1992 review of the field [10].

## 2.2 1993 - Present

In 1993 a new electromagnetic technology for remote sensing was reported by Lawrence Livermore National Laboratories [20]. The new system was called Micropower Impulse Radar (MIR) and arose out of work on a high-speed digitizer being developed for the Nova laser. Thomas McEwan realized that this system could also be adapted as a radar and tested it in a wide range of applications [7].

One of these applications was the remote sensing of vital signs [7]. The MIR system developed for vital signs sensing was very different from that of the Doppler systems described earlier. Instead of using continuous-wave microwaves to sense Doppler shifts, MIR sent out brief pulses of electromagnetic energy. Two parameters were measured in the reflected pulses. The first was the time-of-flight as the pulse traveled from the transmitter, reflected off the target, and traveled back to the radar's receiver. The second measured parameter was the amount of energy contained in the reflected pulse. Both of these parameters were modulated by respiration and heart rate from chest and heart wall motion and by reflectance changes as the heart filled with blood [4, 7]. This technique presents several advantages to a continuous-wave approach, and is described in more detail in the next chapter.

The MIR work by Lawrence Livermore was described in several patents awarded to



that his setup measures, basically making his setup a remote ECG-like device (Private communication from W. R. McGrath, Jet Propulsion Laboratory, California Institute of Technology). A significant portion of the research for this thesis was focused on verifying McGrath's claims by replicating his experimental setup.

## 2.3 Scope of Current Research

There are many current research initiatives related to the work described above, and much more must be done before this technology will be widely accepted for practical use. This thesis project has three primary goals. The first goal, inspired by the work of McGrath, is to evaluate the ability of an amplitude modulated radar system to measure cardiac activity. As mentioned in section 2.1, most of the research regarding remote sensing with continuous wave radar systems was focused on Doppler modulated radar systems.

A second goal of this research is to evaluate the effectiveness of a UWB radar system for measuring cardiac activity in contrast to a radar operating at a fixed-frequency such as the RVSM Doppler radar or the McGrath amplitude radar described earlier. Instead of incorporating signal averaging and parameter measurement in hardware, the UWB system developed for this research uses a high-speed oscilloscope to capture the raw return pulses in order to give the greatest flexibility for signal processing.

Finally, another goal of this research is to determine if cardiac activity recorded by the fixed-frequency or UWB radars is the result of movement (of the chest and/or heart wall) or if it can be attributed to electrical phenomenon as described by McGrath.

The following chapter describes some of the theoretical foundations of the remote sensing techniques used for this research.



## Chapter 3

# Theoretical Background

This chapter gives an overview of some of the theoretical principles that underlie this research. First an overview of radar principles will be given, followed by an explanation of the two kinds of radar that were evaluated. Finally, it will be shown how radar can measure different biological effects caused by the heartbeat.

### 3.1 Radar

Radar is a method of remote sensing and detection that has been in use for many decades. Essentially, radar transmits electromagnetic energy and measures changes in the amplitude, phase, timing, and/or polarization of the returning electromagnetic energy in order to gather information about the object(s) off which the electromagnetic energy is reflected. The parameters we are interested in measuring are the amplitude, phase, and pulse arrival times of the radar.

#### 3.1.1 Amplitude Changes

The amount of power received by radar is determined by a number of factors. These include the gain of the receive and transmit antennas, the path-loss of the electromagnetic wave, the impedance difference between the target and the medium in which the wave travels, and the radar cross section of the target [29]. The radar cross section of the chest is a very difficult parameter to accurately compute, but this is not a major concern since the purpose

of the radars used for this research is to measure changes in these parameters instead of accurate numerical values. The gain of the antennas is measured and calibrated by the manufacturer. The other parameters can be computed with the following equations.

The amount of power reflected by an object with impedance  $Z_2$  from a wave traveling in a medium with impedance  $Z_1$  is determined by the equation:

$$\frac{\Gamma_{ref.}}{\Gamma_{inc.}} = \frac{Z_1 - Z_2}{Z_1 + Z_2} \quad (3.1)$$

where  $\Gamma_{ref.}$  is the power reflected and  $\Gamma_{inc.}$  is the incident power [28]. The impedance of an object can be determined from its relative permittivity  $\epsilon_r$  according to the equation [28]:

$$Z = \sqrt{\frac{\mu_0}{\epsilon_0 \epsilon_r}} \quad (3.2)$$

where  $\mu_0$  is the permeability of a vacuum and  $\epsilon_0$  is the permittivity of free space. The amount of power received by the radar is also affected by the path-loss of the electromagnetic wave as it travels through air. This is determined by the equation:

$$Path Loss = \left(\frac{4\pi df}{c}\right)^2 \quad (3.3)$$

where  $d$  is the distance in meters,  $f$  is the frequency, and  $c$  is the speed of light [30]. By combining the gain of the antennas, the reflectance of the target, and the path loss from the antennas to the target, a good estimate of the maximum received power can be obtained.

### 3.1.2 Phase Changes

When an electromagnetic wave reflects off of a moving object, the frequency of the electromagnetic wave is modulated. This is commonly called the Doppler effect and is the core principle underlying technologies such as police radar guns. The phase of the returning radar wave is determined by the following equation:

$$\theta = \frac{4\pi d}{\lambda} \quad (3.4)$$

where  $d$  is the distance to the target and  $\lambda$  is the wavelength of the radar wave [31, 32]. The change in phase  $\Delta\theta$  caused by a change in position  $\Delta d$  is thus given by:

$$\Delta\theta = \frac{4\pi\Delta d}{\lambda} \quad (3.5)$$

By integrating equation 3.4 with respect to time, the change in phase can be related to frequency with the following equation:

$$f_d(t) = \frac{2fv(t)}{c} \quad (3.6)$$

where  $f_d(t)$  is the Doppler modulated frequency of the returning wave,  $f$  is the frequency of the transmitted wave,  $v(t)$  is the velocity of the moving object, and  $c$  is the speed of light [33, 34]. Using these equations, the change in position of an object such as the chest wall can be accurately measured.

### 3.1.3 Time Difference of Arrival

It takes a finite amount of time for an electromagnetic wave to travel from a transmitter to a target and back again. By measuring the time of flight of the wave the distance to the target can be calculated using the following equation:

$$t = \frac{2d}{c} \quad (3.7)$$

where  $t$  is the time of flight,  $d$  is the distance to the target, and  $c$  is the speed of light. This equation can be used to measure the change in position of a target just like the phase change equation does, but it also provides an accurate calculation of the overall distance to the target whereas the phase equation cannot since it repeats every  $2\pi$ .

### 3.1.4 Types of Radar - UWB versus Fixed-Frequency

Two different kinds of radars were constructed for this thesis work. The first type emits very narrow electromagnetic pulses while the second emits a continuous signal of a fixed frequency. The first system is called ultra-wideband (UWB) radar for reasons that will be discussed below. The second system is similar to more traditional radar and will be

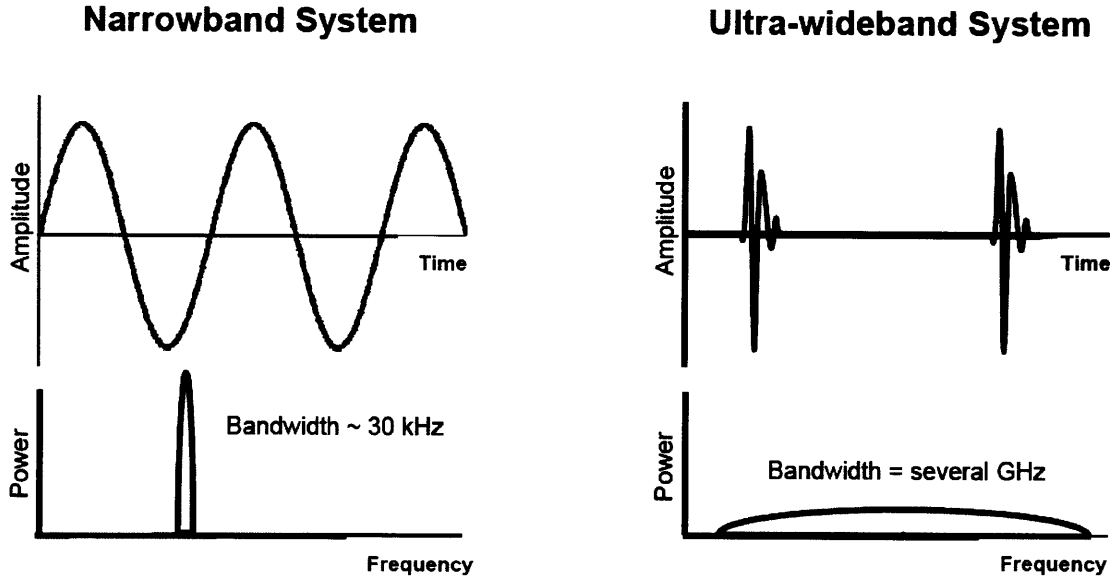


Figure 3-1: Differences between fixed-frequency and UWB signals in time and frequency domains [4]

referred to as the fixed-frequency radar in this thesis. While a detailed description of the physical implementation of these systems will be given in the next chapter, this section serves as a brief introduction to the theory, motivations, and trade-offs involved with these two systems.

Both the UWB and fixed-frequency radars emit an electromagnetic signal that is reflected off the chest of the human subject. However, these signals are very different from each other. As its name implies, the fixed-frequency radar emits a signal with a constant frequency. The UWB radar, on the other hand, emits very brief pulses 60 to several hundred picoseconds wide and 10 V in amplitude. These pulses have a high peak power, but because they are so brief and are sent with relatively long delays between each pulse, the average power is fairly low. These very narrow pulses in time yield a very wide bandwidth in the frequency spectrum. The differences between these two signals in the time and frequency domains are illustrated in Figure 3-1.

A pulsed UWB signal has a number of advantages for use in radar. The brief pulses in time allow the receiver to discriminate pulses reflected by the target from pulses reflected by other objects in cluttered environments. The broad spectrum distributes the power so that the power level at any given frequency is very low. This allows a UWB system to operate in the presence of fixed-frequency systems without causing them interference. Most



importantly, the wide bandwidth of UWB allows it to penetrate a wide range of materials. Different materials transmit, absorb, or reflect electromagnetic signals differently depending on the frequency content of the signal. By covering such a wide frequency spectrum, UWB signals are able to penetrate a greater range of materials than a fixed-frequency signal. The biomedical advantage of this property is to allow a UWB signal to penetrate tissues deeper in the body, such as the heart wall, and thereby provide more diagnostic information [4, 7, 28].

While UWB radar has many advantages over fixed-frequency radar, there are some drawbacks. Fixed-frequency radar uses simpler components and is straightforward to process, while UWB radar requires more complex hardware in order to process the received signals. Also, since the fixed-frequency radar is continuous, it is possible to obtain higher signal-to-noise ratios for the amplitude of the returning signal since there is a much longer time window to collect the returned power relative to the brief spike of power in a UWB signal.

## **3.2 Heartbeats and Effects Observable with Radar**

The human heart is a complex organ that requires precise timing of electrical and mechanical activity in order to provide constant blood flow to the human body. Because of its vital role in sustaining life, numerous methods for measuring its electrical and mechanical functions have been devised over the years. In order to understand them in greater detail a brief physiological examination of the heart is given.

### **3.2.1 Heartbeat**

The heart consists of the left heart and the right heart. Each half consists of a small atrium and a large ventricle with a one-way valve connecting them to prevent the blood from flowing backwards. The right heart collects blood from the rest of the body in the atrium, and when full, the atrium contracts and forces blood into the larger right ventricle. The right ventricle then fills with blood and contracts, forcing the blood to the lungs where it is oxygenated and returned to the left heart, filling the left atrium with blood. Just like the right heart, the left atrium contracts when full, forcing blood into the left ventricle which

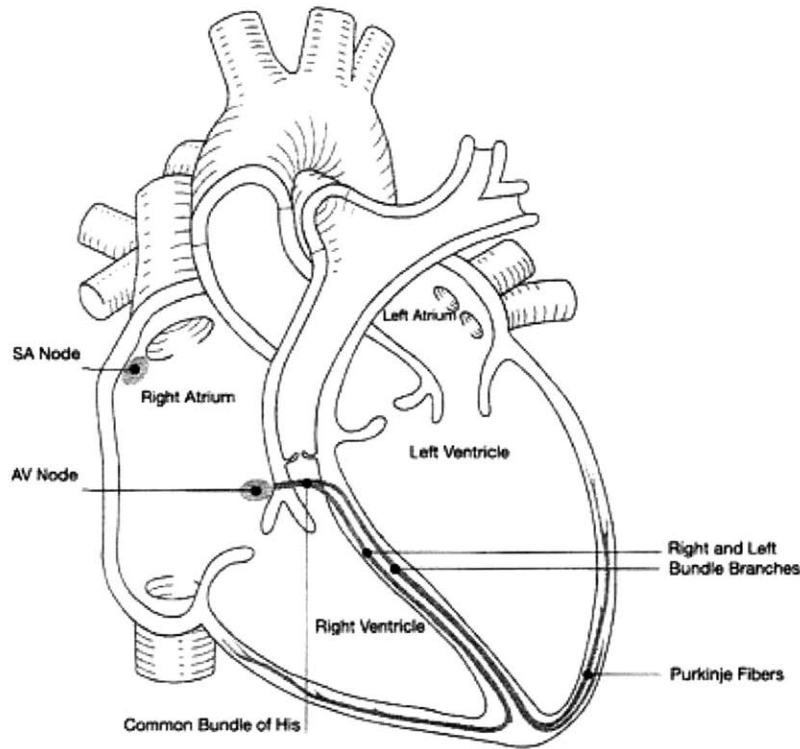


Figure 3-2: Diagram of heart [36]

then fills and contracts, forcing blood to the entire body [35].

This sequence of contractions is controlled by electrical impulses delivered by nerves from a set of cardiac cells called the SA node. The SA node has a special ability which allows it to fire electrical impulses automatically, making it the “pacemaker” of the heart. The impulses from the SA node are delivered to the muscles of the different heart chambers in a very precise and coordinated fashion. Measuring this electrical activity of the heart is the purpose of the electrocardiogram (ECG). By attaching electrodes to the skin of a subject, it is possible to measure these electrical signals in order to diagnose the heart’s condition [35].

A contacting ECG was used in this thesis as a “true” measure of cardiac activity, so it is important to know the basics of the physiology behind the ECG. A normal ECG waveform, such as the one illustrated in Figure 3-3, consists of several characteristic features identified by the letters PQRST. At the beginning of a heartbeat, the nerves of the atrium depolarize at the SA node. This starts a wave of depolarization that sweeps down to another node called the AV node located at the bottom of the atrium and the top of the ventricles. This wave of

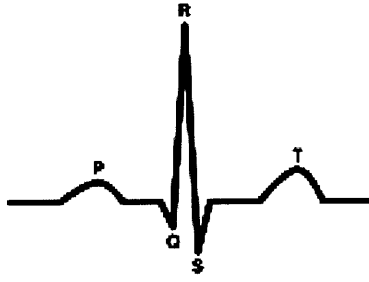


Figure 3-3: Normal ECG waveform with notable signatures labeled [37]

electrical activity causes the atrium to contract and is what forms the P wave in the ECG. The electrical activity is delayed at the AV node, giving time for the atrium to contract, and during this period there is no measurable electrical activity at the surface. After the delay, the electrical activity starts from the AV node and sweeps across the ventricles, first right to left, and then downwards, forming the QRS complex above. After that the cardiac nerve cells are fully depolarized and there is a delay with no electrical activity. The nerve cells of the ventricles then repolarize, forming the T wave in the ECG [35].

While the ECG provides a wealth of diagnostic information thanks to decades of thorough research in the subject, there are other ways to measure cardiac activity. These all focus on measuring the mechanical activity of the heart as the atrium and ventricles contract and the valves open and close. Using an iconic stethoscope or a microphone, the sounds of the moving heart can be recorded and analyzed. A ballistocardiogram measures the amount of force with which the heart forces blood out of the ventricles [31], and an apexcardiogram measures the movement of the chest wall [38, 39]. While none of these measurement techniques were used in this research, they are mentioned here because they have some similarities to the radar results obtained in this thesis.

### 3.2.2 Observable Effects of the Heartbeat with Radar

The heartbeat involves significant physical movement of both the heart itself and the chest wall, and these heartbeat movements can be recorded by radar. A general idea of how the heartbeat will modulate the radar signal can be obtained by using the equations listed earlier.

Using equation 3.1 gives us an idea of how much power will be reflected off the chest by an incident radar signal. In this case, the waves are traveling through free space, and the impedance of free space  $Z_1$  is defined as:

$$Z_1 = \sqrt{\frac{\mu_0}{\varepsilon_0}} = 376.73 \Omega \quad (3.8)$$

where the permeability of free space is  $\mu_0 = 4\pi \times 10^{-7} \frac{H}{m}$  and the permittivity of free space is  $\varepsilon_0 = 8.8542 \times 10^{-12} \frac{F}{m}$  [28]. In order to find the impedance  $Z_2$  of the human chest we use the equation:

$$Z_2 = \sqrt{\frac{\mu_0}{\varepsilon_0 \varepsilon_2}} = 59.57 \Omega \quad (3.9)$$

where the permittivity of skin at the air/chest interface is  $\varepsilon_2 = 40$  at 1 GHz [28, 40]. Substituting  $Z_1$  and  $Z_2$  into equation 3.1 gives:

$$\frac{\Gamma_{ref.}}{\Gamma_{inc.}} = 0.7269 = -1.39 \text{ dB} \quad (3.10)$$

so 72.69% of the incident power will be reflected from the chest at 1 GHz. This percentage is the number most often used and referenced in current literature. However, the radar setups that will be described operate up to 18 GHz. At that frequency, the permittivity of skin becomes  $\varepsilon_2 = 20$  [40]. Substituting that number into equations 3.2 and 3.1 gives:

$$Z_2 = 82.24 \Omega \Rightarrow \frac{\Gamma_{ref.}}{\Gamma_{inc.}} = 0.6345 = -1.98 \text{ dB} \quad (3.11)$$

so 63.45% of the incident power will be reflected from the chest at 18 GHz.

If the distance to the subject is 1 meter ( $d = 1$ ) and the frequency is 18 GHz ( $f = 18 \times 10^9$ ) equation 3.3 gives:

$$Path \ Loss = \left(\frac{4\pi df}{c}\right)^2 = 568,489.21 = 57.55 \text{ dB} \quad (3.12)$$

According to the documentation provided by the manufacturer, the gain of the horn antennas at 18 GHz is approximately 13 dB. Using this information we can estimate the total transmitter to receiver path loss:

$$\begin{aligned}
\textit{Total Path Loss} &= \textit{gain of transmitter antenna} - \textit{path loss to subject} + \\
&\quad + \textit{reflection coefficient} - \textit{path loss from subject} + \\
&\quad + \textit{gain of receiver antenna} & (3.13) \\
&= 13 \textit{ dB} - 57.55 \textit{ dB} - 1.98 \textit{ dB} - 57.55 \textit{ dB} + 13 \textit{ dB} \\
&= -91.08 \textit{ dB}
\end{aligned}$$

The only parameter not included in this estimate is the radar cross section of the human chest, but since the path loss is the greatest factor determining the amplitude of the received signal, the above equation provides a reasonable estimate of the total path loss. However, the radar cross section of the chest changes slightly as the chest moves due to the beating heart. It is difficult to quantitatively predict what the change in radar cross section will be, since small changes in the orientation of the chest can produce significant changes in the radar cross section. Regardless, given a reasonably sensitive receiver, the changes in radar cross section caused by the beating heart always produce a detectable change in the amplitude of the received signal. Therefore, while it is hard to predict the numerical values of the returning radar amplitude, the heartbeats can be detected by measuring the changes of the amplitude over time.

William McGrath of Jet Propulsion Laboratory believes there is a second observable modulation to the amplitude. According to McGrath, as the cardiac nerve cells fire there is a change in the ion concentration of the extracellular fluid. This induces a change in the impedance of the extracellular fluid, changing the reflection coefficient calculated in equation 3.1. Therefore, McGrath believes that the amplitude changes in the returning radar signal contain a small component that is directly related to a traditional ECG measurement (Private communication from W. R. McGrath, Jet Propulsion Laboratory, California Institute of Technology). One goal of the current research is to investigate this claim that the radar can record electrophysiological phenomena such as the ECG.

The movement of the chest wall with each heartbeat varies from subject to subject, but is in the range of  $0.01 - 0.3 \textit{ mm}$  [32, 41, 42]. Using equation 3.5 we can predict the change in phase produced by a movement change of  $\Delta\theta = 0.01 - 0.3 \textit{ mm}$ :

$$\Delta\theta = \frac{4\pi\Delta d}{\lambda} = 0.43^\circ - 12.96^\circ \quad (3.14)$$

While  $0.43^\circ$  may be hard to detect, degree changes on the order of  $12.96^\circ$  are easily detectable.

Finally, chest movement also changes the arrival time of radar pulses. The change in arrival time  $\Delta t$  for chest movements  $\Delta d$  ranging from  $0.01 - 0.3 \text{ mm}$  can be calculated using equation 3.7:

$$\Delta t = \frac{2\Delta d}{c} = 66.67 \text{ fs} - 2 \text{ ps} \quad (3.15)$$

The hardware used in this thesis can only detect time changes on the order of twenty picoseconds, so the radar cannot record heartbeats by measuring changes in the arrival time of the radar pulses. However, the UWB radar can still sense heartbeats by measuring the change in amplitude.

As described above, chest movements induced by heartbeats can be measured by radar. The next section focuses on the radar systems that were constructed to sense these heartbeats and details how they were constructed.

# Chapter 4

## Methods

This chapter will detail the physical construction of the radar systems, the signal processing used in each, and the methods that were used to collect data from human subjects. The chapter is divided into five sections: a description of the hardware and signal processing used in each of two radar systems; descriptions of extra testing devices that were used; descriptions of the experiments conducted to determine the radar modulation's source, and finally the test protocol.

### 4.1 Ultra-Wideband Radar System

When planning the UWB radar system it was decided to focus on the signal processing aspects of the project instead of spending time developing complex, custom hardware. As a result, the UWB radar system was constructed using off the shelf components and test equipment. As described before, UWB radar consists of a transmitter that emits very sharp, short pulses of electromagnetic energy, and a receiver that processes these signals.

There are two main types of processing strategies. The first strategy opens a receive gate for a narrow window of time after each pulse is sent and averages the power received in that time window over numerous pulse repetitions. By calibrating the receive gate to open exactly when the pulse energy returns from the chest or heart wall, movements of these walls can be detected as changing average power levels. The second, less common processing strategy measures the changes in the time-of-arrival of the returning pulse. Both of these methods use custom electronic circuits to transmit and receive the UWB pulses.

In this thesis, both strategies were implemented by changing the signal processing used on the received data. However, only results from the first strategy proved useful.

#### 4.1.1 UWB Radar Hardware

The UWB radar system was constructed using a pulse generator (Picosecond Pulse Labs model 10,060A) for the transmitter, a high speed oscilloscope (Tektronix Digital Phosphor Oscilloscope (DPO) 72004) for the receiver, and two ETS-Lindgren 3115 broadband horn antennas. This approach provided a large degree of flexibility and avoided time wasted developing and debugging electronic hardware.

The pulse generator has adjustable pulse width, amplitude, and repetition rate, and is capable of producing pulses with rise times as fast as 55 ps, pulse widths as short as 100 ps, and amplitudes of 10 V. In order to capture pulse widths as narrow as 100 ps, we required an oscilloscope with a very high sample rate. Also, by definition, a UWB radar pulse has a large bandwidth, so the analog bandwidth of the oscilloscope also needed to be very wide. In theory, a pulse with a rise time of 55 ps has frequency content up to 18 GHz. Finally, the oscilloscope needed the capability to capture very short windows of time with comparatively long down time between windows over an extended period of time (4-10 seconds). The DPO 72004 met these requirements with a sample rate of 50 billion samples per second and an analog bandwidth of 20 GHz. It also had a capability called FastFrames that allowed it to capture multiple, short time windows as described above.

A diagram of the UWB radar system is shown in Figure 4-1. The UWB pulse generated by the pulse generator was fed into a broadband horn antenna. This antenna is designed to operate at frequencies from 0.75 - 18 GHz and provides 10-16 dB of gain. After the pulses are reflected off the chest of the human subject, they were received by a second, identical horn antenna connected directly to an oscilloscope. The oscilloscope also received a trigger signal from the pulse generator every time the pulse generator sent a pulse. This trigger gave the oscilloscope a reliable reference for opening the receive window, and allowed the oscilloscope to compare the transit time of multiple pulses sent by the pulse generator to the oscilloscope. This strategy allowed both processing strategies described earlier to be implemented. The average power level within the receive window as well as the change in transit time of the pulse can be calculated in the signal processing stage.



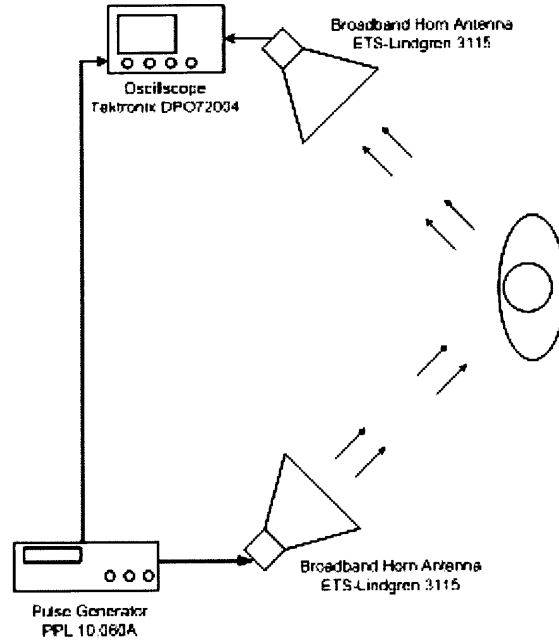


Figure 4-1: Hardware for UWB Radar

Finally, high quality coaxial cables were used to connect the pulse generator and oscilloscope to the horn antennas. At first, general purpose coaxial cable was used, but it eventually became clear that the high frequency components of the pulses were being severely attenuated. The cable was replaced with Gore Phaseflex coaxial cable rated up to 18 GHz and the high frequency components of the pulse were preserved.

#### 4.1.2 Safety Considerations

Before testing with human subjects it was necessary to ensure that the radar system was safe for this use. While a number of RF safety standards exist, one of the most widely used standards is the IEEE C95.1 [43]. This standard gives maximum permissible exposure (MPE) power levels for frequencies ranging from 3 kHz to 300 GHz. The lowest MPE power level is  $0.2 \text{ mW/cm}^2$  for frequencies from 100-300 MHz. At higher frequencies the MPE power level is higher, up to  $10 \text{ mW/cm}^2$ .

The spectrum of the UWB pulse is very broad, theoretically reaching all the way to 18 GHz. This makes it hard to analyze using the template in the C95.1 standard since its spectrum covers several frequency bands that have different MPE power levels. A conservative approach is to limit the total power per  $\text{cm}^2$  of the UWB pulse radiated by the antenna to

be less than the lowest MPE power level of  $0.2 \text{ mW/cm}^2$ .

The pulse generator has a maximum output of 10 V. The coaxial cable and antenna are matched at  $50\Omega$ , so the instantaneous peak power of the pulse generator is:

$$\text{Peak Power} = \frac{V^2}{R} = 2 \text{ W} \quad (4.1)$$

To find the average power we consider the pulse width and pulse repetition rate. The maximum ratings of the pulse generator are a 10 ns pulse width and a repetition rate of 100 KHz. This gives an average power of:

$$\text{Average Power} = \text{Peak Power} \times \text{pulse width} \times \text{pulse rate} = 2 \text{ mW} \quad (4.2)$$

This is the total average power that enters the transmit antenna. The transmit antenna then spreads this power over a wide area depending on its geometry. The horn antenna has a maximum possible gain of 17 dB and is 15 cm deep. The antenna gain is defined as:

$$\text{Antenna Gain} = \frac{\text{Power Boresight}}{\text{Power Isotropic}} \quad (4.3)$$

To estimate the power delivered to a subject standing right next to the horn antenna (worst case scenario) we multiply the isotropic power by the antenna gain. Even though the user would be in the near field of the antenna and equation 4.3 is valid only for the far field, this approach is conservative because the power in the near field can only be less than the power calculation using far field equations [44]. Using far field equations, the isotropic power delivered 15 cm away by the antenna with an average input power of 2 mW is:

$$\text{Isotropic Power} = \frac{\text{Power}}{4\pi r^2} = \frac{2}{4\pi 15^2} \text{ mW/cm}^2 = 0.707 \text{ }\mu\text{W/cm}^2 \quad (4.4)$$

Multiplying the isotropic power by the gain of the antenna gives us the incident power on the subject:

$$\text{Incident Power} = 0.707 \text{ }\mu\text{W/cm}^2 \times 10^{17 \text{ dB}/10} = 35.43 \text{ }\mu\text{W/cm}^2 \quad (4.5)$$

This is well below the conservative MPE power level of  $0.2 \text{ mW/cm}^2$  established above,

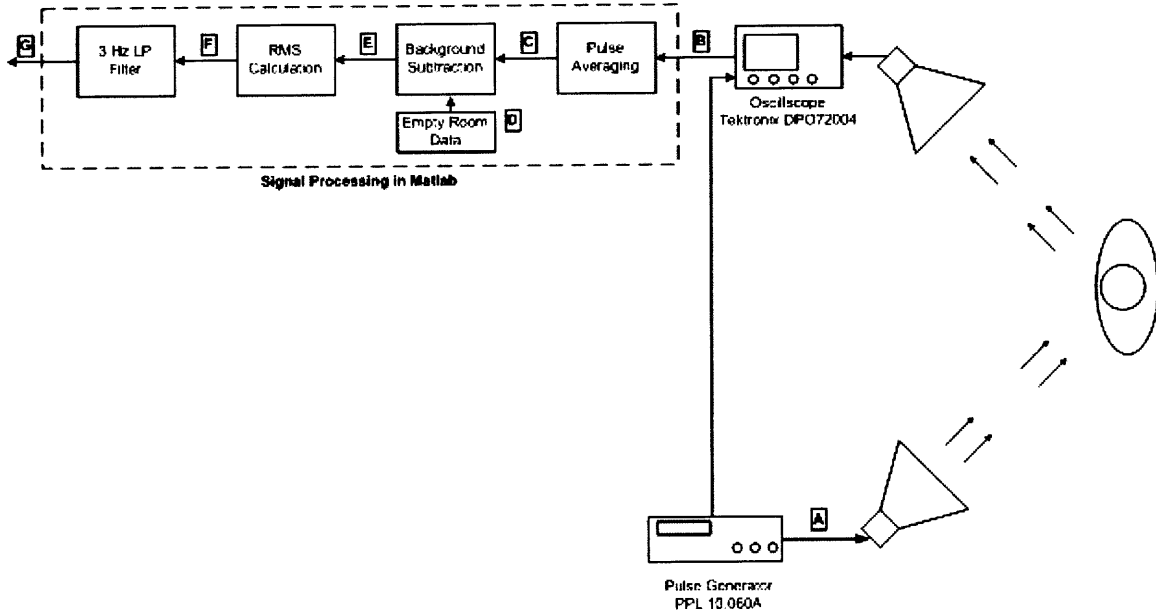


Figure 4-2: UWB Radar System

making the UWB radar system safe for human subject testing.

### 4.1.3 UWB Radar Signal Processing

This section details each stage of the UWB radar, describing the purpose and associated processing with example waveforms. A diagram illustrating the overall system is shown in Figure 4-2.

The first step is generating the UWB pulse with the pulse generator. The three settings that control the UWB pulse are the pulse amplitude, pulse repetition rate, and pulse width. The pulse amplitude was chosen to be the maximum possible 10 V in order to improve the signal-to-noise ratio of the returning UWB pulse. The repetition rate was set to 4000 pulses per second. This was established by trial and error, and represents a compromise that provides sufficient time resolution while also permitting the averaging of many pulses without creating unmanageably large data files.

The pulse width parameter was difficult to choose. A major consideration when choosing the pulse width is the amount of ringing in the signal caused by the extremely sharp step hitting the antenna. Pulse widths greater than a 1-2 ns are wide enough that the ringing caused by the rising edge does not significantly overlap with the ringing caused by the falling edge. However, in order to capture the return from the entire pulse, the window

length of the scope must be several nanoseconds long, producing undesirably large file sizes. For pulse widths from 200 ps to 2 ns wide, the ringing caused by the rising and falling edges overlaps and confuses the returns. Very short pulse widths less than 200 ps do not have significant destructive effects from the ringing since the rising and falling edges are so close in time that the ringing caused by one edge is indistinguishable from the ringing caused by the other, thereby merging into one coherent waveform. Short pulse widths also have the advantage of requiring short record windows, and so for these reasons, pulse widths of 60 ps wide were used, as illustrated in Figures 4-3 and 4-4.

As can be seen in Figure 4-3, the “60 ps” pulse is not truly 60 ps wide but has a full width, half maximum of 140 ps. This is because the rise time of the pulse generator alone is 55 ps, so in order to rise and fall it should take at least 110 ps. However, decreasing the pulse width below 110 ps still seems to slightly decrease the pulse width at the sacrifice of some amplitude. Also, note the amplitude of the pulse in Figure 4-3 is only 0.5 V since a 10 V pulse could damage the oscilloscope. The spectrum of the pulse reveals that the power is mainly concentrated from 0-3 GHz. However, power can be detected all the way up to 10 GHz.

When the pulse reaches the transmit antenna, significant ringing occurs due to the sharp step hitting a resonant device. This pulse is broadcast by the transmit antenna and then received by the second antenna and sampled by the oscilloscope. The received signal is also affected by antenna cross talk and reflections off of other nearby objects in the environment, but since these components do not change over time, they can be removed from the signal as described later in this section.

Figures 4-5 and 4-6 are plots of a pulse transmitted directly, line-of-sight to the receive antenna. Figure 4-5 shows the ringing caused by the antenna. Figure 4-6 shows that the spectrum of the received signal has the low frequency components removed. This is expected since the horn antenna significantly attenuates signals below 750 MHz. Between 750 MHz and 6 GHz the spectrum of the received signal is attenuated roughly 20 dB more than the same range in the spectrum of the transmitted signal. Above 6 GHz the shape of the spectrum is largely unchanged.

The oscilloscope uses the FastFrames capability to receive each pulse but ignore the dead time in between pulses. FastFrames works by segmenting the buffer into many small

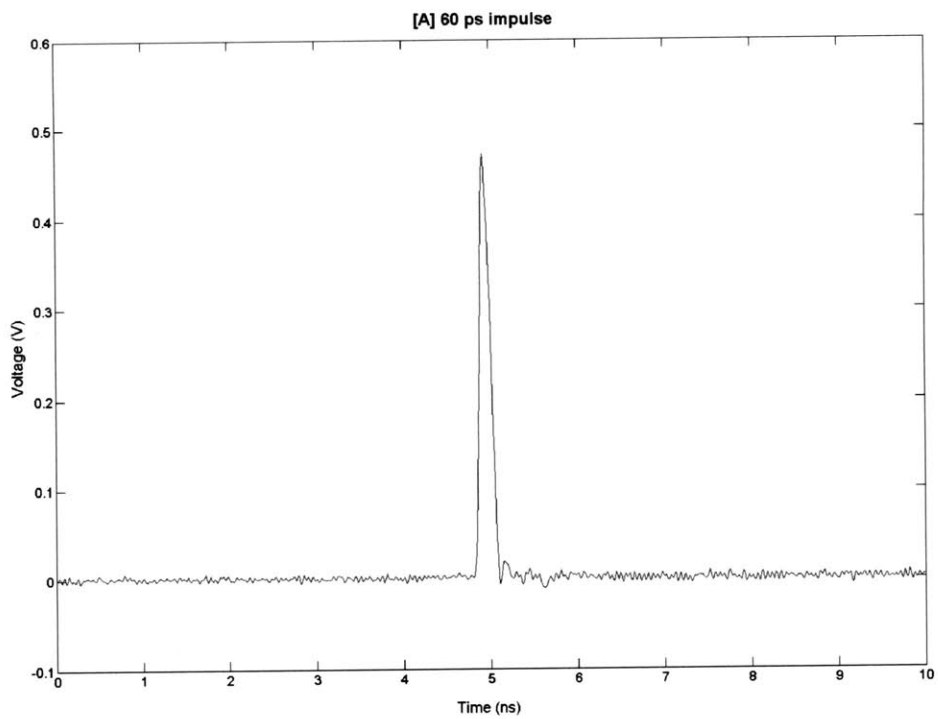


Figure 4-3: Waveform A - 60 ps pulse from pulse generator

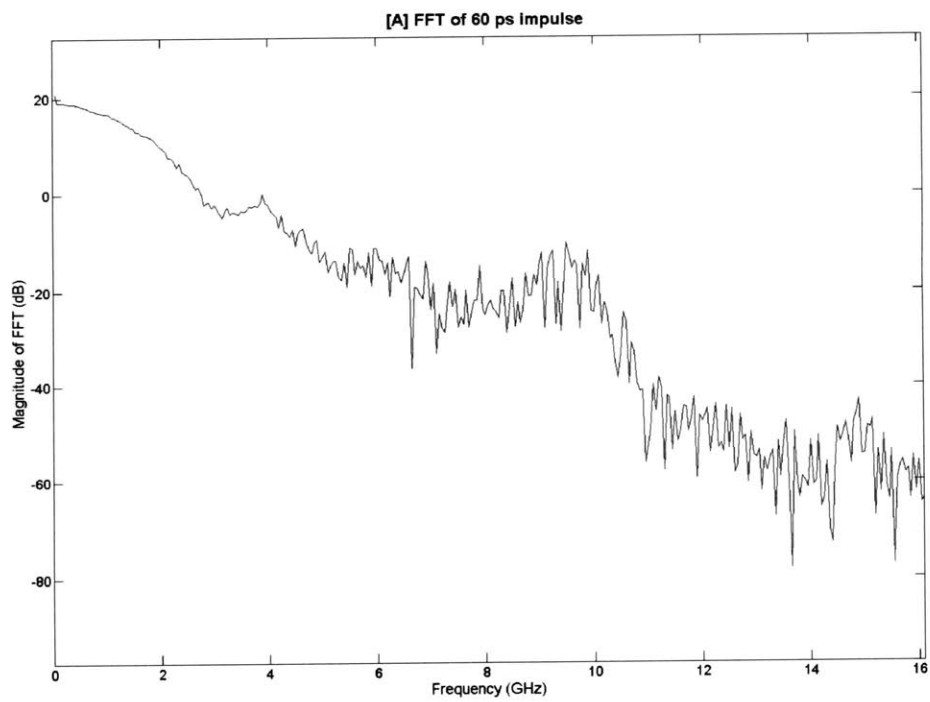


Figure 4-4: Waveform A - Frequency spectrum of 60 ps pulse

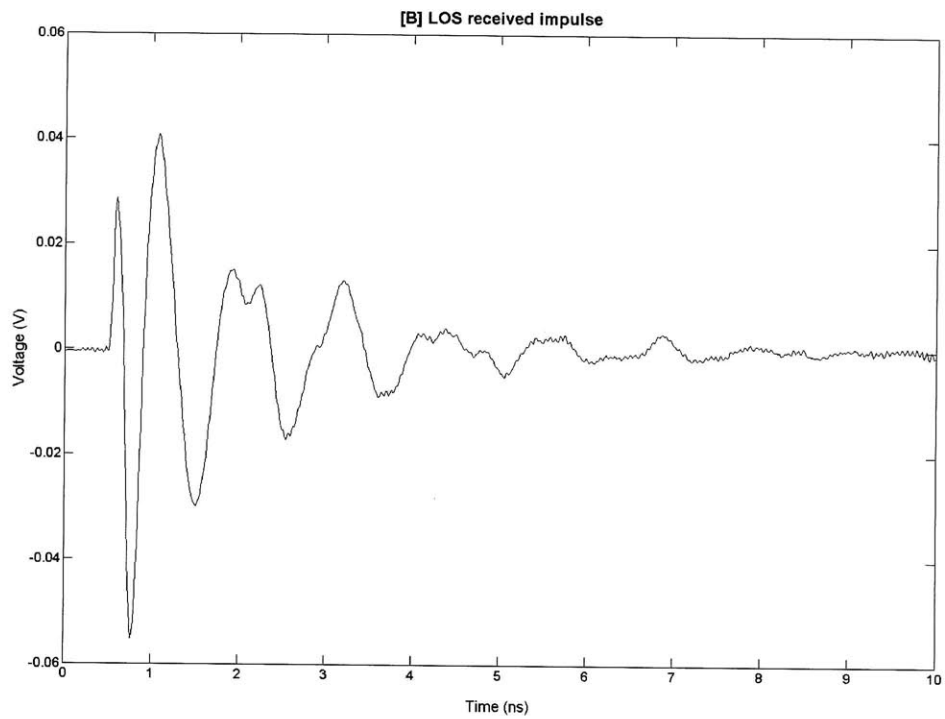


Figure 4-5: Waveform B - Received pulse transmitted line of sight

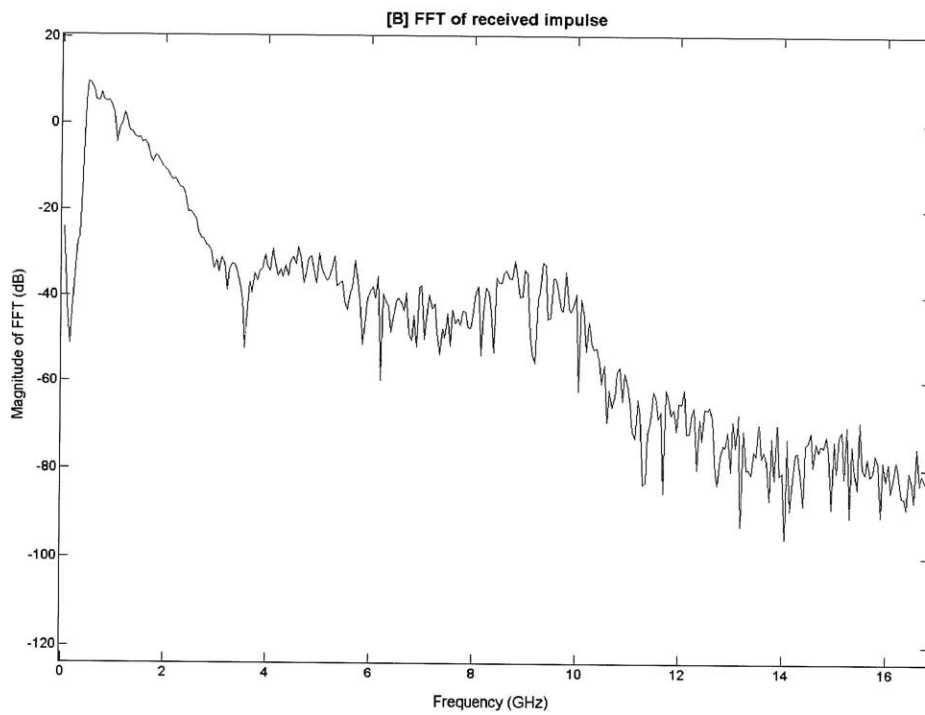


Figure 4-6: Waveform B - Frequency spectrum of received pulse transmitted line of sight

windows. Each time a trigger is received, the oscilloscope delays for several nanoseconds to allow time for the pulse to travel from the transmit antenna, reflect off the subject, and return to the receive antenna. This value is calibrated by the operator depending on the position of the subject, but for subjects 0.5 m away values around 9 ns were used and then fine tuned so that the start of the pulse occurred within the first 1 ns of the receive window. After the delay, the oscilloscope records for 10 ns at 50 Gsamples/s, puts the data in the FastFrame window, and waits for the next trigger. After receiving all the pulses, the operator saves the waveform as a Tektronix .wfm file that can be read into Matlab for additional processing. The FastFrames capability proves to be an effective way to replicate the “receive gate” mentioned earlier, and allows record times up to 10 seconds by not storing the signal received between pulses.

The received signal is corrupted by antenna cross talk, but since cross talk doesn't change over time it is possible to reduce this cross-talk by subtraction. Before testing a human subject, we record the UWB radar returns from the empty room for one second. The antennas are positioned as in Figure 4-2, but point to an empty chair instead of a human subject. This recording is conducted each time the antennas are configured or a large object in the testing area is moved. The one second recording contains 4000 pulse returns, and these are averaged to give a signal representing the time-invariant antenna cross-talk and reflections from nearby objects. An example of empty room data is shown in Figure 4-7.

Because the received pulse is often very noisy, the first step when collecting data from a human subject is to average 10 consecutive pulses in order to improve the signal-to-noise ratio. The results of this averaging are illustrated in Figure 4-8. While the averaging produces a fairly clean signal compared to a single pulse, the pulse reflected from the chest is corrupted by the antenna cross-talk. In order to remove some of the antenna cross-talk contained in the signal, the average empty room pulse return is subtracted from the human subject pulse returns. The result of the subtraction is shown in Figure 4-9.

The next step is to extract the heartbeat from this intermediate signal. The transmitted pulses are modulated in their amplitude and in the timing of their return according to the equations in chapter 3.

Preliminary results confirmed that the timing of the returning pulses varied too little to extract the time-of-arrival information, so we focused on the amplitude modulation of the

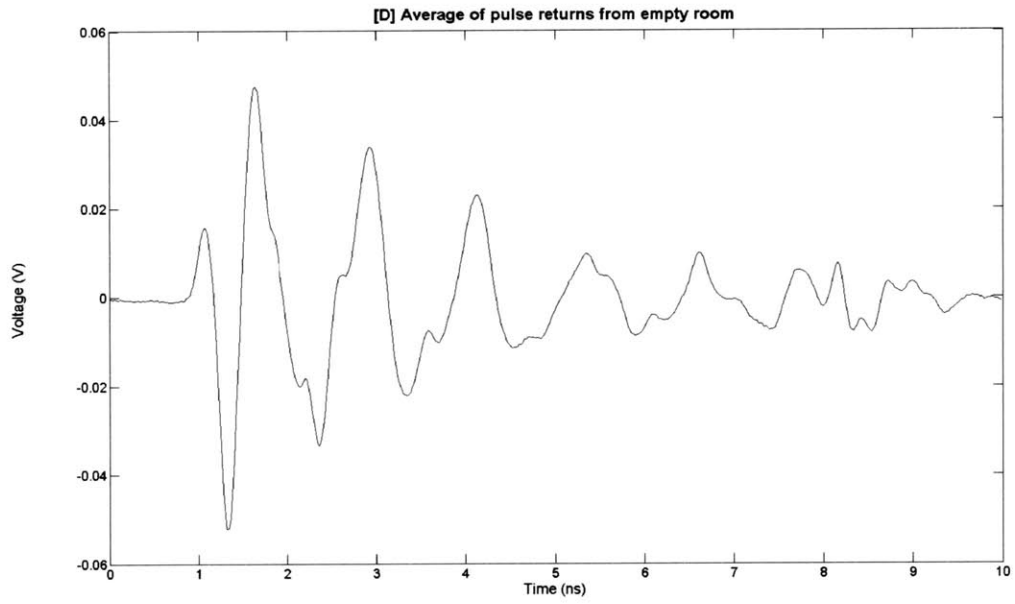


Figure 4-7: Waveform D - Average of pulse returns from empty room

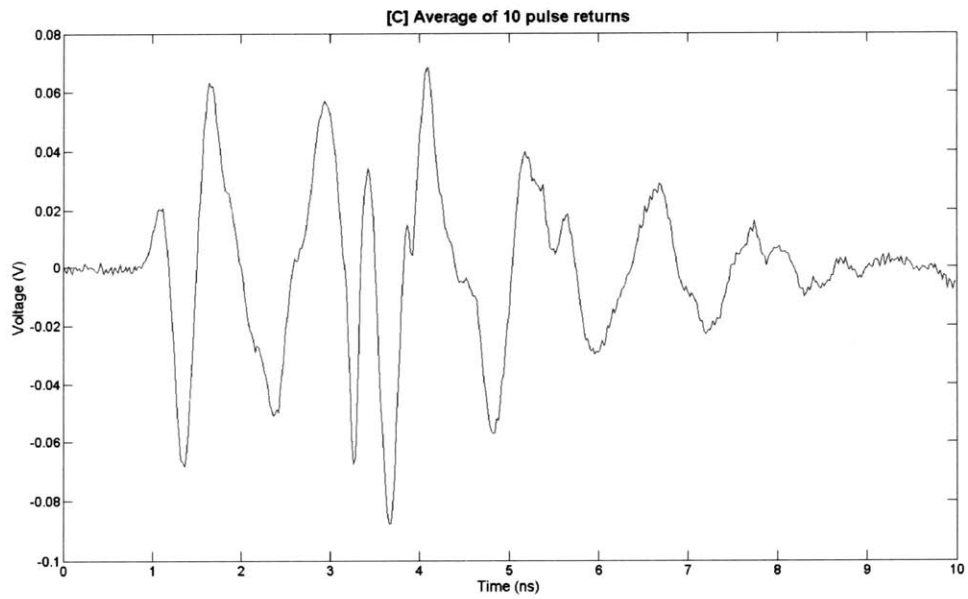


Figure 4-8: Waveform C - Average of 10 received pulses reflected off of human subject



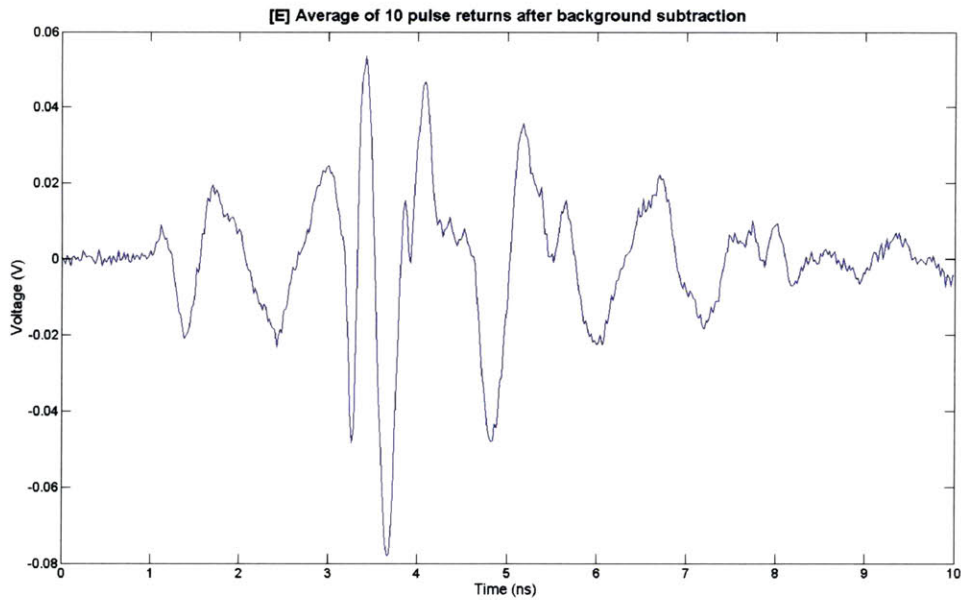


Figure 4-9: Waveform E - Subtraction of empty room pulses from a human subject pulse return

returning pulse. A simple technique that works fairly well is to take the root mean squared (RMS) value of the data points in the pulse window. This gives a single RMS value for each set of averaged pulse returns. A plot of the RMS values is shown in Figure 4-10.

These RMS values were then filtered with either a 10 Hz or 3 Hz FIR low pass filter. This eliminated the high frequency noise and revealed the low frequency components from the heartbeat. The effects of the 3 Hz low pass filter are shown in Figure 4-11. While it is not very clear, the amplitude modulation from the heartbeat can be seen as large bumps in the signal.

There are many different avenues for further work and improvements to the UWB radar system; these will be discussed in chapter 6. However, due to the unreliable and noisy returns from the system and the much better results obtained with the fixed frequency radar, we decided to focus the current project primarily on the fixed-frequency radar system detailed in the next section.

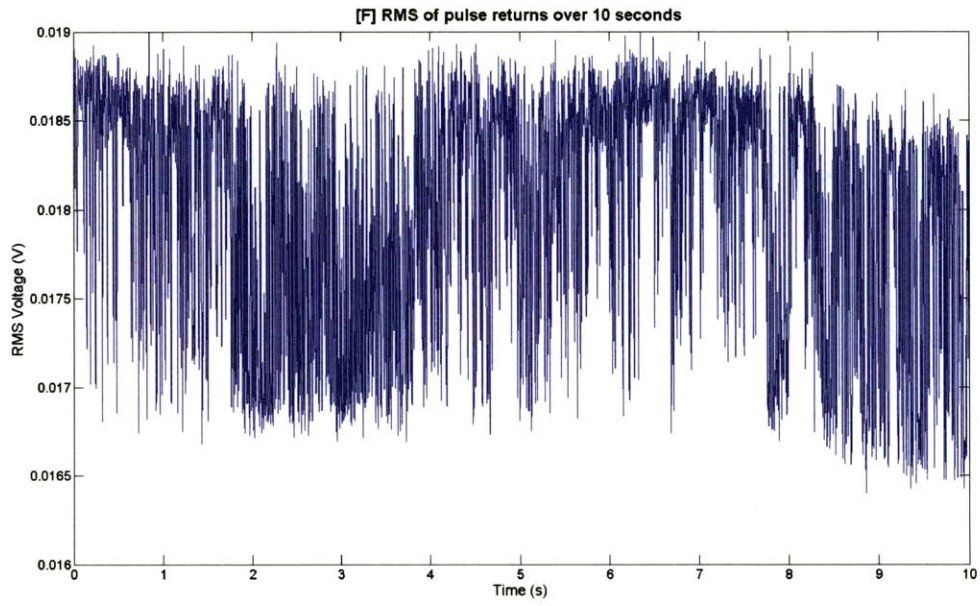


Figure 4-10: Waveform F - RMS values of averaged pulse returns

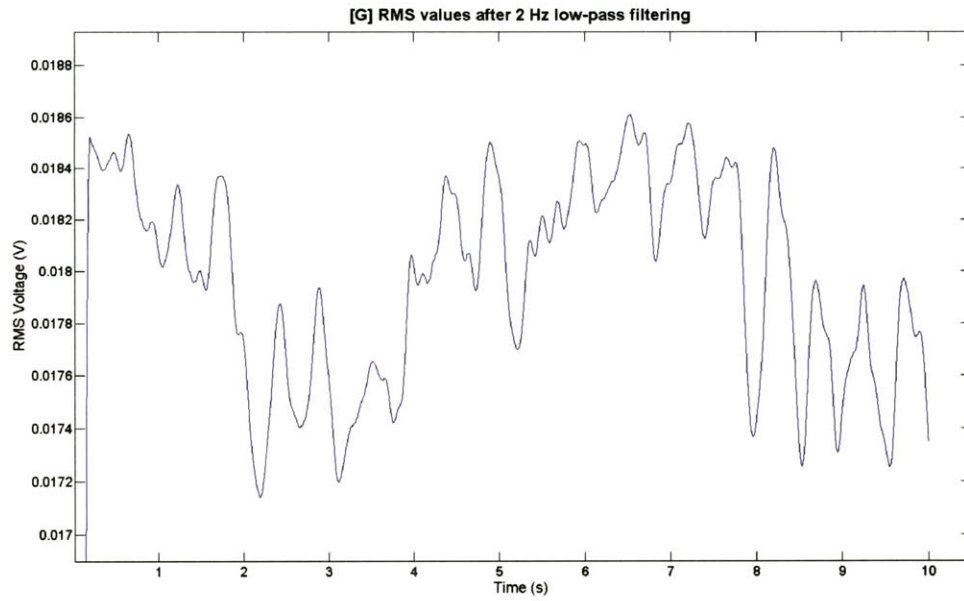


Figure 4-11: Waveform G - RMS values filtered with 3 Hz low pass filter

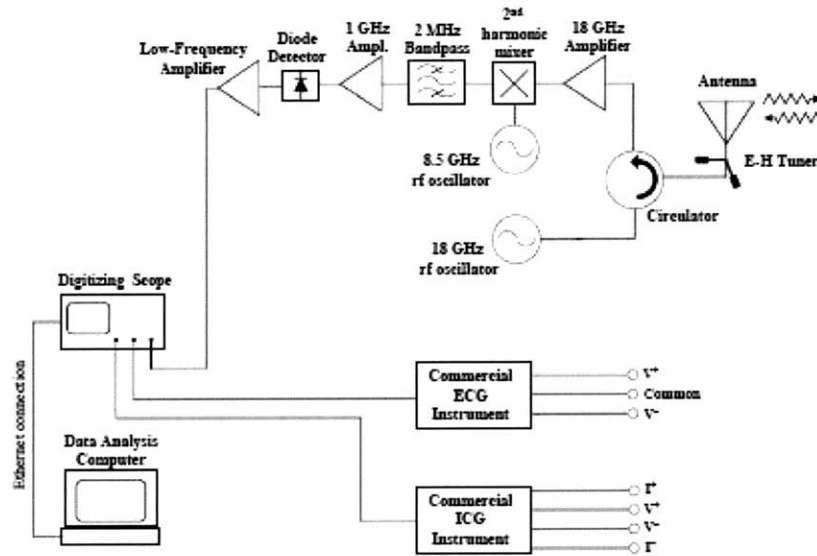


Figure 4-12: Fixed frequency radar setup by McGrath

## 4.2 Fixed Frequency Radar Setup

The motivation for a fixed frequency radar setup came from an unpublished manuscript by William R. McGrath of Jet Propulsion Laboratory (JPL). As discussed previously, McGrath described a system that could be used to sense ECG-like signals remotely using fixed frequency radar. In an effort to replicate McGrath's results, a fixed frequency radar was constructed similar to the one he described. An illustration of the radar from his manuscript is shown in Figure 4-12.

The radar constructed by McGrath illuminated the subject with an 18 GHz, 0 dBm signal. The return signal was received with the same antenna, amplified, and mixed with 8.5 GHz. A bandpass filter selected the second harmonic (1 GHz) from the output of the mixer and the signal was then amplified before being fed to a diode detector. The output of the diode detector was proportional to the power of the 1 GHz input signal. In summary, McGrath's radar emits 18 GHz radiation and measures the amount of power that comes back. Our fixed frequency radar was constructed to perform the same function.

### 4.2.1 Fixed Frequency Hardware

Similar to the UWB radar, our version of the fixed frequency radar was constructed using test equipment to avoid spending time developing a radar system with custom hardware. The radar hardware needed to accomplish three main functions: 1) transmit an 18 GHz signal, 2) receive the reflected signal and mix it down to a more usable frequency, and 3) measure parameters of the resulting signal, such as amplitude, in order to extract information about the heartbeat of the human subject. In our fixed frequency radar these three functions are performed by three separate pieces of test equipment.

The 18 GHz signal is generated by an Agilent 8673G 2-26 GHz Synthesized Signal Generator. This piece of equipment is simply set to generate 18 GHz with a power output of 0 dBm. It is connected to one of the same broadband horn antennas used in the UWB radar system: an ETS-Lindgren 3115 rated for frequencies from 0.75 - 18 GHz. At 18 GHz the horn antenna has a gain of 13 dB and a half power beamwidth of  $10^\circ$ . The horn antennas are connected with Gore Phaseflex coaxial cable rated up to 18 GHz.

The return signal is received by a second, identical horn antenna connected to the input of an Agilent 8566B 100 Hz - 22 GHz Spectrum Analyzer. The spectrum analyzer performs the second function of the system: mixing the reflected 18 GHz signal down to a more usable frequency. A spectrum analyzer usually mixes (multiplies) its input with a local oscillator (LO) that slowly sweeps its frequency across a set range. This mixing produces an output whose frequency is the input frequency minus the LO frequency. This process of mixing an input signal to produce a lower frequency output signal is called down mixing or down converting. There are also many harmonics of the input and LO signals in the output, so a bandpass filter is used to isolate the exact desired harmonic. The output power of the bandpass filter is measured, and since the center frequency of the filter and the current frequency of the local oscillator are known, it is possible to calculate the frequency of the input signal at which the observed power level occurs. By sweeping the local oscillator frequency, a picture of the input signal's power spectrum is obtained. For signal quality issues, this Agilent spectrum analyzer actually downmixes the input signal twice, but the principle is the same.

The diagram of the spectrum analyzer in Figure 4-13 is simplified for clarity and a more accurate representation of the 18 GHz signal chain inside the spectrum analyzer is shown

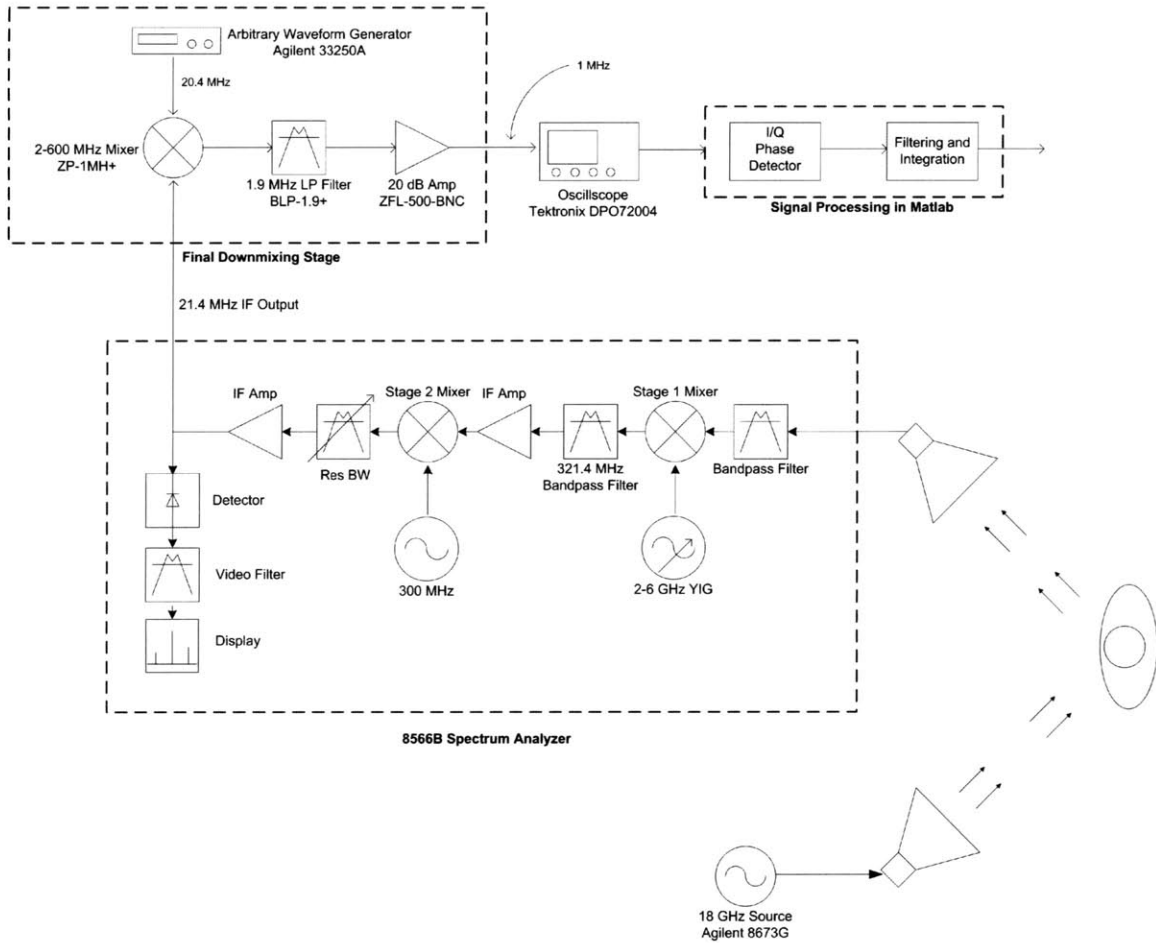


Figure 4-13: Fixed Frequency Radar System

in Figure 4-14. This diagram was redrawn from the Agilent 8566B repair manual as best as the poor quality of the document allowed. There are two main differences between the two figures. The first is the mixing strategy of the first converter. Instead of a traditional three-port mixer, the first mixer couples the local oscillator frequency into the same line as the intermediate frequency. By placing a bandpass filter at the end of this line, the 321.4 MHz intermediate frequency can still be isolated from the local oscillator frequency and the rest of the harmonics. While this first mixer uses a different topology than normal, the function is identical to that of a standard three-port mixer.

The second difference is the added amplification and attenuation stages after the second mixer. The 21.4 MHz preamplifier filters out the harmonics from the output and amplifies the signal. The purpose of the stages following the preamplifier is to offset the frequency dependent attenuation differences of the first hardware components in the spectrum analyzer's

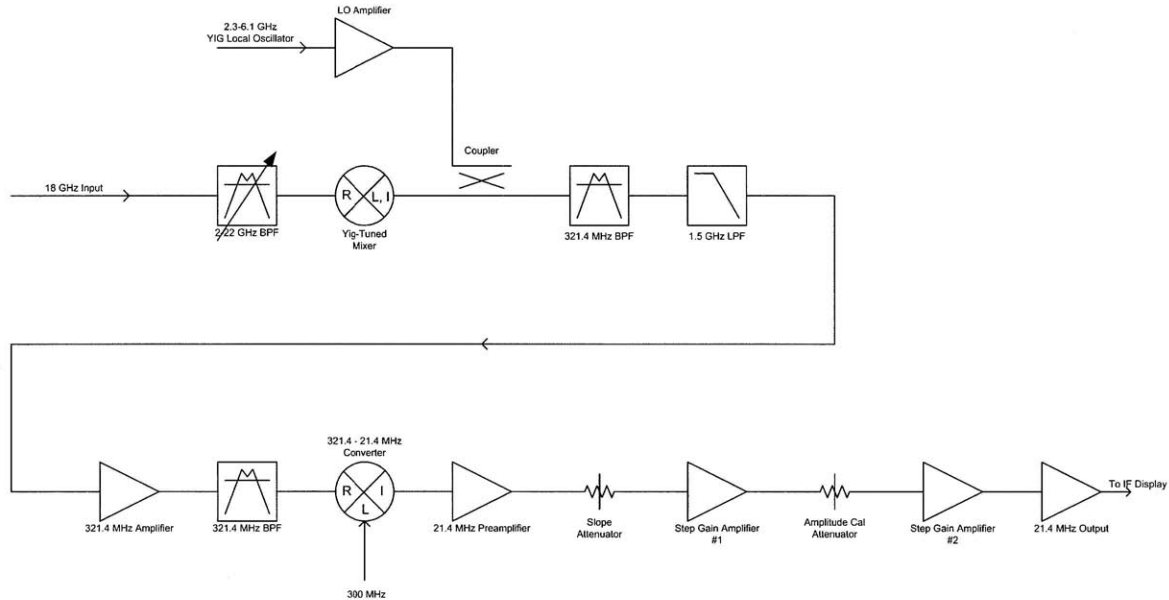


Figure 4-14: More accurate representation of 18 GHz signal chain inside the 8566B spectrum analyzer

signal chain. While the inside of the spectrum analyzer is fairly complex, its functionality is well represented by the two-stage down conversion in Figure 4-13.

Instead of using the spectrum analyzer to obtain the power levels of the input signal at a range of frequencies, we are only interested in the power level of the input signal at a particular frequency - 18 GHz. We can use the spectrum analyzer to measure this by setting the center frequency to 18 GHz and the frequency span to 0 Hz. This effectively turns the spectrum analyzer into a giant, two stage down converter. The spectrum analyzer first converts the input signal from 18 GHz down to 321.4 MHz, and then a second mixing stage converts the 321.4 MHz signal down to 21.4 MHz, called the intermediate frequency (IF). The spectrum analyzer measures the power of the IF and plots the value on the display. Usually the display sweeps from left to right along with the sweeping LO frequency, plotting the power as a function of frequency. In our case the frequency span is zero, but the display still slowly sweeps from left to right, effectively plotting the power of 18 GHz as a function of time.

While the display of the spectrum analyzer produces the desired output, the analog equipment does not provide a means to record the final signal for further processing. However, the spectrum analyzer produces an output signal consisting of the 21.4 MHz IF signal. By recording the IF output of the spectrum analyzer with the Tektronix DPO 72004 os-

cilloscope described previously, the power can be calculated and then further processed in Matlab. This method allows much more flexibility in the final processing, and also has the great advantage that by recording the full IF signal, we are preserving not only the power but also the frequency information of the signal.

Originally the 21.4 MHz IF was recorded directly by the oscilloscope. The minimum sampling rate offered by the oscilloscope above the Nyquist frequency is 62.5 Msamples/s. Since the maximum record length per channel of the oscilloscope is 250 Msamples, only 4 seconds of data could be recorded at a time. Also, because the sampling rate was so close to the Nyquist limit, detecting phase changes in the IF signal was not feasible. In order to solve these problems, a simple, third mixing stage was constructed external to the spectrum analyzer to mix the 21.4 MHz signal down even further to 1 MHz.

The final mixing stage was constructed using inexpensive components purchased from Minicircuits. A 2-600 MHz mixer (Minicircuits model ZP-1MH+) with a 13 dBm LO drive level followed by a 1.9 MHz low pass filter (Minicircuits model BLP-1.9+) was used to convert the 21.4 MHz down to 1 MHz. A general purpose Agilent 33250A 80 MHz Function / Arbitrary Waveform Generator set to 20.4 MHz at 13 dBm was used as the local oscillator. The output of the filter was amplified by a 20 dB, 0.05-500 MHz amplifier (Minicircuits model ZFL-500-BNC).

The 1 MHz output of the final mixing stage is recorded by the oscilloscope. Because the frequency of the input signal is lower than the 21.4 MHz output of the spectrum analyzer originally recorded by the oscilloscope, we now have much more flexibility in selecting the scope settings. In order to produce good resolution for measuring the phase change of the signal, the sampling rate of the oscilloscope was set to 25 Msamples/s, producing a record length of 10 s. If an even longer record length is desired, the sampling rate of the scope can be lowered. To keep the same oversampling ratio, the output frequency of the final mixing stage can be lowered as well by raising the local oscillator frequency. However, because the analog filter in the final mixing stage has a cutoff of 1.9 MHz, the sampling rate of the oscilloscope should not be lowered below 3.8 MHz to avoid aliasing.

After the 1 MHz signal is recorded by the oscilloscope, the rest of the fixed-frequency system consists of signal processing steps in Matlab. These steps are detailed in section 4.2.4. In order to preserve the signal for future analysis, the entire waveform is saved as

a Tektronix .wfm file. This format preserves all the information in the most compact way possible. For the signal processing steps in Matlab, this file is parsed by a Matlab routine to import the recorded signal into the Matlab environment.

## 4.2.2 Safety Considerations

Just as with the UWB radar, it was necessary to ensure that the radar was safe for human subject testing. The IEEE C95.1 standard gives  $10/mW/cm^2$  as the highest maximum permissible exposure (MPE) power level for frequencies of 18 GHz.

The signal generator transmits 18 GHz with a power level of 0 dBm (1 mW). The transmit horn antenna is the same as that used for the UWB case, so the same equations and analysis can be used. The horn antenna has a maximum possible gain of 17 dB and is 15 cm deep. Antenna gain is defined by equation 4.3.

To estimate the power delivered to the subject standing right next to the horn antenna we multiply the isotropic power by the antenna gain. Even though the user would be in the near field of the antenna and equation 4.3 is valid only for the far field, this approach is conservative because the power in the near field can only be less than the power calculated using far field equations [44]. Using far field equations, the isotropic power delivered 15 cm away by the antenna with an input power of 1 mW is:

$$Isotropic\ Power = \frac{1}{4\pi 15^2} mW/cm^2 = 0.354 \mu W/cm^2 \quad (4.6)$$

Multiplying the isotropic power by the gain of the antenna gives us the incident power on the subject:

$$Incident\ Power = 0.354 \mu W/cm^2 \times 10^{17 dB/10} = 17.74 \mu W/cm^2 \quad (4.7)$$

This is far under the 18 GHz MPE power level of  $10mW/cm^2$  given by the IEEE, making the fixed frequency radar setup safe for human subject testing.



### 4.2.3 Frequency Sweep Experiment

The initial data collected with the fixed frequency radar revealed that high frequency components of the returned signal were attenuated. In order to verify this observation and diagnose the problem, a frequency sweep experiment was designed to test the radar system. ECG signals have a useful frequency spectrum up to roughly 30 Hz, so the experiment was designed to see if the spectrum analyzer attenuated the 18 GHz signal when it was modulated by a signal with frequency components up to 40 Hz.

For the experiment, the transmit and receive antennas were separated by 0.5 meters and pointed directly at each other. A signal generator transmitted an 18 GHz signal between the antennas, the spectrum analyzer downconverted the signal, and the IF output was recorded by the oscilloscope. The 18 GHz signal was amplitude modulated by an arbitrary waveform generator set to produce a frequency sweep from 0.5 - 40 Hz over a 4 second time period.

The experiment confirmed the initial observations - the spectrum analyzer severely attenuated any modulating waveform components above several Hz. We determined that this was due to the RES (resolution) filter bandwidth setting on the spectrum analyzer. The RES filter is a bandpass filter that determines the resolution of the frequency sweep on the spectrum analyzer. By setting the bandwidth of the RES filter to a small value, only a very small window of the input signal's spectrum is measured at any one time. When the user decreases the span of the frequency sweep, the spectrum analyzer automatically sets the bandwidth of the RES filter to smaller and smaller values to give better resolution. When used in the radar system, the spectrum analyzer was set to have a frequency span of zero, so the spectrum analyzer set the bandwidth of the RES filter to its smallest possible value of 10 Hz. Therefore, if the 18 GHz signal was modulated by a signal with frequency components above 10 Hz, the RES filter significantly attenuated those high frequency components.

The solution to this problem was simply to override the default RES filter bandwidth setting with a higher value. The results of several RES filter settings are shown in Figures 4-15 and 4-16.

Based on the results shown above, we decided to use a RES filter bandwidth setting of 300 Hz in the remainder of this work. The 300 Hz setting did not appear to attenuate any signals below 40 Hz, but at the same time filtered out noise at higher frequencies.

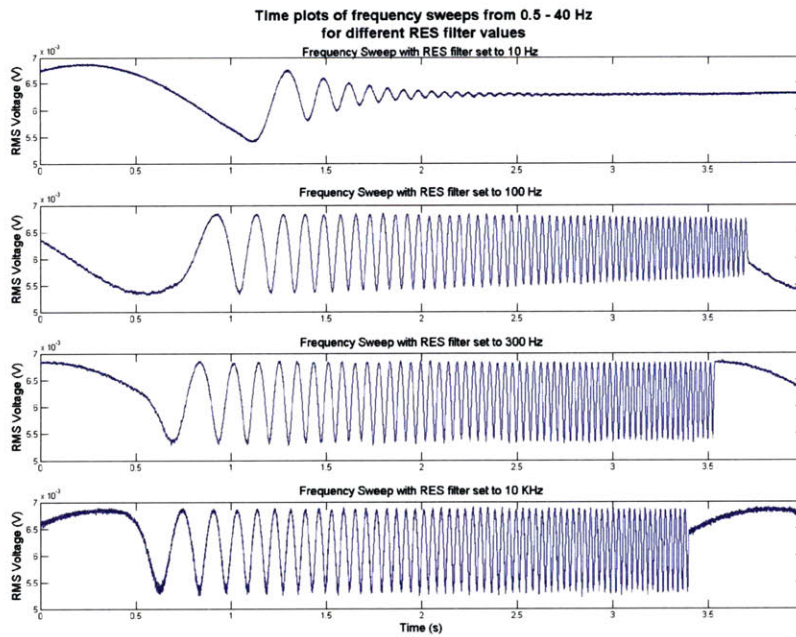


Figure 4-15: Results of amplitude modulating the 18 GHz signal with a frequency sweep from 0.5 - 40 Hz with RES filter bandwidth settings of 10, 100, 300, and 10,000 Hz

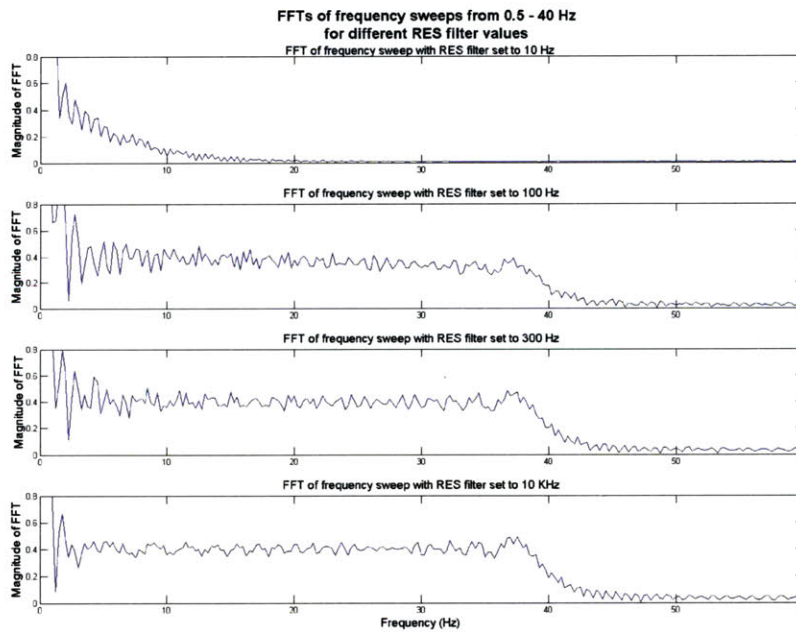


Figure 4-16: Frequency spectrum of results from Figure 4-15

#### 4.2.4 Fixed Frequency Radar Signal Processing

The signal processing used with the fixed frequency radar can be divided into two parts. The first part involves extracting the amplitude and phase modulation of the 18 GHz signal through an I/Q demodulator. The second part involves filtering the amplitude and phase signals to reveal the heartbeat information contained in each.

##### Demodulation

I/Q, or quadrature, demodulation is a popular technique for demodulating frequency modulated communications. An I/Q demodulator works by splitting the input into two channels and converting each channel to baseband by mixing with a local oscillator of the same frequency as the center frequency of the input. However, the local oscillators of the two channels are shifted by 90 degrees from each other. The outputs of the two mixers are filtered to remove harmonics and the result is an imaginary (I) and real (Q) channel at baseband. These two channels can then be used to calculate the phase of the incoming signal by taking the inverse tangent of their ratio [45].

The mathematical proof for the demodulator is given below. If the input is a signal of frequency  $\omega$  radians per second with a time dependent phase of  $\varphi(t)$ , we can express it in terms of complex exponentials according to Euler's Formula:

$$\sin(\omega t + \varphi(t)) = \frac{e^{j(\omega t + \varphi(t))} - e^{-j(\omega t + \varphi(t))}}{2j} \quad (4.8)$$

Multiplying this by the local oscillators gives:

$$\begin{aligned} \sin(\omega t + \varphi(t)) \times \sin \omega t &= \frac{e^{j2\omega t} e^{j\varphi(t)} - e^{-j\varphi(t)} - e^{j\varphi(t)} + e^{-j2\omega t} e^{-j\varphi(t)}}{-4} \\ &= \frac{1}{2} \cos(\varphi(t)) - \frac{1}{2} \cos(2\omega t + \varphi(t)) \\ \sin(\omega t + \varphi(t)) \times \cos \omega t &= \frac{e^{j2\omega t} e^{j\varphi(t)} - e^{-j\varphi(t)} + e^{j\varphi(t)} - e^{-j2\omega t} e^{-j\varphi(t)}}{4j} \\ &= \frac{1}{2} \sin(\varphi(t)) + \frac{1}{2} \sin(2\omega t + \varphi(t)) \end{aligned} \quad (4.9)$$

The low pass filter following each mixer removes the image at double the input frequency.

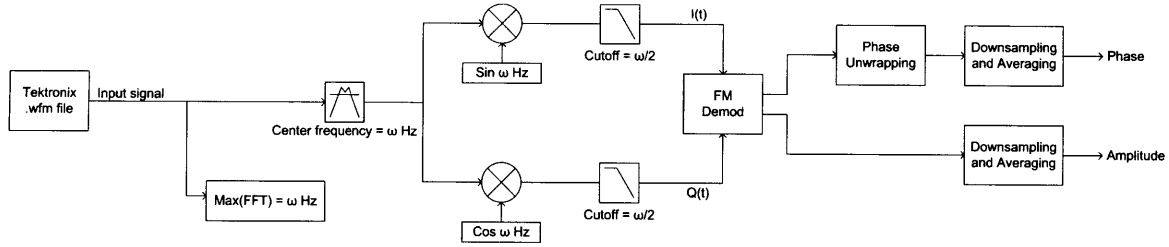


Figure 4-17: Block diagram of the FM demodulator for phase and amplitude detection

The remaining components are defined as  $I(t)$  (imaginary channel) and  $Q(t)$  (real channel):

$$I(t) = \frac{1}{2} \cos(\varphi(t)) \quad (4.10)$$

$$Q(t) = \frac{1}{2} \sin(\varphi(t))$$

From  $I(t)$  and  $Q(t)$ , we can solve for  $\varphi(t)$  using:

$$\arctan\left(\frac{Q(t)}{I(t)}\right) = \arctan\left(\frac{\frac{1}{2} \sin(\varphi(t))}{\frac{1}{2} \cos(\varphi(t))}\right) = \varphi(t) \quad (4.11)$$

The amplitude of the signal can also be calculated using  $I(t)$  and  $Q(t)$ :

$$Amplitude = \frac{2 \times I(t)}{\cos(\varphi(t))} = \frac{2 \times Q(t)}{\sin(\varphi(t))} = \frac{I(t)}{\cos(\varphi(t))} + \frac{Q(t)}{\sin(\varphi(t))} \quad (4.12)$$

The I/Q demodulator is often implemented in analog circuitry, but the same functionality can be replicated using digital signal processing techniques. Calculating the phase from the I and Q channels, called FM demodulation, is also easily done digitally using equation 4.11. The I/Q and FM demodulation scheme described above is done digitally within Matlab, and is the first step of signal processing performed on the recorded signals. A block diagram of the system is shown in Figure 4-17.

The first step in the FM demodulator involves parsing the Tektronix .wfm file in order to extract the recorded signal. The parser is an efficiency enhanced version of a community developed Matlab function written by Randy White [46]. Because the entire oscilloscope buffer of 250 million points has been saved, it is impractical to parse the entire file at once. For most systems, trying to process a huge, 250 million length buffer in Matlab will

quickly lead to memory errors. To get around this, the system processes the file in large segments and downsamples the phase and amplitude output by averaging wide windows of consecutive data points. While the size of these segments and windows are configurable, the settings used are: 1) processing data in 1 million length segments, and 2) averaging 2500 consecutive data points to form a single output data point. For a recording 10 seconds long that used the full 250 million point buffer, this downsampling gives an effective sampling rate of 10 KHz, giving sufficient bandwidth for the input signals of interest and yielding data lengths of manageable size.

The next step is to determine the center frequency of the recorded signal. While this is known to be 1 MHz, the oscilloscope, spectrum analyzer, and AWG in the final conversion stage are not synchronized in any way, so it is necessary to determine the exact frequency of the recorded signal within Matlab. This is accomplished by parsing a large segment (25 million points) from the file and calculating its FFT. The frequency at the maximum magnitude in the first half of the FFT is used as the center frequency. That center frequency is used to calculate multiple parameters in the rest of the demodulator.

After the center frequency is calculated, the demodulator reads in segments of data and processes each completely before moving on to the next data segment. At some points in the processing chain, portions of the data segment currently being processed are saved to append to the next data segment - for example, to provide the initial values for applying an FIR filter to the next data segment.

The first step in processing each segment is filtering with an FIR bandpass filter with a center frequency as determined above and a cutoff of  $\pm 5$  KHz. Since the final output is downsampled to 10 KHz, a 5 KHz filter bandwidth is chosen to avoid unnecessary aliasing. One thousand coefficient FIR filters are used in all filtering stages because their constant group delay over frequency is highly desirable. The bandpass filter removes any leftover harmonics from previous mixing stages and ensures that the input signal to the I/Q demodulator is as clean as possible.

After filtering, one cosine wave and one sine wave are generated at the center frequency calculated previously. These waves continue seamlessly from their value in the previous data segment - they do not start at the same point for each data segment. The  $I(t)$  and  $Q(t)$  channels are then formed by separately multiplying the output of the bandpass filter

with the sine wave and the cosine wave. The newly formed  $I(t)$  and  $Q(t)$  channels are then filtered by a low pass, 1000 coefficient FIR filter with a cutoff at one-half the center frequency. This removes the image at twice the center frequency generated by mixing with the sine and cosine waves.

Now that the  $I(t)$  and  $Q(t)$  channels have been formed, the next step takes the inverse tangent of  $Q(t)$  divided by  $I(t)$  in order to determine the phase of the signal. However, as the phase changes, there are times when the calculated phase will exceed  $+\pi$  or  $-\pi$ , causing it to jump  $2\pi$  in the other direction. This is called wrapped phase, and in order to be more useful, these jumps of  $2\pi$  are removed in a phase unwrapping process. A custom unwrapping operation was written since the Matlab unwrapping function did not handle noisy phase signals very well. The custom unwrapping operation looks for a large, sudden jump in the phase, but it also ensures that these jumps are isolated events and not part of a trend to prevent unwrapping a natural but sudden change in phase. This unwrapping operation is included in the code listing in Appendix A.

The amplitude of the input signal is computed using equation 4.12. Since  $I(t)$ ,  $Q(t)$ ,  $\cos(\varphi(t))$ , and  $\sin(\varphi(t))$  have already been computed, this is a simple matter of division and addition.

The final step in processing takes windows of the amplitude and phase data, averages the values in each window, and uses the result as the data points for the final output. The length of the window is chosen to be 2500 points long so that the final effective sample rate is 10 KHz. As mentioned previously, this greatly reduces the amount of data stored for further processing and is far above any frequency of interest. After all data segments have been processed, the result is turned over to the next section for further filtering in order to reveal the heartbeat signatures contained within. The Matlab code used to implement this demodulation is included in Appendix A.

## Filtering

The phase output of the FM demodulator usually has a constant rate of decay or increase. This is due to the slight frequency difference between the actual center frequency of the recorded signal and the center frequency computed and used by the demodulator. This frequency difference translates to a constant rate of phase change. In order to remove this

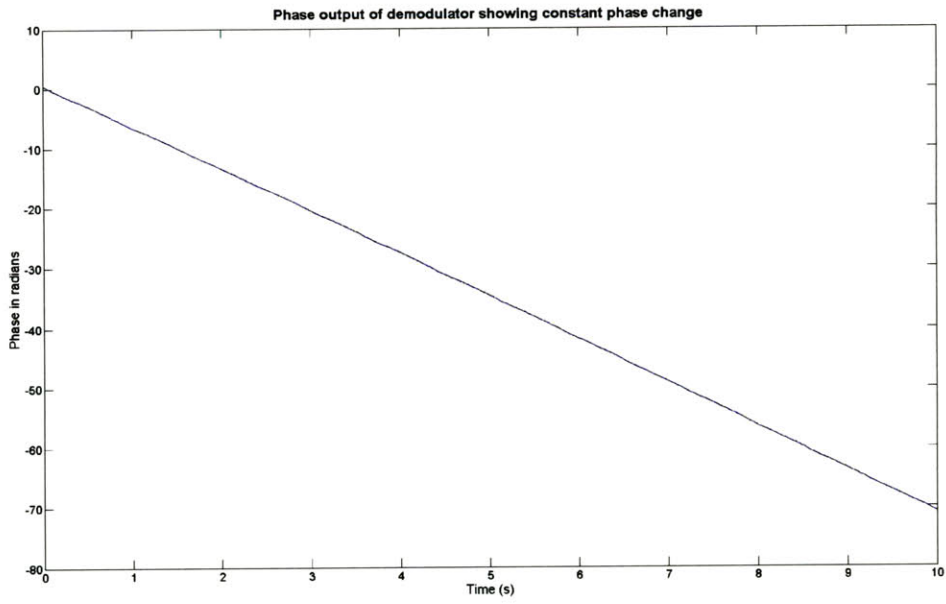


Figure 4-18: Phase output before line subtraction

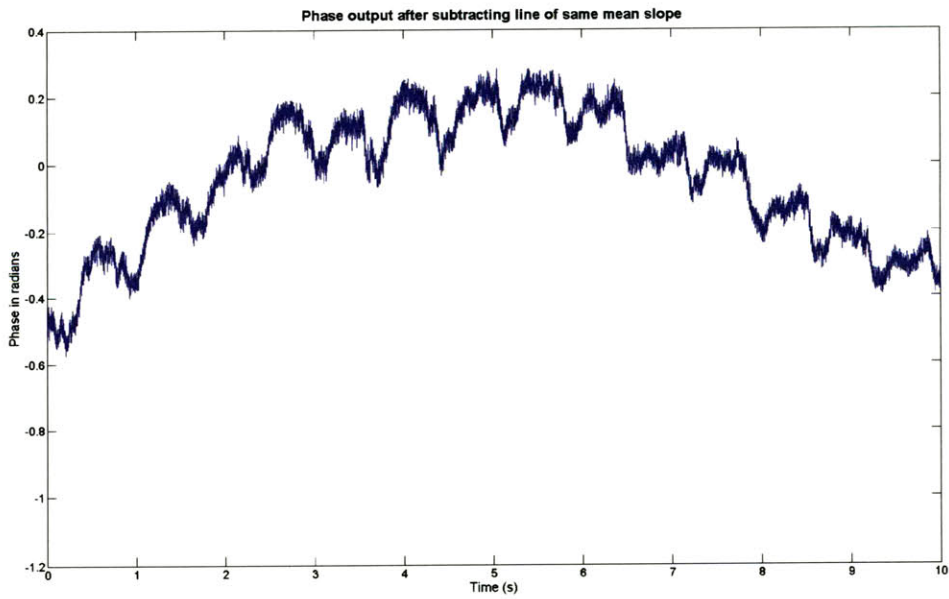


Figure 4-19: Phase output after line subtraction

constant change from the phase signal, the phase data could be high pass filtered. However, this produces unwanted effects in the output signal. Another method is to subtract from the phase data a line that has the same average slope as the phase data. This removes the constant phase change, but does not add any unwanted effects to the output data. Figures 4-18 and 4-19 show the effects of this line subtraction operation.

The main function of the filtering stage is to remove components of the frequency spectrum that are unnecessary. The following two filters are applied to both the radar phase after line subtraction and the radar amplitude. The first filter removes some of the very low frequency components caused by drift or very slow body motions. This filter is a 2nd order, 0.5 Hz highpass Butterworth filter. A Butterworth filter was chosen because it can remove strong low frequency components that an FIR filter could not handle without an excessively large number of coefficients. The second filter is a 1000 coefficient, 30 Hz lowpass FIR filter. The FIR filter was chosen because of its constant group delay. This filter effectively removes high frequency noise from the radar channels. The Matlab files that generate these filters can be found in Appendix A.

## 4.3 Other Devices

In order to gather a “true” measure of cardiac function, the outputs of two monitoring devices were recorded by the oscilloscope at the same time as the radar. One device is an ECG monitor for measuring the electrical activity of the heart. The second device is an accelerometer for measuring chest movements caused by the heartbeat. Their operation is described below.

### 4.3.1 ECG Monitor

For this project we needed an inexpensive ECG monitor and used an ECG1C Electrocardiogram Heart Monitor, purchased from Ramsey Electronics. The monitor has two differential probes and one ground probe, comes with a set of ECGP10 probe patches, and runs off of a 9 V battery. The monitor works adequately when proper contact with the skin is made.

A bottle of Buh-Bump ECG electrode cream was purchased to increase the contact between the electrodes and the skin. A number of different electrode positions were tried,



and the most reliable results were found when the differential electrodes were placed on opposite sides of the chest just below the shoulder, with the ground electrode attached to the left or right ankle. The oscilloscope sampled the data using a P6246 differential probe. This probe served as a high-impedance buffer, allowing the oscilloscope to sample weakly driven signals. The oscilloscope differential probe was connected directly across resistor R13 inside the ECG monitor since a less filtered signal could be obtained at that point. The gain of the monitor was set so that the ECG signal was clearly visible in the oscilloscope. For most subjects this required the gain to be set to about 3/4 of the full value.

The output of the ECG monitor was windowed in the same way as the amplitude and phase outputs of the demodulator in section 4.2.4.1. The signal was then filtered with the same 30 Hz, 1000 coefficient lowpass FIR filter described in section 4.2.4.2.

### 4.3.2 Accelerometer

In order to verify that the heartbeat signatures recorded by the radar came from chest movement and not some other physiological effect, a small accelerometer board was constructed to measure the movement of the chest wall. The accelerometer was from Freescale Semiconductor (part number MMA1260EG). It was chosen for its high sensitivity, small number of external components, and 1-D sensing axis.

The recommended application circuit from the product data sheet is shown in Figure 4-20. The ST pin was tied to ground and the STATUS line was left open. The accelerometer and external components were mounted on a 9162 surfboard from Capital Advanced Technologies. The accelerometer used a 5 V external power supply, and the oscilloscope recorded its output through a TCA-1MEG buffer amplifier from Tektronix. The accelerometer was mounted on the chest three inches to the left of the base of the sternum.

The accelerometer measures the acceleration of the chest. In order to truly compare the accelerometer with the radar signals, the accelerometer data needs to be integrated twice to yield position. First, the accelerometer data is windowed and 30 Hz low pass filtered just like the ECG signal. The integral is calculated by a simple cumulative summation. However, this often adds large low frequency components to the signal, and these are removed with a 8th order, high-pass Butterworth filter with a cutoff frequency of 1 Hz, the values of which were chosen by trial and error.

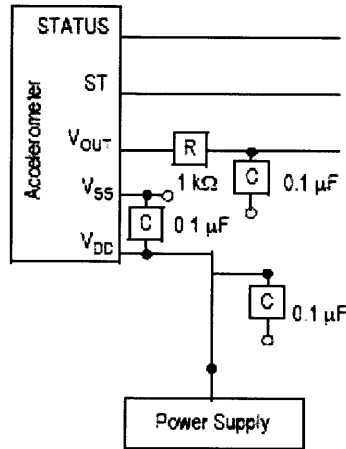


Figure 4-20: Recommended application circuit for accelerometer

## 4.4 Radar Modulation Experimental Methods

Two experiments were conducted to identify the source of the radar’s amplitude modulation. The first experiment attempted to replicate and measure electrical activity in a very simple physiological analog. The second experiment measured chest movement and determined if the chest movement correlated with the radar returns. The methods used for each experiment are discussed below.

### 4.4.1 Cardiac Electrical Analog

The goal of this experiment was to construct a simple test setup that replicated the same electrical characteristics as the human body. The physiological analog consisted of a circular basin containing 4 liters of water mixed with saline tablets that replicated the salinity and pH of the human body. Four electrodes were inserted into the basin at equal distances from each other. Two electrodes were a shared ground, while the other two electrodes were driven by two sinusoids with a phase offset of 90 degrees and a fixed frequency that could be selected in the range 4-53 Hz. The purpose of the electrodes was to create a circulating electrical field that the radar might be able to record.

The sinusoidal signals had a peak voltage in the range 0 - 5 V and passed through either a 50  $\Omega$  or 1 M $\Omega$  resistor to limit the current. The transmit and receive antennas were placed over the basin and pointed at symmetric angles towards the center of the basin. Many

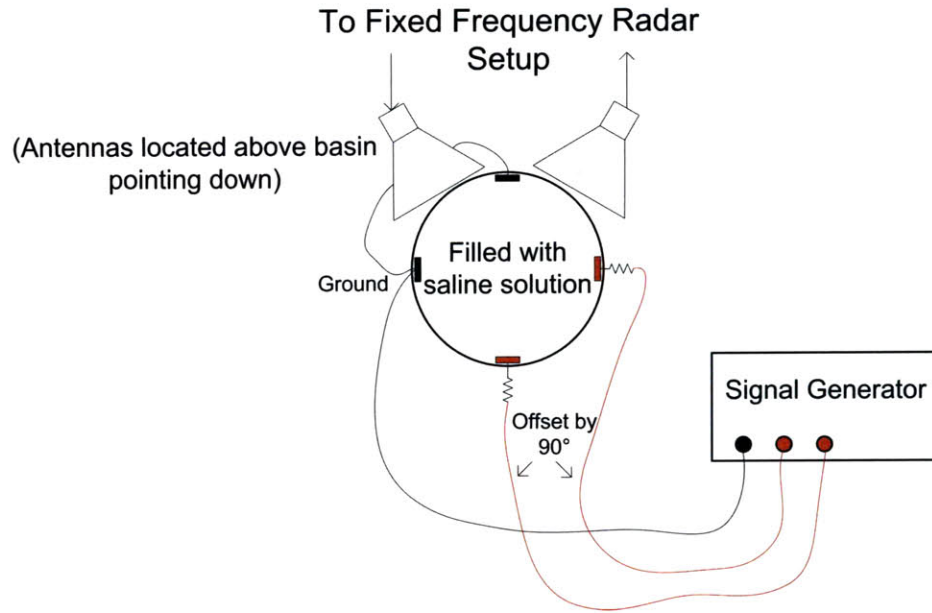


Figure 4-21: Physiological analog experiment

permutations of different drive frequencies, drive voltages, resistor values, and electrode configurations were setup and recorded with the radar for 4 seconds.

The radar amplitude was calculated by taking windows of the oscilloscope waveform and computing the RMS voltage of the windowed data. The resulting waveform was filtered with two, 1000 coefficient FIR filters. The first filter low pass filtered the data with a 60 Hz cutoff. The second filter high pass filtered the data with a 5 Hz cutoff. The raw, low passed, high and low passed, and FFT versions of the signal were examined for signs of the driving electrical signal. The results are discussed in section 5.2.1.

#### 4.4.2 Chest Accelerometer Experiment

The goal of this experiment was to measure the movement of the chest and determine how well those movements correlated with the radar amplitude. The accelerometer described in section 4.3.2 was mounted on the chest roughly three inches to the subject's left of the base of the sternum. This point appeared to have more movement caused by heartbeats than any other spot on the chest.

The subject was positioned roughly 0.5 meters directly in front of the transmit antenna with the receive antenna to the subject's left. The radar data was recorded for four seconds.

Both the radar and accelerometer data was windowed and the RMS voltage of each window calculated. These RMS values formed the radar and accelerometer waveforms.

Both waveforms were low pass filtered with a 60 Hz, 1000 coefficient FIR filter. This removed much of the unnecessary noise at higher frequencies. The radar often has large low frequency bumps in it caused by the heartbeat. These bumps clearly show the heart rate, but they also obscure the smaller amplitude, high frequency components in the radar. According to McGrath, it is these high frequency components that correspond to the QRS complex in the ECG signal. In order to compare the high frequency components in the radar with the QRS complex in the ECG, the waveforms were high pass filtered with a 5 Hz, 1000 coefficient FIR filter to remove the low frequency bumps in the radar and preserve the high frequency spikes. The accelerometer data is double integrated by performing two cumulative summations. This produces a signal with strong low frequency components, so in order to reveal the high frequency components corresponding to the heartbeat, both signals are high pass filtered with an 8th order, 1 Hz high pass Butterworth filter. This filtering is not strictly necessary for the ECG signal since it has already been high pass filtered at 5 Hz. However, both waveforms are processed with the same filters in order to apply the same group delay effects to the waveforms to facilitate accurate timing comparison.

The results of this experiment are discussed in section 5.2.1.

## 4.5 Subject Testing Protocol

The steps used to collect data from human subjects with the fixed-frequency radar system, ECG monitor, and accelerometer are specified in this section. A diagram illustrating the entire test setup is shown in Figure 4-22.

1. Set the signal generator to transmit 18 GHz at a power level of 0 dBm.
2. Set the spectrum analyzer with 18 GHz center frequency and 1 GHz frequency span. Find the peak of the received 18 GHz and center it in the display. Then decrease the frequency span to 10 MHz, find the 18 GHz peak, and center it. Decrease the frequency span to 1 MHz and repeat until the frequency span is at 100 Hz and the 18 GHz signal is centered. Then set the frequency span to 0 Hz and then set the RES filter to 300 Hz.
3. Disable the output of the signal generator.

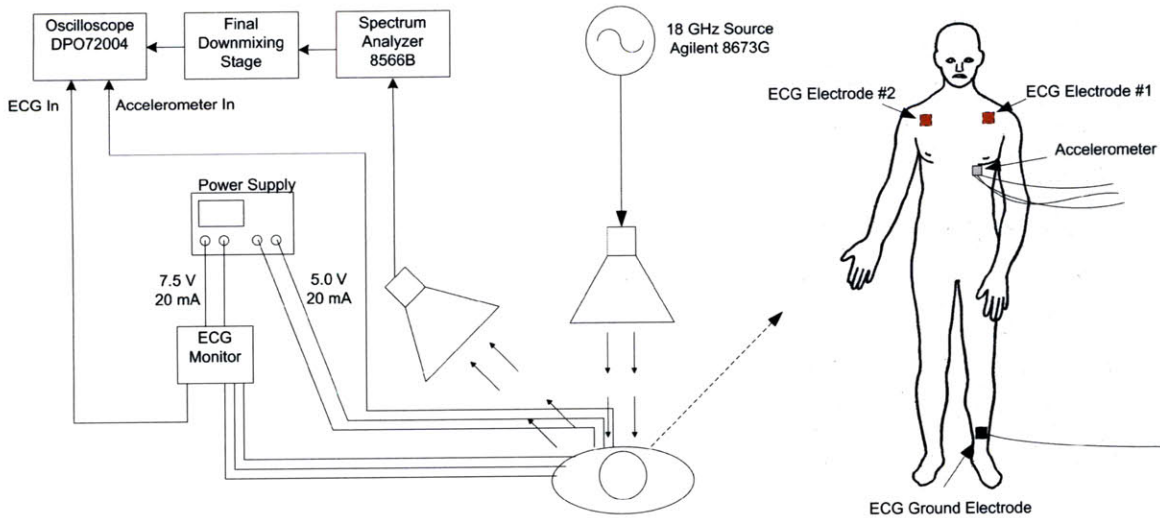


Figure 4-22: Test setup showing all connections between equipment [47]

4. Set the oscilloscope to record for 10 seconds with a sample rate of 25 Msamples/s. Set the ECG channel of the oscilloscope to have a 2 V/division step, the accelerometer channel to have a 1 V/division step, and the IF channel to have a 50 mV/division step.
5. Affix the differential ECG electrodes just below the subject's shoulders and the ground electrode on the left or right ankle. Use electrode gel and tape to secure if needed.
6. Affix the accelerometer 3 inches to the left of the base of the subject's sternum just below the left breast.
7. Seat the subject in a chair with back support no more than 0.5 meters away from antennas with the antennas 0.3 meters apart. Adjust the antennas to be at the same height as the subject's heart. Have the subject face the transmit antenna and position the chair such that receiving antenna is located to the subjects left at an angle of 30-45 degrees. Boresight both antennas to the center of the subject's chest.
8. Turn on the output of the signal generator.
9. Ask subject to breathe normally.
10. Take a 10 second, single data capture with oscilloscope.
11. Save waveforms from all three channels as Tektronix waveform files (.wfm).
12. Repeat steps 9-11.
13. Repeat steps 10-11 two times, but ask the subject to hold his breath during the 10 second recording.
14. Ask the subject to turn to his left and face the receive antenna.
15. Repeat steps 10-11 two times. The first time ask the subject to breathe normally, and the second time ask the subject to hold his breath during the 10 second recording.

16. Swap the transmit and receive coaxial cables at the antennas.
17. Repeat steps 10-11 two times. The first time ask the subject to breathe normally, and the second time ask the subject to hold his breath during the 10 second recording.
18. Ask the subject to turn to his right and face the receive antenna.
19. Repeat steps 10-11 two times. The first time ask the subject to breathe normally, and the second time ask the subject to hold his breath during the 10 second recording.
20. Swap the transmit and receive coaxial cables at the antennas, returning them to their original positions.
21. Ask the subject to roll the chair to the marked position 1 meter away.
22. Repeat steps 10-11 two times. The first time ask the subject to breathe normally, and the second time ask the subject to hold his breath during the 10 second recording.
23. Ask the subject to roll the chair to the marked position 3 meter away.
24. Repeat steps 10-11 two times. The first time ask the subject to breathe normally, and the second time ask the subject to hold his breath during the 10 second recording.

This protocol was used to test 8 male and 4 female subjects. The results are presented in section 5.2.2.

# Chapter 5

## Results

The results of the thesis research are organized into two sections. The first section describes the results obtained using the UWB radar system, while the second section describes the results from the fixed frequency radar. The bulk of the analysis is dedicated to the second section, since the fixed frequency radar became the focus of this thesis research. The analysis focuses on whether the radars are able to record heartbeat signatures, what the characteristics of these heartbeat signatures are, and what factors, both environmental and physiological, affect these results.

### 5.1 UWB Radar Results

The UWB radar system described in section 4.1 was tested on the author on multiple occasions. The author positioned himself 0.5 meters directly in front of the two antennas and held his breath for 10 seconds. The antennas were separated by roughly 0.3 meters, positioned at chest level, and pointed at the center of the chest.

The results of the UWB radar proved to be erratic and unreliable. The heartbeat signatures, if present at all, were frequently indistinguishable from the large amount of noise in the output.

Figure 5-1 shows the amplitude output of the UWB radar in one of the clearest of the results collected together with the output of the ECG monitor recorded simultaneously. The first 2 seconds contain movement artifacts caused by the subject and should be ignored. The

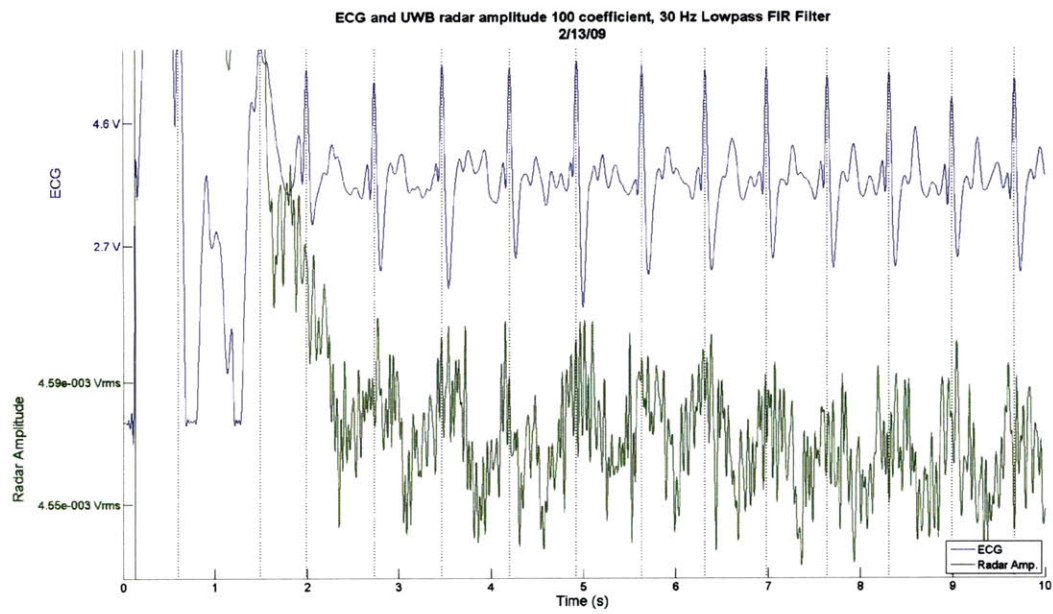


Figure 5-1: UWB radar amplitude with 30 Hz lowpass filter

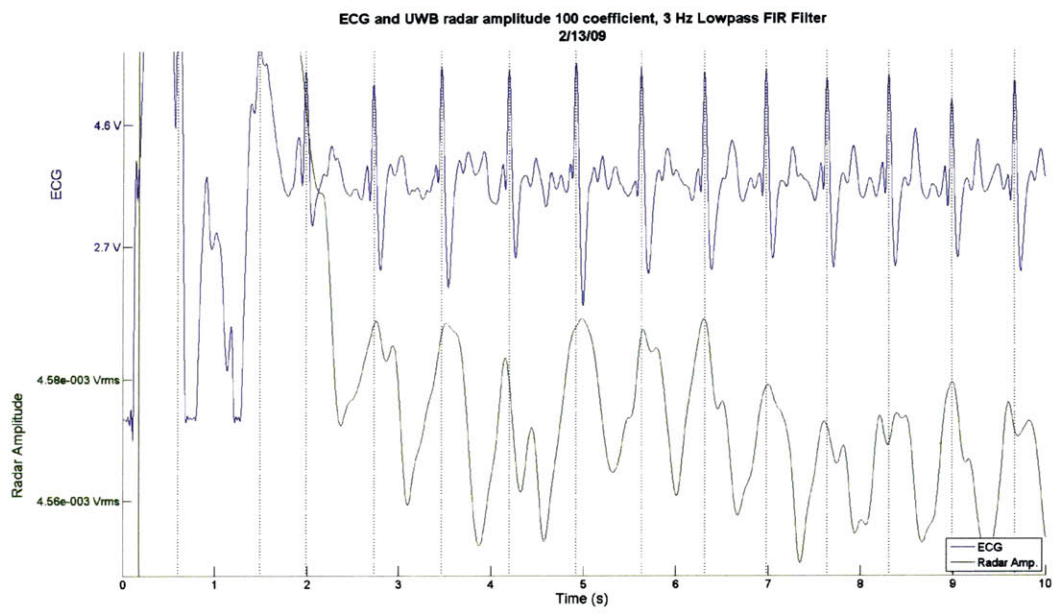


Figure 5-2: UWB radar amplitude with 3 Hz lowpass filter



radar output illustrated in Figure 5-1 is lowpass filtered by a 30 Hz, 1000 coefficient FIR filter. This filter removes some high frequency components, but the output is still quite noisy and it is difficult to distinguish the heartbeat signatures. The features temporally correlated with the ECG monitor output can be more clearly seen by low pass filtering the radar output with a cutoff of 3 Hz as shown in Figure 5-2.

While the UWB radar system was sometimes able to record heartbeat signatures as shown in Figures 5-1 and 5-2, the output is very noisy and requires strong low pass filtering to extract the heartbeat signatures. Often the noise overwhelms the heartbeat signatures, making them impossible to measure at all. Many different chest positions, antenna positions, and pulse parameters were adjusted, but the results were the same or worse. Time difference of arrival modulation was also analyzed, but as equation 3.15 suggested, the radar system was unable to distinguish the small changes in pulse arrival time caused by the moving chest.

In order to build a more reliable UWB radar, custom hardware would have to be designed. Even though the oscilloscope used in the radar is extremely fast, it is still not fast enough to detect changes in the pulse arrival times. Also, the oscilloscope has a fairly small number of effective bits: 5.4. This small number of bits prevents highly accurate captures of the pulse amplitude, which possibly contributes to the noisy results described above. Antenna ringing is another problem that can only be partially addressed by the signal processing steps described in section 4.1.3. Designing antennas specifically for transmitting UWB pulses may improve signal quality and produce better results.

Due to the unreliable nature of the UWB radar system, this thesis research focused on the fixed frequency radar system which showed much higher reliability and clearer heartbeat signatures.

## 5.2 Fixed Frequency Radar Results

There are two sets of results regarding the fixed frequency radar. The first section details the results of the experiments conducted to determine the source of the radar's modulation. The second section discusses the results of the human subject testing.

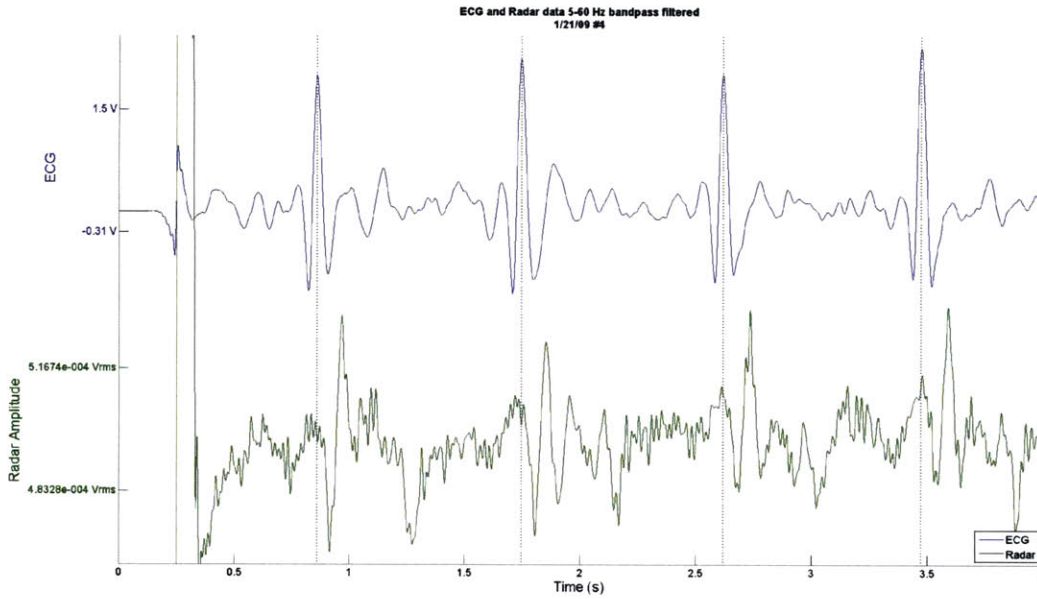


Figure 5-3: ECG and radar amplitude highpass filtered without delay

### 5.2.1 Movement vs. Impedance Results

As discussed in sections 2.2 and 2.3 of this thesis, there are two competing theories regarding the physiological source of amplitude modulation in fixed frequency radars. While most researchers agree that the radar amplitude is modulated by chest movement, Dr. William McGrath of Jet Propulsion Laboratory believes that the radar amplitude is also modulated by impedance changes in the chest caused by cardiac electrical activity. One goal of this thesis was to test this claim and attempt to replicate McGrath's results.

Figure 5-3 shows one result obtained during initial testing on the author using the settings and procedures described in Section 4.4.2. In order to compare the QRS complex in the ECG to the radar data, both waveforms were highpass filtered at 5 Hz to eliminate strong low-frequency components in the radar waveform that interfered with the comparison. This comparison revealed high frequency spikes following 100 milliseconds behind the QRS complex recorded by the ECG monitor. In other data sets, the high frequency components in the radar amplitude appeared consistently 90-130 milliseconds behind the QRS complex from the ECG monitor.

By delaying the ECG data so that the spikes in the ECG and radar signals occurred at the same time, the two signals showed noticeable correlation, as shown in Figure 5-4. The

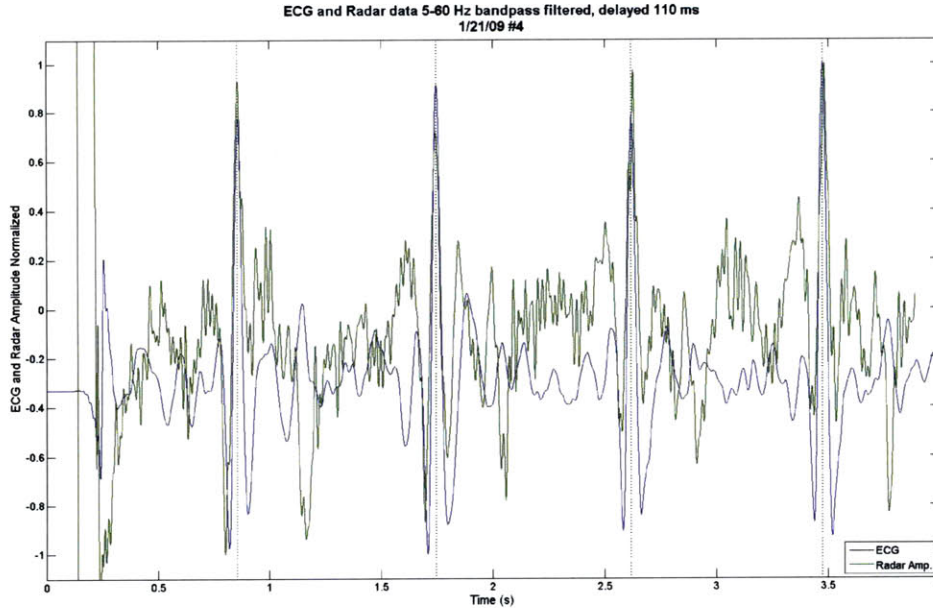


Figure 5-4: ECG and radar amplitude highpass filtered, delayed 110 ms, and overlaid; correlation = 0.46

correlation coefficient was calculated to be 0.46 for the data recorded from 0.37 seconds to 4.0 seconds. (The data prior to 0.37 seconds was corrupted by filtering artifacts.) The ECG signal has corresponding components in the radar signal around the QRS complex as well as an inverted component around the T wave. These correlations provided preliminary evidence that the radar might be recording cardiac electrical activity, as McGrath asserted.

However, there were two unexplained problems with this initial data. The first was the 90-130 millisecond delay between the spikes in the signals, which is far longer than that which could be explained by the time required for any kind of physiological electrical propagation. The second problem was that, while there was significant correlation between the ECG and radar signals, there were also significant differences. The radar signal often contained large low frequency components not present in the ECG signal. There were also timing differences between the peaks and valleys around the QRS complex and its corresponding components in the radar signal. Given these differences, additional experiments were conducted to confirm McGrath's assertion.

The first experiment used the radar to try to record electrical currents injected into a solution with the same salinity as the human body. If the radar was able to record this circulating current in the physiological analog, then it would be a positive sign that

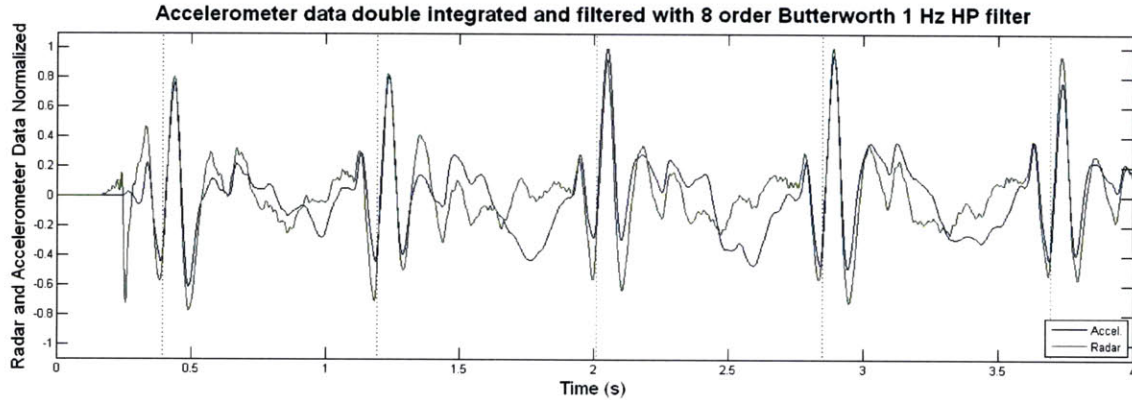


Figure 5-5: Comparison of accelerometer data and radar amplitude; correlation = 0.80

recording electrical currents from the heart was also possible. The exact testing setup is described in detail in section 4.4.1. Many different drive frequencies, resistances, and electrode configurations were tried, but no sign of the electrical currents were recorded. This negative result is not conclusive, since the physiological analog used is extremely simplified, but it does cast doubt on McGrath's assertion.

As mentioned earlier, the competing theory to McGrath's claim is that the radar amplitude is modulated by chest movement. This theory was tested in the second experiment by mounting an accelerometer on the chest of the author and comparing the output with the radar amplitude. The radar amplitude is modulated by the radar cross section of the target, and this is determined by the position of the chest. Since the output of the radar is determined by chest position, not acceleration, the output of the accelerometer was double integrated and filtered to yield position in order to produce a valid comparison with the radar.

The result of this experiment showed very clear correlation between the radar's amplitude and the accelerometer data, as shown in Figure 5-5. No delay was necessary to synchronize the waveforms as was necessary in the case of the ECG monitor, and the correlation between the radar and accelerometer data was roughly 0.80 - substantially higher than the correlation of 0.46 between the ECG and radar waveforms.

The ECG monitor measures electrical cardiac activity and the accelerometer measures mechanical cardiac activity, but most importantly, they are both measuring cardiac activity. It is therefore not surprising that both the ECG and the accelerometer waveforms had substantial correlations with the heartbeat signatures in the radar data. However, the much

higher degree of correlation between the radar waveform and the accelerometer waveform indicates that the radar senses the heartbeat not through impedance changes, but through chest motion.

### 5.2.2 Human Subject Testing Results

The fixed frequency radar was tested on a group of 12 human subjects according to the protocol described in section 4.5. There were three effects studied during human subject testing. The first was the effect of breathing on the ability of the radar to sense heartbeats. Since the radar depends on chest movement to record heartbeats, the large chest movements caused by breathing could seriously impact the radar’s ability to record heartbeats. The second was the effect of the orientation of the subject’s chest relative to the radar. The heartbeat does not cause the chest wall to move symmetrically, so the orientation of the chest could significantly affect the results. The final effect studied was the distance between the subject and the radar. The farther away the subject is from the radar, the weaker the returning signal will be, making it harder to measure the heartbeat. The effect of other variables such as the subject’s build and gender will also be discussed.

<b>Data Set #</b>	<b>Breathing</b>	<b>Transmitter Orientation</b>	<b>Receiver Orientation</b>	<b>Distance</b>
1	Yes	Center	Left (30°-50°)	< 0.5 m
2	Yes	Center	Left (30°-50°)	< 0.5 m
3	No	Center	Left (30°-50°)	< 0.5 m
4	No	Center	Left (30°-50°)	< 0.5 m
5	Yes	Right (30°-50°)	Center	< 0.5 m
6	No	Right (30°-50°)	Center	< 0.5 m
7	Yes	Center	Right (30°-50°)	< 0.5 m
8	No	Center	Right (30°-50°)	< 0.5 m
9	Yes	Left (30°-50°)	Center	< 0.5 m
10	No	Left (30°-50°)	Center	< 0.5 m
11	Yes	Center	Left (15°-30°)	1 m
12	No	Center	Left (15°-30°)	1 m
13	Yes	Center	Left (5°-15°)	3 m
14	No	Center	Left (5°-15°)	3 m

Table 5.1: Variables for each data set

Fourteen data sets were collected with each human subject, and three variables were adjusted during the data collection: breathing, orientation, and distance. A list of the different permutations tested for each subject is given in Table 5.1. The transmitter and



receiver orientations define where the antennas were placed relative to the subject. For example, in data set #1, the subject is directly facing the transmitter antenna while the receive antenna is located to the subject's left roughly 40°. The exact placement of the equipment is described in section 4.5. Conditions for data sets 1-2 and 3-4 are identical in order to test the degree of repeatability within the same subject.

The remainder of this section is divided into two parts. The first focuses on the ability of the radar to record heartbeats and the effect of the variables studied. The second part discusses the characteristics of the heartbeat signatures and the variables that affect those characteristics.

### **Heartbeat Detection Results**

For each data set collected, the amplitude and phase outputs of the radar were analyzed and compared to the ECG and accelerometer data to determine if either radar output contained signatures corresponding to the heartbeat, as measured by the ECG monitor and accelerometer. Each data set was classified into one of three categories. Category 1 data sets have clear heartbeat signatures in one or both of the radar outputs. Category 2 data sets have heartbeat signatures that are noisy or sporadic but still detectable by a human observer (the author). Category 3 data sets contain no heartbeat signatures or signatures that are unusable due to high noise and inconsistency.

An example data set from each category is given in Figures 5-6, 5-7, and 5-8. The category 1 example has clear heartbeat signatures in both radar channels; however, many category 1 data sets have clear signatures in only one channel. This can be seen in the category 2 example, where the amplitude radar channel shows some heartbeat signatures, while the phase channel does not. However, the heartbeat signatures in the amplitude channel in figure 5-7 are inconsistent after the first four seconds, which is why the data set has been given a category 2 classification. The category 3 example lacks repeatable heartbeat signatures.

An overview of the results from human subject testing is shown in Table 5.2. Every data set collected from each of the 12 test subjects is classified into one of the three categories described above and displayed with color coding. The radar channel that clearly shows the heartbeat signatures in each data set is indicated as either the amplitude (Amp), phase, or

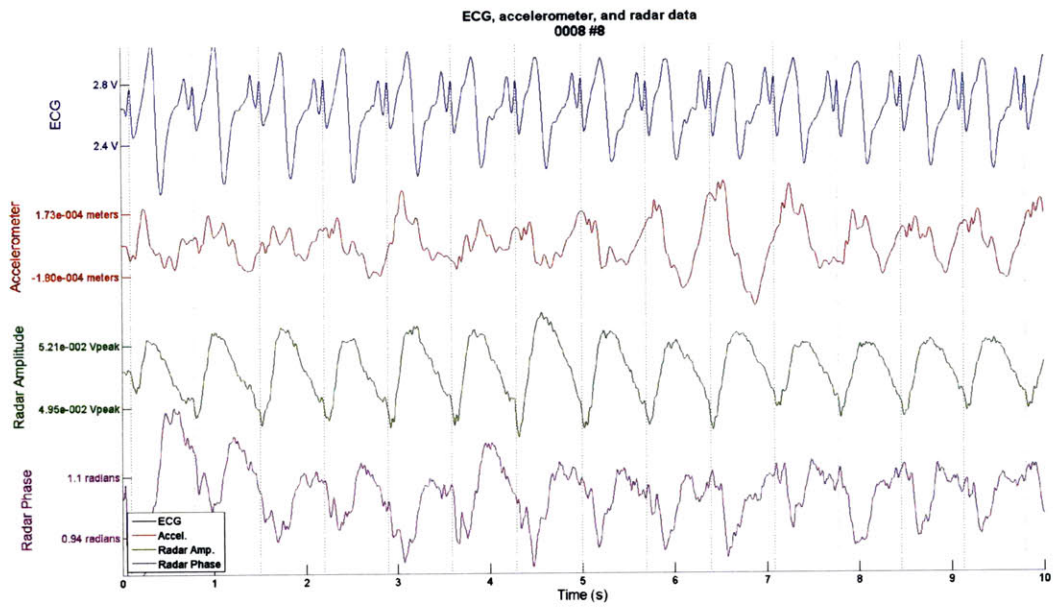


Figure 5-6: Example of category 1 data set

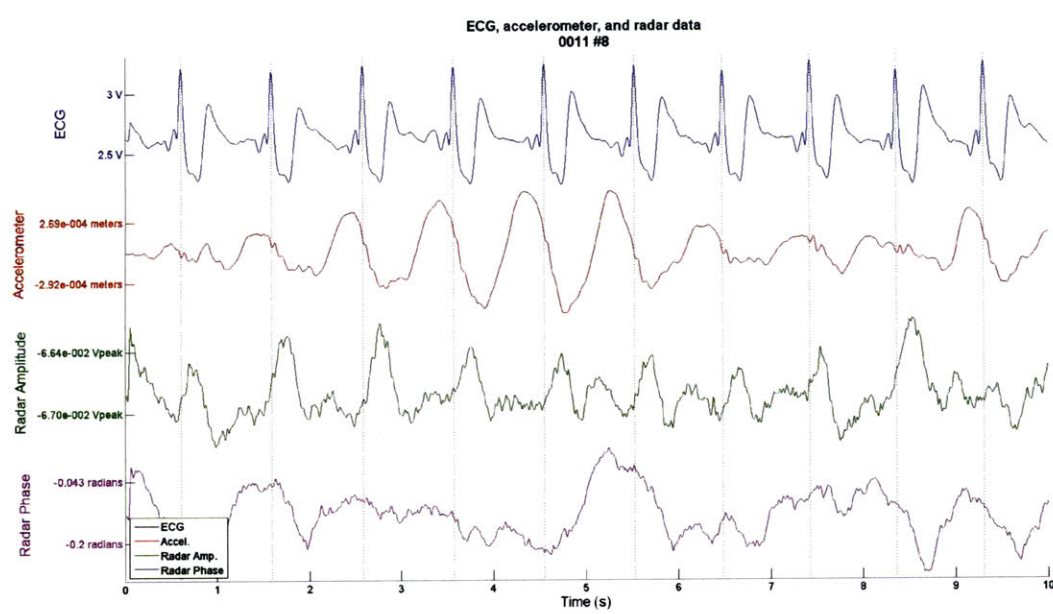


Figure 5-7: Example of category 2 data set

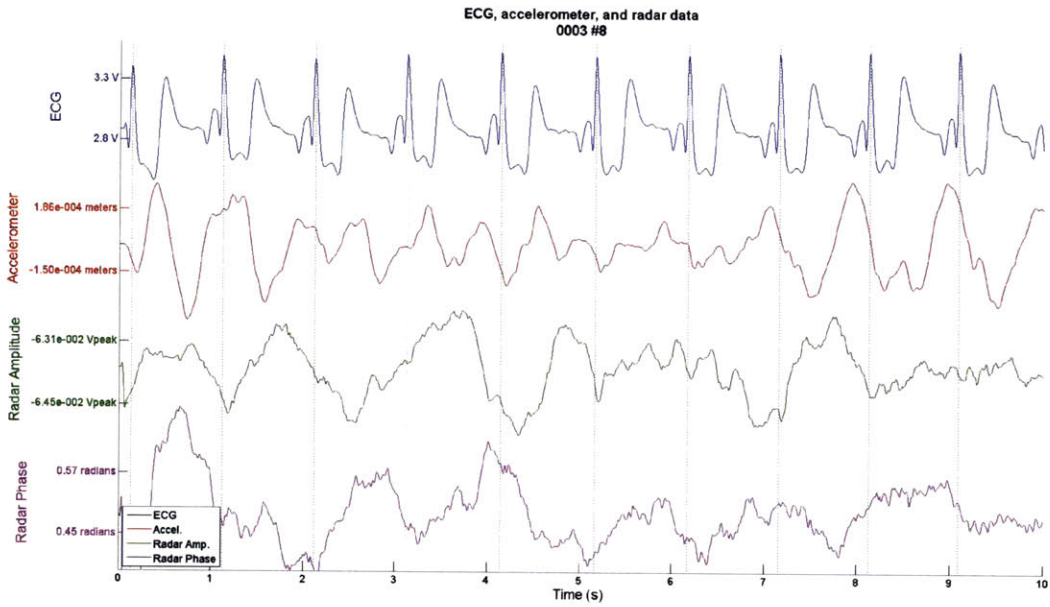


Figure 5-8: Example of category 3 data set

both. The table also notes the gender and approximate build of each human subject. The build is based on the relative chest size of each test subject and is an approximate measure determined by visual inspection.

When testing the subjects at the 1 and 3 meter distances (data sets #11-14), it was discovered that background movement in the room could disturb the results even when the source was several meters away. Sometimes this background movement is strong enough to cause ringing in the amplitude and phase channels or enough noise to completely obscure the heartbeat signatures. When such background corruption is evident in the radar signal, the corresponding data is marked by an 'x' in the table. For subject 0006, data sets 11-14 accidentally had the antennas swapped so that the receive antenna was in the center and the transmit antenna was to the subject's left. Those data sets have been marked with a star, even though swapping the antennas should not have a substantial effect on the results.



Subject Number	0003	0004	0005	0006	0007	0008	0009	0010	0011	0012	0013	0014
Gender	F	M	M	F	M	F	M	M	M	M	F	M
Build	Med	Med	Heavy	Lean	Med	Lean	Med	Heavy	Lean	Lean	Med	Heavy
Data Set												
1		2 - Phase				2 - Both	2 - Phase	2 - Phase				
2		2 - Both				2 - Both	1 - Both					
3		2 - Amp		1 - Both	1 - Both	1 - Both	1 - Both	2 - Both	1 - Amp	1 - Both		2 - Amp
4	1 - Both	1 - Phase		1 - Both	2 - Both	1 - Both	1 - Both	2 - Amp	1 - Amp	1 - Both	2 - Both	1 - Amp
5		2 - Phase				2 - Both						
6	2 - Amp	1 - Phase		1 - Phase	2 - Amp	1 - Both	1 - Amp			1 - Both		
7		1 - Both				2 - Both						
8		1 - Phase		1 - Amp	2 - Amp	1 - Both	1 - Amp		2 - Amp	2 - Both		
9						1 - Both						
10	2 - Phase	1 - Phase	2 - Both	1 - Both	1 - Both	1 - Both			2 - Amp	1 - Both	2 - Both	2 - Both
11												
12	1 - Both	<del>2 - Amp</del>		*			2 - Amp		1 - Phase			
13				*								
14				*	1 - Amp					2 - Amp		

Category 1  
 Category 2  
 Category 3  
 Corrupted by environment  
 \* Receive antenna center, transmit antenna left

Table 5.2: Data set category matrix. Also shows which radar channel showed heartbeat signatures

The first of the three variables tested was the effect of breathing. In order to isolate heartbeats in data collected while breathing, the filter values were modified. Instead of high pass filtering the radar amplitude and phase at 0.5 Hz, the cutoff was increased to 2 Hz. This is necessary to eliminate the stronger low frequency components caused by breathing that are not present in non-breathing data sets. There is no cutoff frequency that is perfect for all data sets, but 2 Hz seemed to give the most improvement and was used to produce the results shown in Table 5.2 for data sets #1, 2, 5, 7, 9, 11 and 13.

Figure 5-9 shows an example of data collected while the subject was breathing. For this example, the order of the high pass filter used on the accelerometer data was changed from 8 to 2 in order to allow most of the low frequency components from the breathing to pass through. The radar channels have their high pass filters removed altogether in order to show how the radar channels track with the breathing. Both the amplitude and phase channels vary slowly with the breathing as measured by the accelerometer.

Figure 5-10 shows the result of high pass filtering the radar channels with a 2nd order, 2 Hz high pass Butterworth filter. The accelerometer high pass filter order is increased from 2 to 8. While not as clear as some data sets, the phase channel, and especially the amplitude channel, have repeating structures that correspond to the heartbeat.

While it is sometimes possible to reliably isolate heartbeat signatures while the subject is breathing, the large amounts of chest motion that breathing causes can drown out the motion from the heartbeat. This effect is evident in the results. Even with the modification to the highpass filter cutoff, the vast majority (72 out of 84) of data sets for conditions with breathing (#1, 2, 5, 7, 9, 11, 13) were classified as category 3.

The second of the three variables tested was the effect of the orientation of the chest. These conditions addressed two questions: which side of the chest was the best for sensing heartbeats, and whether swapping the transmit and receive antennae would affect the results.

Data sets 1-4 and 9-10 had one antenna facing the left side of the subject with the other facing the center, while data sets 5-8 had one antenna facing the right side of the subject with the other facing center. It is important to compare the data sets with breathing (#1,2,5,7,9) only to other data sets with breathing and likewise for data sets without breathing (#3,4,6,8,10). Non-breathing data sets with an antenna on the left (#3,4, 10)

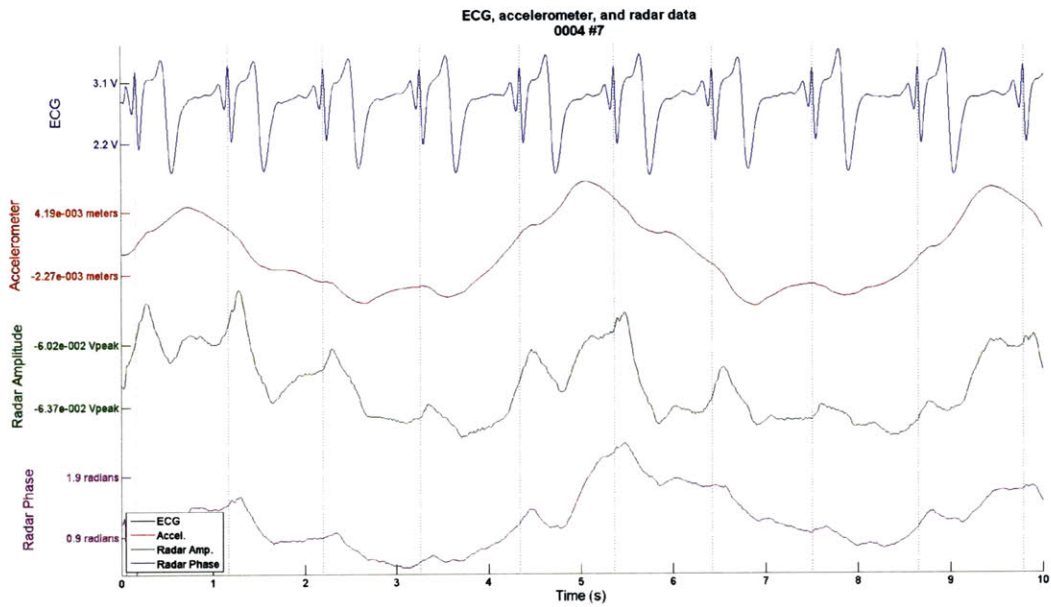


Figure 5-9: Breathing as recorded by radar; no high pass filtering on radar and 2nd order, 1 Hz highpass Butterworth filter on accelerometer

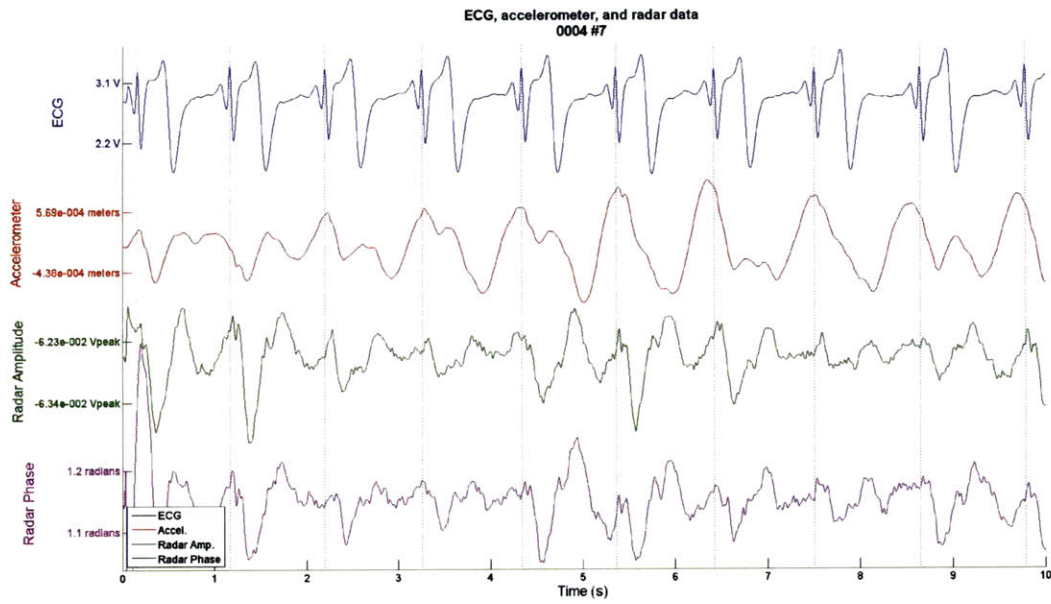


Figure 5-10: Breathing filtered out to reveal heartbeat signatures

produced reliable heartbeat signatures 30 out of 36 times while non-breathing data sets with an antenna on the right (#6, 8) did so 14 out of 24 times. Breathing data sets with an antenna on the left (#1, 2, 9) provided reliable heartbeat signatures 8 out of 36 times, and breathing data sets with an antenna on the right (#5, 7) did so 4 out of 24 times. Left side antenna data sets had higher yields of 83% and 22% for non-breathing and breathing conditions respectively compared with the right side yields of 58% and 17%. However, data set 9, a left side antenna data set with breathing, recorded fewer heartbeats than either of the other right sided antenna data sets with breathing. This indicates that the data has substantial variation, so even though data sets with an antenna on the left side had better results on average, more investigation with larger data sets should be conducted to determine the optimal antenna orientations.

Data sets 6 vs. 8 and 3-4 vs. 10 are compared to determine the effect of swapping the receive and transmit antennas. Data sets 6 and 8 both have yields of 58% (both 7/12), and data sets 3-4 and 10 both have yields of 83% (20/24 and 10/12 respectively). The rate at which heartbeats are successfully recorded stays the same between these data sets, which suggests that swapping which antenna receives and which transmits does not have a significant impact on the results.

The third variable that was tested was the effect of distance on the results. Table 5.2 shows that, as the distance between the subject and the antenna increases, the ability to record the heartbeat in non-breathing data sets drops from 44 out of 60 at 0.5 m (data sets #3,4,6,8, 10) to 6 out of 24 at 1.0 or 3.0 m (data sets #12, 14). This reduced performance is not surprising since the longer distance increases the path loss, thereby decreasing the amplitude of the returning signal. The farther the subject is from the antenna, the less focused the incident radar signal. This prevents the radar from focusing on the region of interest on the chest and makes the heartbeat signatures more difficult to distinguish. The increased distance also increases the ability of background movements to corrupt the results, with 9 out of the 48 data sets at the farther distances in Table 5.2 (data sets 11-14) corrupted by background movement. The data shows that with increased distance the radar's ability to record heartbeats diminishes.

It appears that the build of the subject may also impact the ability of the radar to record heartbeats. In general, data from subjects with lean and medium builds was more

likely to be classified as Type 1 or Type 2. The heavier the build of the subject, the more tissue there is between the heart and the outside world. It is possible that the chest motions caused by the heartbeat are more attenuated by this extra tissue, making the heartbeats harder to detect.

Human subject testing showed that the fixed frequency radar system is able to record heartbeats under a variety of conditions, but in order to be more robust to distance, orientation, and especially breathing, further improvements are needed. Possible future enhancements to the hardware and the signal processing will be discussed in chapter 6.

### **Characteristics of Heartbeat Signatures**

The previous section discussed the ability of the radar system to record heartbeat signatures. However, these heartbeat signatures can vary widely between subjects and even vary within the same subject. A number of examples are given in the figures below.

Looking closely at the amplitude channel of the radar results, we can see that the appearance of the heartbeat signatures varies significantly. Subjects 0003 and 0006 have slowly varying bumps in one or both radar channels that coincide with the ECG. Subject 0012 has high frequency, downward spikes following each QRS complex, while subject 0014 has downward spikes superimposed on low frequency bumps. There is even a good deal of variability between subjects in their ECG and accelerometer waveforms, but this is expected since the position of the electrodes and accelerometer varies from subject to subject. Subject 0014 also demonstrates that one channel of the radar may clearly see heartbeat signatures while the other channel sees nothing at all.

The phase output of the radar most often records heartbeat signatures as low frequency bumps as seen in the examples below. If looked at closely, sometimes high-frequency components can be seen soon after the QRS complex in the ECG such as in subject 0012. The amplitude output of the radar seems to be more variable than the phase. Sometimes high-frequency spikes can be seen, usually occurring roughly 100 ms after the QRS complex. These are probably due to sudden heart movements caused by the contracting ventricles. This causes corresponding sudden movements at the chest wall, but presumably there is a 100 ms delay from electrical stimulus to mechanical contraction and chest wall movement.

There does not seem to be any correlation between transmitter/receiver orientation and

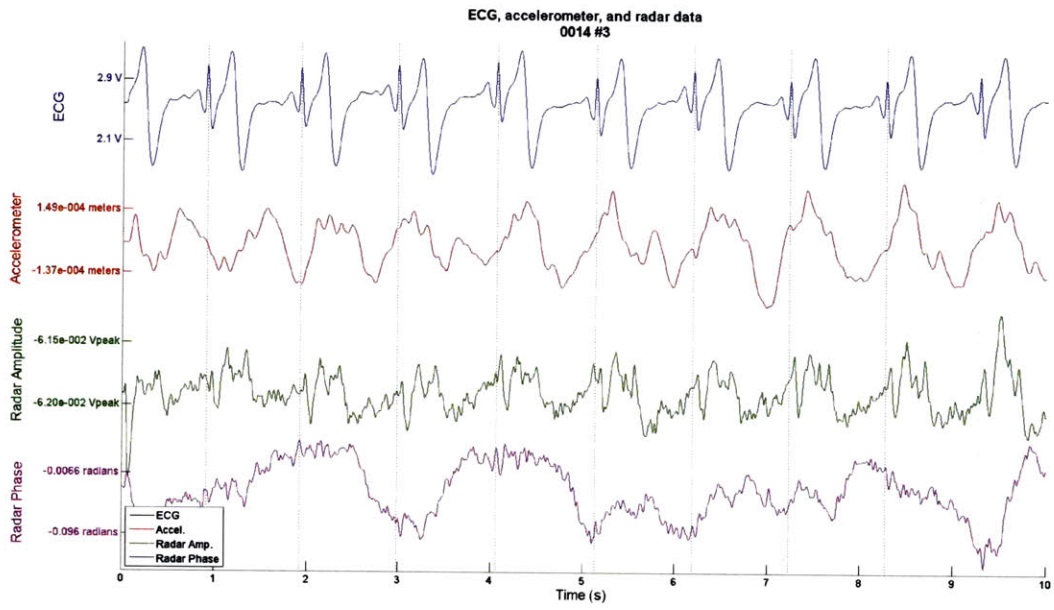


Figure 5-11: Subject 0014, data set #3

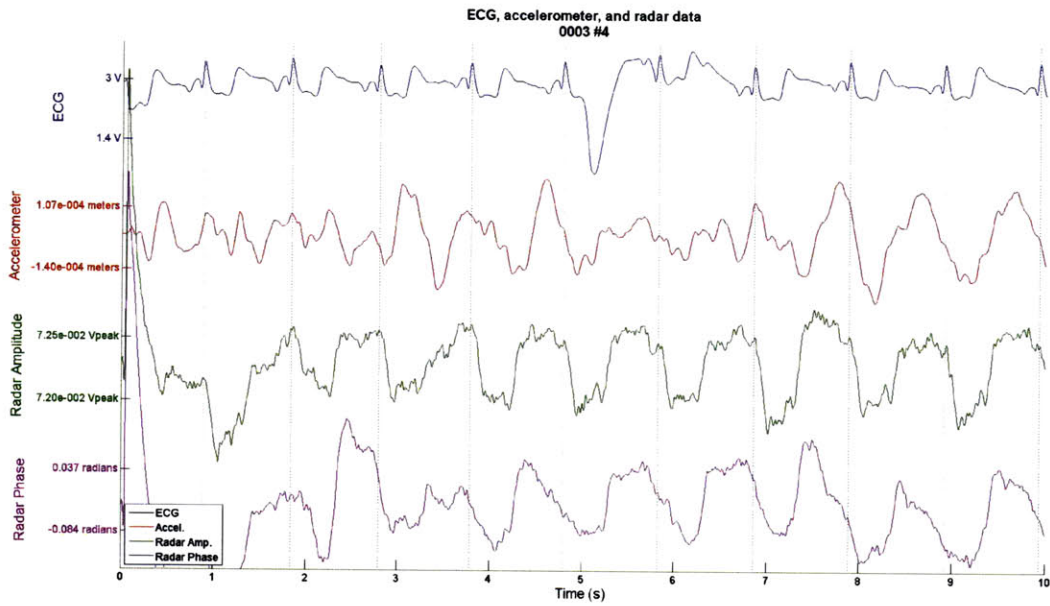


Figure 5-12: Subject 0003, data set #4



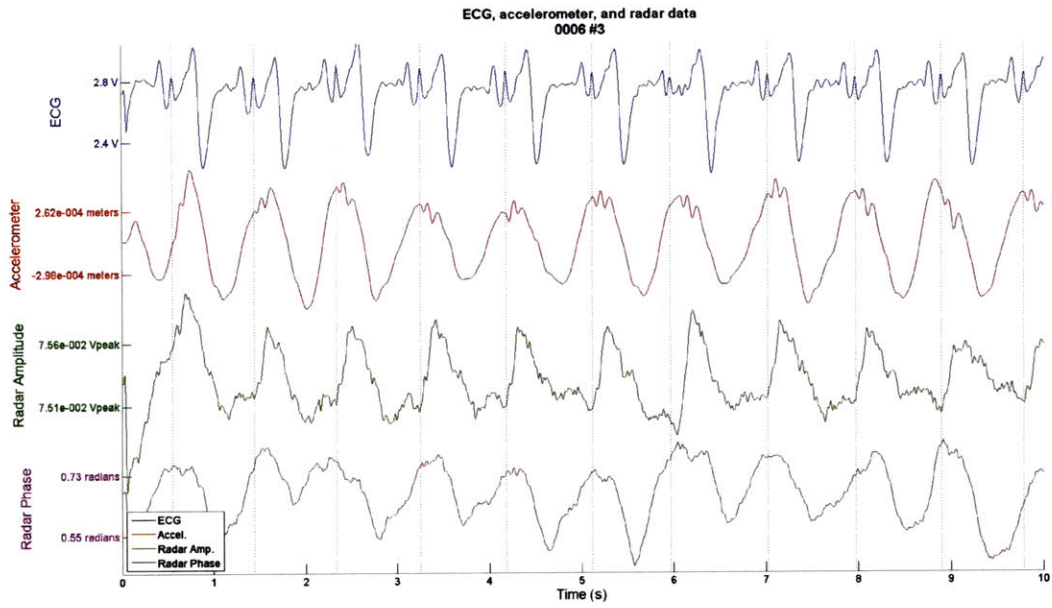


Figure 5-13: Subject 0006, data set #3

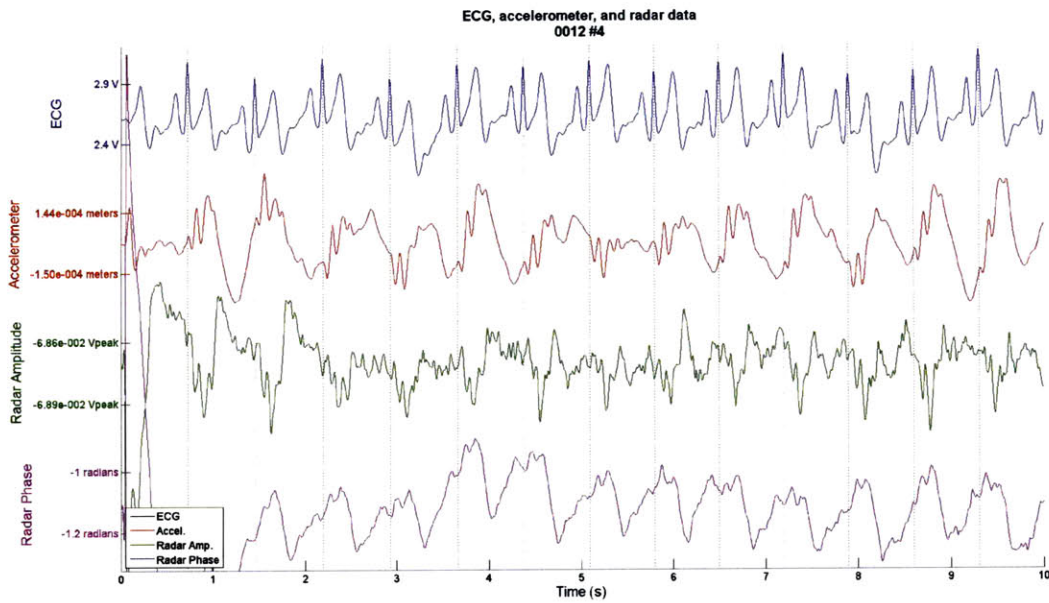


Figure 5-14: Subject 0012, data set #4

the types of heartbeat signatures seen. Breathing does appear to have some effect however. It appears that as the subject fills his or her lungs with air, the heartbeat signatures became more pronounced. This can be seen in Figures 5-9 and 5-10 from 0-2 seconds and from 4-6 seconds.

As the distance between the antennas and the subject increases, the amplitude of the signatures decreases. Figures 5-15 and 5-16 illustrate this decrease in amplitude as the distance to subject 0007 increases from 0.5 meters to 3 meters. The range in amplitude at a distance of 0.5 meters is 14.6 mV, while the range at 3 meters decreases to 0.08 mV. In order to overcome this significant drop in amplitude, antennas with a greater gain and narrower beamwidth would be necessary to focus the microwaves.

It is important to note that useful information is obtained from both the amplitude and phase channels of the radar. Often heartbeat signatures appear in one channel but not the other. Other times, the heartbeat signature will appear in one channel, but then attenuate and become clearer in the other channel.

It is hypothesized that the heartbeat signatures can sometimes appear in only one channel because while the two channels are related, they have importance differences. It is possible that some chest wall movements do not affect the radar cross section, and therefore are recorded as a phase change but not as an amplitude change. On the other hand, a chest movement could cause different motions in opposite directions that would cancel out the phase changes measured by the radar, but at the same time produce a significant change in the radar cross section, making the chest movement observable by the radar amplitude but not the radar phase.

While the data collected is highly variable and the appearances of the heartbeat signatures vary, by monitoring both the radar's amplitude and phase channels it is often possible to observe repeating changes that correspond to the heartbeat.

The system studied here successfully recorded cardiac activity for a variety of orientations with a varied group of human subjects. In the next chapter this thesis concludes with a summary of the results and a discussion of potential improvements and future work.



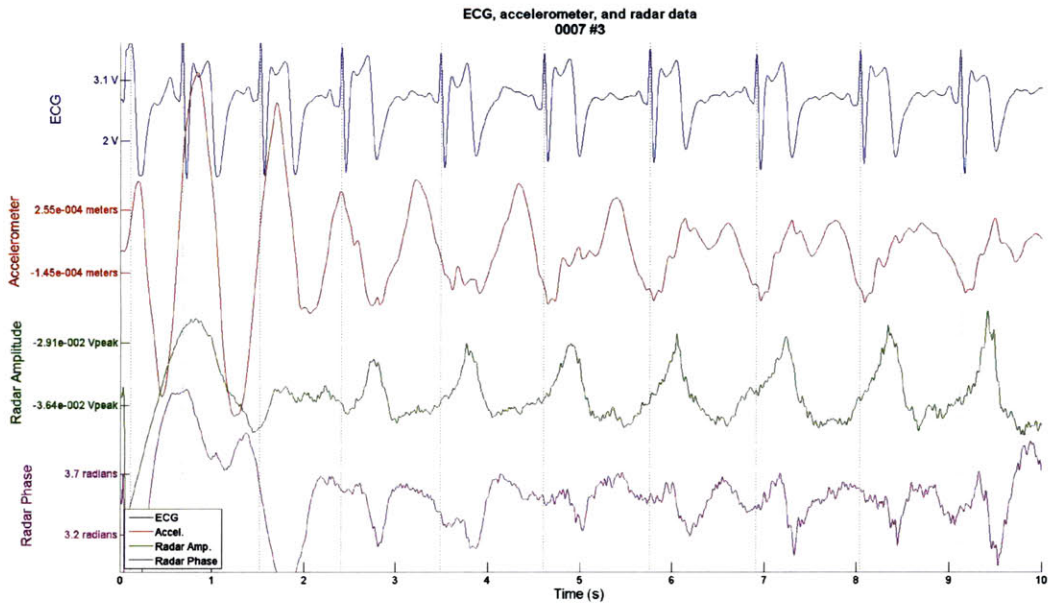


Figure 5-15: Heartbeat signatures from 0.5 meters; 14.6 mV range in amplitude

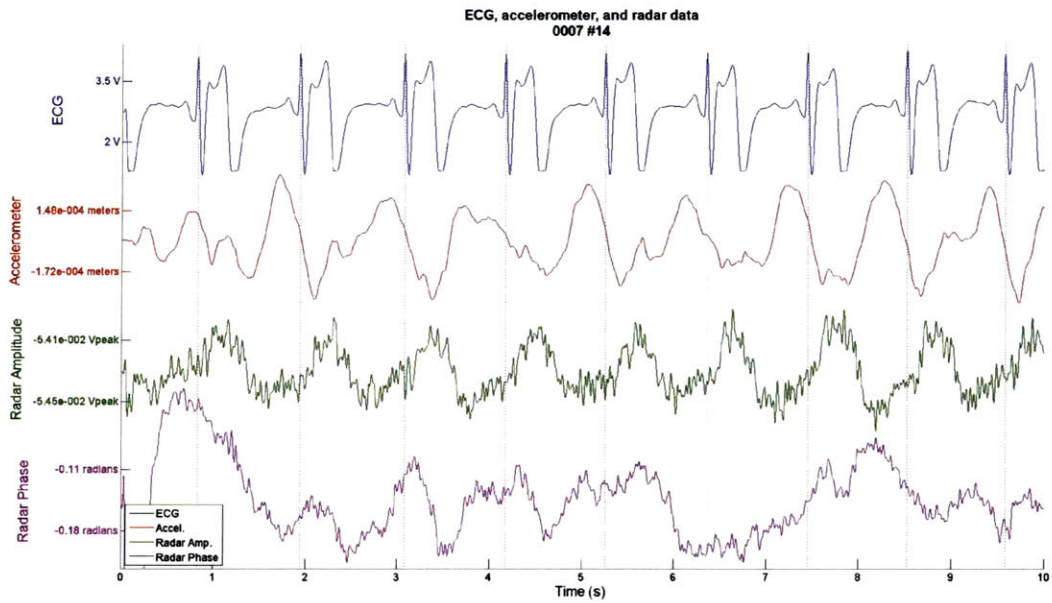


Figure 5-16: Heartbeat signatures from 3 meters; 0.08 mV range in amplitude



# Chapter 6

## Conclusions

This chapter summarizes the results of the thesis research. It also discusses the limitations of the current system and concludes with possible improvements to the system and potential future research.

### 6.1 Summary of Results

This thesis research had three original goals. The first was to determine the ability of an amplitude modulated radar system, as opposed to a Doppler modulated radar system, to sense cardiac activity remotely. The second goal was to compare the effectiveness of UWB and fixed frequency radar systems for sensing cardiac activity. Finally, the thesis tried to verify William McGrath's claim that fixed-frequency, amplitude modulated radar was capable of remotely detecting cardiac electrical activity, such as that detected by an ECG.

The thesis determined that an amplitude modulated radar system can record cardiac activity. A system was constructed that was able to simultaneously measure the amplitude and phase of the returning radar signal. The system was tested on a group of 12 human subjects and successfully obtained heartbeat signatures for every test subject under some of the conditions tested. The most successful test conditions were when the subject was not breathing, less than 0.5 meters away, and had one of the antennas on the left side. It was also found that both the amplitude and phase channels should be monitored since sometimes heartbeat signatures appear in only one of the channels. The ability of the amplitude modulated radar to record heartbeats was highly variable, however. Performance is affected

by many parameters such as the distance to the subject, movement and orientation of the subject, and the subject's build. Also, the heartbeat signatures in the radar results were identified by a human observer with the aid of ECG and accelerometer data as the "true" measure of cardiac activity. For many data sets, it would have been hard to identify heartbeat signatures without this "true" standard. Despite these limitations, this thesis showed that an amplitude radar system can successfully be used to record cardiac activity without direct physical contact.

A UWB radar was also constructed and tested on the author. It was found to be very noisy and unreliable. While it was at times able to record heartbeats, the output was too noisy and required such severe filtering in order to be usable that it eliminated large amounts of useful spectrum. Given the unreliable nature of the system and the poor results compared to the fixed-frequency system, it was decided to focus on the fixed frequency radar for the majority of this thesis project.

Finally, the thesis tested McGrath's claim of remote monitoring of cardiac electrical activity. Initial results seemed promising, since by delaying the ECG waveform 100 ms, the high pass filtered ECG and radar amplitude showed reasonable correlation. However, an experiment was conducted using an accelerometer mounted on the chest. Comparing the double integrated accelerometer signal with the radar amplitude showed nearly perfect correlation with no time delay. This seems to conclusively point to chest movement, rather than impedance changes from electrical activity, to be the true source of amplitude modulation in the radar data.

The fixed frequency radar system has a variety of possible applications. One is monitoring the vital signs of burn victims in hospitals. Since burn victims don't have healthy skin to attach ECG electrodes to, a radar based system would prove useful. Battlefield medics could also use a hand held version of the radar to tell if casualties on the battlefield are dead or alive before exposing themselves to harm while giving aid. Other potential applications of these kinds of radar systems are given in chapter 1.

While the fixed frequency radar system did successfully record heartbeat signatures from a variety of subjects, it does have some significant limitations. Most importantly, it is very sensitive to movement. Breathing alone can corrupt the data, and larger body movements completely overwhelm the tiny signals from the heartbeat. The system quickly loses its

ability to record heartbeats as the distance between the subject and antennas increases. The radar also relies on post-processing in Matlab in order to process and filter the results. A real-time system would require considerable processing power. Finally, the radar results vary substantially. While it is usually possible for a human observer to identify heartbeat signatures under ideal conditions, the appearance of the signatures themselves can change significantly, preventing their use for diagnostic purposes and hindering the development of algorithms to extract heartbeat signatures automatically.

## 6.2 Possible Improvements and Further Research

A number of improvements could be made to the amplitude radar system in order to solve some of its current limitations. The first is to reduce the variability of the radar system performance so that it more reliably records heartbeats at close distances. A simple step would be to use higher gain antennas to focus the radar signal into a tighter beam. The more focused microwaves would reduce the variability of the chest position and movement recorded by the radar. It would also increase the usable range of the radar. Reliability could also be improved if there was a better understanding of how the shape and movement of the chest wall affects the radar channels. Research investigating this problem and modeling the radar cross section of the chest would be very useful.

Another important area of research is finding ways to mitigate non-cardiac body movements in order to record heartbeats from subjects that are not completely motionless. Some groups have already made promising progress in this arena using multiple transmitters and receivers [48], but there is still much work left to do.

The UWB radar system constructed in this project proved to be unreliable and did not give good results. However, there were a few data records that showed clear heartbeat signatures, suggesting that future UWB radar research might be warranted. However, a different hardware system should be used that can more accurately measure both the amplitude of the returning pulse and its arrival time. Antennas designed specifically for UWB purposes could also yield significant improvements by reducing antenna ringing. Finally, more advanced signal processing, such as wavelet based approaches, could give more accurate and noise free results.

Using radar to remotely sense heartbeats is a very exciting area of research that has real potential to significantly change many aspects of health care and other industries. It will be interesting to observe future developments in this field.

# Appendix A

## Code Listing

```

1  %%%%%%%%%%%%%%%%%%%%%%%%%%%%%%%%%%%%%%%%%%%%%%%%%%%%%%%%%%%%%%%%%%%%%%%%%
2  % UWB_analysis.m
3  %%%%%%%%%%%%%%%%%%%%%%%%%%%%%%%%%%%%%%%%%%%%%%%%%%%%%%%%%%%%%%%%%%%%%%%%%
4  %% Get data
5  clear all; clc;
6
7  date = '2/13/09';
8
9  % Specify files to load ECG, radar, and empty room waveforms from
10 [temp, data_ecg, temp2] = wfm_ascii_dpo_FF('UWB Data\Jon_2_13_09_3_ECG.wfm');
11 [temp, data_rdr, temp2] = wfm_ascii_dpo_FF('UWB Data\Jon_2_13_09_3_RDR.wfm');
12 [temp, data_room, temp2] = wfm_ascii_dpo_FF('UWB Data\Room_2_13_09_1.wfm');
13
14 % Get size of waveforms
15 [num_frames, frame_length] = size(data_ecg);
16
17 % Number of waveforms to average together
18 num_avg = 10;
19
20 % Size of font
21 fsize = 17;
22
23 % Initialize variables
24 ecg = zeros([num_frames/num_avg 1]);
25 amp = zeros([num_frames/num_avg 1]);
26 toa = zeros([num_frames/num_avg 1]);
27
28 % Average all pulse returns from empty room
29 room_avg = mean(data_room);
30
31
32 %% Process data
33 for i=1:num_frames
34
35     % If averaging multiple waveforms for amp, only form a new data point
36     % every num_avg frames
37     if (~mod(i,num_avg))
38         % Compute average of num_avg waveforms and take mean in the case of
39         % ecg, and RMS in case of amp
40         ecg(i/num_avg) = mean(mean(data_ecg((i-num_avg)+1:i,:),1));
41         amp(i/num_avg) = sqrt(mean((mean(data_rdr((i-num_avg)+1:i,:),1)-room_avg).^2));
42     end
43
44     % Compute the location at which the peak of the returning pulse occurs
45     [jnk, toa(i)] = max(mean(data_rdr(i,:),1)-room_avg);
46
47 end
48
49 % Convert to toa to seconds
50 toa = toa * 20e-12;
51
52
53 %% Filter data
54 % Filter ECG with 30 Hz LP
55 % Filter amp and toa with 3 Hz LP, but they are of different lengths so
56 % keep filters separate
57 nyquist_toa = 2000;
58 nyquist_amp = nyquist_toa / num_avg;
59 numcoef_toa = nyquist_toa / 2;
60 numcoef_amp = nyquist_amp / 2;
61

```



```

62 t_amp = (1:length(ecg)) * (10 / length(ecg));
63 t_toa = (1:length(toa)) * (10 / length(toa));
64
65 b_1 = fir1(numcoef_toa, 3/nyquist_toa);
66 b_2 = fir1(numcoef_amp, 3/nyquist_amp);
67 b_3 = fir1(numcoef_amp, 30/nyquist_amp);
68
69 f_toa_1 = filter(b_1, 1, toa);
70 f_amp_1 = filter(b_2, 1, amp);
71 f_ecg_1 = filter(b_3, 1, ecg);
72
73
74 %% Plot Data
75 % Normalize channels for plotting
76 ecg_max = max(f_ecg_1(nyquist_amp*6:end));
77 amp_max = max(f_amp_1(nyquist_amp*6:end));
78 toa_max = max(f_toa_1(nyquist_toa*6:end));
79
80 ecg_min = min(f_ecg_1(nyquist_amp*6:end));
81 amp_min = min(f_amp_1(nyquist_amp*6:end));
82 toa_min = min(f_toa_1(nyquist_toa*6:end));
83
84 ecg_scale = 2 / (ecg_max - ecg_min);
85 amp_scale = 2 / (amp_max - amp_min);
86 toa_scale = 2 / (toa_max - toa_min);
87
88 ecg_tran = 1 - (ecg_max * ecg_scale);
89 amp_tran = 1 - (amp_max * amp_scale);
90 toa_tran = 1 - (toa_max * toa_scale);
91
92 f_ecg_norm = (f_ecg_1 * ecg_scale) + ecg_tran;
93 f_amp_norm = (f_amp_1 * amp_scale) + amp_tran;
94 f_toa_norm = (f_toa_1 * toa_scale) + toa_tran;
95
96 ecg_step = (ecg_max - ecg_min) / 4;
97 amp_step = (amp_max - amp_min) / 4;
98 toa_step = (toa_max - toa_min) / 4;
99
100 % Plot waveforms
101 figure('Color','w');
102 axes('position',[.1 .6 .8 .25]);
103 axis([0, 10, -1.05, 1.1]);
104 set(gca,'ytick',[-0.5 0.5],'yticklabel',[sprintf('%12.2g V', ecg_min+ecg_step); sprintf('%12
    .2g V', ecg_max-ecg_step)],'ycolor','b','xtick',[],'xcolor','w','FontSize',fsize-4);
105 ylabel('ECG','FontSize',fsize);
106
107 axes('position',[.1 .35 .8 .25]);
108 axis([0, 10, -1.05, 1.05]);
109 set(gca,'ytick',[-0.5 0.5],'yticklabel',[sprintf('%12.4e V', amp_min+amp_step); sprintf('%12
    4e V', amp_max-amp_step)],'ycolor',[0 0.5 0],'xtick',[],'xcolor','w','FontSize',fsize-4);
110 ylabel('Radar Amplitude','FontSize',fsize);
111 xlabel('Time (s)','FontSize',fsize);
112
113 axes('position',[.1 .1 .8 .25]);
114 axis([0, 10, -1.1, 1.05]);
115 set(gca,'ytick',[-0.5 0.5],'yticklabel',[sprintf('%12.4e sec', toa_min+toa_step); sprintf('%12
    4e sec', toa_max-toa_step)],'ycolor','r','FontSize',fsize-4);
116 ylabel('Radar Pulse Return Time','FontSize',fsize);
117 xlabel('Time (s)','FontSize',fsize);
118
119 axes('position',[.1 .1 .8 .75],'FontSize',fsize-4);

```

```

120 hold on;
121 plot(t_amp, f_ecg_norm, 'b')
122 plot(t_amp, f_amp_norm - 2.1, 'Color', [0 0.5 0]);
123 plot(t_toa, f_toa_norm - 4.2, 'Color', 'r');
124 [pks, locs] = findpeaks(f_ecg_norm(2*numcoef_amp:end), 'minpeakheight', 0.5, 'minpeakdistance',
    , nyquist_amp*.15);
125 locs = locs + 2*numcoef_amp;
126 line([t_amp(locs); t_amp(locs)], {ones(1,length(locs))*-5.3; ones(1,length(locs))*1.1}, '
    LineStyle', ':', 'Color', 'k', 'LineWidth', 2);
127 hold off;
128
129 axis([0 10 -5.3 1.1]);
130 set(gca, 'ytick', [], 'xtick', [], 'Color', 'none');
131 legend('ECG', 'Radar Amp', 'Radar Time', 'Location', 'SouthWest');
132
133 title({'ECG and UWB pulse amplitude and return time'; date}, 'FontSize', fsize, 'FontWeight', '
    bold');

```

```

1  %%%%%%%%%%%%%%%%%%%%%%%%%%%%%%%%%%%%%%%%%%%%%%%%%%%%%%%%%%%%%%%%%%%%%%%%%
2  % wfm_ascii_dpo_FF.m
3  %%%%%%%%%%%%%%%%%%%%%%%%%%%%%%%%%%%%%%%%%%%%%%%%%%%%%%%%%%%%%%%%%%%%%%%%%
4
5  function [out_descript, outdata, timedata] = wfm_ascii_dpo_FF(fname, data_start, data_stop)
6  % Modified by Jonathan Burnham to implement fast frame and speed up reading
7  % large data sets offset by large amounts
8  %
9  % Converts TSD5/6/7k and DPO7k 70k wfm file to ASCII format
10 % with time array
11 %
12 % data_start and data_stop input arguments are optional
13 % and can be used to read parts of file
14 %
15 % To do: implement fast frame, pixel maps
16 %
17
18 out = [];
19 if nargin==0
20     fname='';
21 end
22
23 if isempty(fname)
24     [filename, pname]=uigetfile({'*.wfm', 'Tektronix Waveform Files (*.wfm)';'*.*', 'All Files
25     (*.*)'}, 'Choose Tektronix WFM file');
26     fname=[pname filename];
27 end
28 %---Open file
29 fd = fopen(fname, 'r');
30 if fd==-1
31     error('Problem opening file "%s"', fname)
32 end
33
34 %---Determine byte ordering, then close and reopen with proper byte ordering
35 ByteOrder = fread(fd, 1, 'ushort');
36 if ByteOrder==61680
37     fclose(fd);
38     fd = fopen(fname, 'r', 'ieee-be');
39 else
40     fclose(fd);
41     fd = fopen(fname, 'r', 'ieee-le');
42 end
43
44 %---WFM static file information
45 out.ByteOrder = fread(fd, 1, 'ushort');
46 out.VersionNum = fread(fd, 8, '*char');
47 if ~any(strcmp(out.VersionNum, {'WFM#001'; 'WFM#002'; 'WFM#003'}))
48     fclose(fd);
49     error('File "%s" is not a valid WFM file', fname)
50 end
51 out.NumDigitsInByteCount = fread(fd, 1, 'char');
52 out.NumBytesToEOF = fread(fd, 1, 'long');
53 out.NumBytesPerPoint = fread(fd, 1, 'char');
54 out.ByteOffsetToCurveBuffer = fread(fd, 1, 'long');
55 out.HorZoomScale = fread(fd, 1, 'long');
56 out.HorZoomPos = fread(fd, 1, 'float32');
57 out.VerZoomScale = fread(fd, 1, 'double');
58 out.VerZoomPos = fread(fd, 1, 'float32');
59 out.WaveformLabel = fread(fd, 32, '*char');
60 out.N = fread(fd, 1, 'ulong');

```

```

61 out.HeaderSize          = fread(fd, 1, 'ushort' );
62
63 %---WFM header
64 out.SetType             = fread(fd, 1, 'int'   );
65 out.WfmCnt              = fread(fd, 1, 'ulong' );
66 jnk                    = fread(fd,36, 'uchar' ); % Skip these for now
67 out.DataType           = fread(fd, 1, 'int'   );
68 jnk                    = fread(fd,20, 'uchar' ); % Skip these for now
69 out.numReqFrames       = fread(fd, 1, 'ulong' );
70 out.numAcqFrames       = fread(fd, 1, 'ulong' );
71 switch out.VersionNum
72 case {':WFM#002' ':WFM#003'}
73     jnk                 = fread(fd, 1, 'ushort'); % Skip these for now
74 end
75 jnk                    = fread(fd,12, 'uchar' ); % Skip these for now
76
77 %---Explicit Dimension 1/2
78 s = [];
79 for n=1:2
80     s.DimScale          = fread(fd, 1, 'double');
81     s.DimOffset         = fread(fd, 1, 'double');
82     s.DimSize           = fread(fd, 1, 'ulong' );
83     s.Units             = fread(fd,20, '*char' );
84     s.DimExtentMin      = fread(fd, 1, 'double');
85     s.DimExtentMax      = fread(fd, 1, 'double');
86     s.DimResolution     = fread(fd, 1, 'double');
87     s.DimRefPoint       = fread(fd, 1, 'double');
88     s.Format            = fread(fd, 1, 'int'   );
89     s.StorageType       = fread(fd, 1, 'int'   );
90     jnk                 = fread(fd,20, 'uchar' ); % Skip these for now
91     s.UserScale         = fread(fd, 1, 'double');
92     s.UserUnits         = fread(fd,20, '*char' );
93     s.UserOffset        = fread(fd, 1, 'double');
94     switch out.VersionNum
95     case ':WFM#003'
96         s.PointDensity  = fread(fd, 1, 'double');
97     otherwise
98         s.PointDensity  = fread(fd, 1, 'ulong' );
99     end
100    s.HRef               = fread(fd, 1, 'double');
101    s.TrigDelay          = fread(fd, 1, 'double');
102    out.ExplicitDimension(n) = s;
103 end
104
105 %---Implicit Dimension 1/2
106 s = [];
107 for n=1:2
108     s.DimScale          = fread(fd, 1, 'double');
109     s.DimOffset         = fread(fd, 1, 'double');
110     s.DimSize           = fread(fd, 1, 'ulong' );
111     s.Units             = fread(fd,20, '*char' );
112     jnk                 = fread(fd,16, 'uchar' ); % Skip these for now
113     s.DimResolution     = fread(fd, 1, 'double');
114     jnk                 = fread(fd,12, 'uchar' ); % Skip these for now
115     s.UserScale         = fread(fd, 1, 'double');
116     s.UserUnits         = fread(fd,20, '*char' );
117     s.UserOffset        = fread(fd, 1, 'double');
118     switch out.VersionNum
119     case ':WFM#003'
120         s.PointDensity  = fread(fd, 1, 'double');
121     otherwise

```

```

122     s.PointDensity      = fread(fd, 1, 'ulong' );
123     end
124     s.HRef              = fread(fd, 1, 'double' );
125     s.TrigDelay         = fread(fd, 1, 'double' );
126     out.ImplicitDimension(n) = s;
127 end
128
129 %---Time Base 1/2 Information
130 s=[];
131 for n=1:2
132     s.RealPointSpacing  = fread(fd, 1, 'ulong' );
133     s.Sweep             = fread(fd, 1, 'int'   );
134     s.TypeOfBase       = fread(fd, 1, 'int'   );
135     out.TimeBase(n) = s;
136 end
137
138 %---WFM Update Spec
139 jnk = fread(fd, 24, 'uchar'); % Skip these for now
140
141 %---WFM Curve Information
142 jnk = fread(fd, 10, 'uchar'); % Skip these for now
143 PrechargeStartOffset = fread(fd, 1, 'ulong' );
144 DataStartOffset      = fread(fd, 1, 'ulong' );
145 PostchargeStartOffset = fread(fd, 1, 'ulong' );
146 PostchargeStopOffset = fread(fd, 1, 'ulong' );
147 EndOfCurveBufferOffset = fread(fd, 1, 'ulong' );
148
149 out.CurveSizeInBytes = PostchargeStartOffset - DataStartOffset;
150 out.CurveSize = out.CurveSizeInBytes / out.NumBytesPerPoint;
151
152 %---FastFrame Frames
153 if out.N > 0
154     % We are dealing with fast frames
155     fseek(fd, out.N * 24, 'cof');
156
157     % Initialize data and offset variables
158     outdata = zeros([out.numAcqFrames out.CurveSize]);
159     buffer_offsets = zeros([out.numAcqFrames 2]);
160
161     buffer_offsets(1,1) = DataStartOffset;
162     buffer_offsets(1,2) = EndOfCurveBufferOffset - PostchargeStartOffset;
163
164     % Loop through and get offset information for all of the frames Store
165     % info so we know how many bytes to skip in between frames
166     for i=2:out.numAcqFrames
167
168         jnk = fread(fd, 10, 'uchar');
169         PrechargeStartOffset = fread(fd, 1, 'ulong');
170         DataStartOffset      = fread(fd, 1, 'ulong');
171         PostchargeStartOffset = fread(fd, 1, 'ulong');
172         PostchargeStopOffset = fread(fd, 1, 'ulong');
173         EndOfCurveBufferOffset = fread(fd, 1, 'ulong');
174
175         buffer_offsets(i,1) = DataStartOffset;
176         buffer_offsets(i,2) = EndOfCurveBufferOffset - PostchargeStartOffset;
177
178     end
179
180     % Now go through the curvebuffer and extract all the frames
181     for i=1:out.numAcqFrames
182

```

```

183     jnk = fread(fd,buffer_offsets(i,1),'uchar');
184     switch out.NumBytesPerPoint
185     case 1
186         y = fread(fd,out.CurveSize,'*int8');
187     case 2
188         y = fread(fd,out.CurveSize,'*int16');
189     end
190
191     outdata(i,:) = (out.ExplicitDimension(1,1).DimOffset) + (out.ExplicitDimension(1,1)
192         .DimScale)*double(y);
193
194     jnk = fread(fd,buffer_offsets(i,2),'uchar');
195
196 end
197
198 t = out.ImplicitDimension(1,1).DimOffset + out.ImplicitDimension(1,1).DimScale*(1:
199     out.CurveSize);
200 out_descript.Fs = 1/out.ImplicitDimension(1,1).DimScale;
201 out_descript.Ts = out.ImplicitDimension(1,1).DimScale;
202 out_descript.N = out.CurveSize;
203 out_descript.byte = out.NumBytesPerPoint;
204 timedata = t;
205
206 else
207     %---Curve Buffer: no fast frames
208     jnk = fread(fd,DataStartOffset,'uchar'); % Skip precharge
209
210     if nargin<3
211         data_start = 1;
212         data_stop = out.CurveSize;
213     end
214     switch out.NumBytesPerPoint
215     case 1
216         if data_start > 1
217             % jnk = fread(fd,data_start-1,'*int8');
218             fseek(fd, data_start-1, 'cof');
219             out.CurveData = fread(fd,data_stop-data_start+1,'*int8');
220         else
221             out.CurveData = fread(fd,data_stop,'*int8');
222         end
223     case 2
224         if data_start > 1
225             % out.CurveData = fread(fd,data_start-1,'*int16');
226             fseek(fd, (data_start-1)*2, 'cof');
227             out.CurveData = fread(fd,data_stop-data_start+1,'*int16');
228         else
229             out.CurveData = fread(fd,data_stop,'*int16');
230         end
231     end
232
233     y = (out.ExplicitDimension(1,1).DimOffset) + (out.ExplicitDimension(1,1).DimScale)*double(
234         out.CurveData);
235     t = out.ImplicitDimension(1,1).DimOffset + out.ImplicitDimension(1,1).DimScale*(data_start
236         :data_stop);
237     out_descript.Fs = 1/out.ImplicitDimension(1,1).DimScale;
238     out_descript.Ts = out.ImplicitDimension(1,1).DimScale;
239     out_descript.N = out.CurveSize;
240     out_descript.byte = out.NumBytesPerPoint;
241     outdata = y;
242     timedata = t;
243
244 end

```

```
240 end
241
242
243 %---Close file
244 fclose (fd);
245 %E_DimOffset = out.ExplicitDimension(1,1) DimOffset;
246 %E_DimScale = out.ExplicitDimension(1,1) DimScale;
247 %E_CurveData = out.CurveData;
248 %I_DimOffset = out.ImplicitDimension(1,1) DimOffset;
249 %I_DimScale = out.ImplicitDimension(1,1) DimScale
```

```

1 %%%%%%%%%%%%%%%%%%%%%%%%%%%%%%%%%%%%%%%%%%%%%%%%%%%%%%%%%%%%%%%%%%%%%%%%%
2 % Fixed-frequency-analysis.m
3 %%%%%%%%%%%%%%%%%%%%%%%%%%%%%%%%%%%%%%%%%%%%%%%%%%%%%%%%%%%%%%%%%%%%%%%%%
4 %% Collect data
5 clear all; clc;
6
7 % Subject number, date, and sequence number of data to plot
8 subj-num = '0008';
9 date = '4/8/09';
10 seq-num = 8;
11
12 % Base font size for plots
13 fsize = 17;
14
15 % Read in data
16 [accel_data, ecg_data, amp_data, phase_data, t] = get_data(subj-num, date, seq-num);
17
18 %% Do processing
19 num_coef = 1000;
20 nyquist = 5000;
21
22 % Center accelerometer values for filtering
23 accel_mean = mean(accel_data);
24 accel = accel_data - accel_mean;
25 % Convert to meters/s^2
26 % accel is in volts: data sheet says 1.2 V/g, g = 9.8 m/s^2
27 accel = accel * (1/1.2) * 9.8;
28
29 % Center ecg values for filtering
30 ecg_mean = mean(ecg_data);
31 ecg = ecg_data - ecg_mean;
32
33 % Center amplitude values for filtering
34 amp_mean = mean(amp_data);
35 amp = amp_data - amp_mean;
36
37 % Subtract out constant phase change
38 % Estimate slope by taking mean of diff. Only look at everything after
39 % first second since initial data is often unusual
40 slope = mean(diff(phase_data(2*nyquist:end)));
41 % Calculate line with that slope that runs through first data point
42 line_data = slope*(1:length(phase_data))' - slope + phase_data(1);
43 % Subtract line from phase to give
44 phase_nl = phase_data - line_data;
45 % Center phase values for filtering
46 phase_mean = mean(phase_nl);
47 phase_nl = phase_nl - phase_mean;
48
49
50 % Make FIR filter coefficients for different filters
51 b_1 = fir1(num_coef, 30/nyquist);
52 [z,p,k] = butter(2, 0.5/nyquist, 'high');
53 [sos,g] = zp2sos(z,p,k);
54 h_05_HP = dfilt.df2sos(sos,g);
55 [z,p,k] = butter(8, 1/nyquist, 'high');
56 [sos,g] = zp2sos(z,p,k);
57 h_2_HP = dfilt.df2sos(sos,g);
58
59 % 0.5 Hz high pass filter phase and rdr
60 f_phase_1 = filter(h_05_HP, phase_nl);
61 f_amp_1 = filter(h_05_HP, amp);

```



```

62
63 % Low pass filter all channels with 30 Hz LP filter
64 f_accel_2 = filter(b_1, 1, accel);
65 f_ecg_2 = filter(b_1, 1, ecg);
66 f_amp_2 = filter(b_1, 1, f_amp_1);
67 f_phase_2 = filter(b_1, 1, f_phase_1);
68
69 % Double integrate acc and filter
70 f_accel_2 = cumsum(cumsum(f_accel_2));
71 f_accel_2 = filter(h_2_HP, f_accel_2);
72
73
74
75 %% Plot results
76 % Normalize channels for plotting on a -1 to +1 axis
77 f_ecg_2 = f_ecg_2 + ecg_mean;
78 f_amp_2 = f_amp_2 + amp_mean;
79 f_accel_2 = f_accel_2 * (1/(2*nyquist))^2;
80 f_phase_2 = f_phase_2 + phase_mean;
81
82 ecg_max = max(f_ecg_2(nyquist*6:end));
83 accel_max = max(f_accel_2(nyquist*6:end));
84 amp_max = max(f_amp_2(nyquist*6:end));
85 phase_max = max(f_phase_2(nyquist*6:end));
86
87 ecg_min = min(f_ecg_2(nyquist*6:end));
88 accel_min = min(f_accel_2(nyquist*6:end));
89 amp_min = min(f_amp_2(nyquist*6:end));
90 phase_min = min(f_phase_2(nyquist*6:end));
91
92 ecg_scale = 2 / (ecg_max - ecg_min);
93 accel_scale = 2 / (accel_max - accel_min);
94 amp_scale = 2 / (amp_max - amp_min);
95 phase_scale = 2 / (phase_max - phase_min);
96
97 ecg_tran = 1 - (ecg_max * ecg_scale);
98 accel_tran = 1 - (accel_max * accel_scale);
99 amp_tran = 1 - (amp_max * amp_scale);
100 phase_tran = 1 - (phase_max * phase_scale);
101
102 f_accel_norm = (f_accel_2 * accel_scale) + accel_tran;
103 f_ecg_norm = (f_ecg_2 * ecg_scale) + ecg_tran;
104 f_amp_norm = (f_amp_2 * amp_scale) + amp_tran;
105 f_phase_norm = (f_phase_2 * phase_scale) + phase_tran;
106
107 ecg_step = (ecg_max - ecg_min) / 4;
108 accel_step = (accel_max - accel_min) / 4;
109 amp_step = (amp_max - amp_min) / 4;
110 phase_step = (phase_max - phase_min) / 4;
111
112
113 % Plot four channels in same window
114 figure('Color','w');
115 axes('position',[.1 .7 .8 .2]);
116 axis([0 10 -1.05 1.1]);
117 set(gca,'ytick',[-0.5 0.5],'yticklabel',[sprintf('%12.2g V', ecg_min+ecg_step); sprintf('%12
    .2g V', ecg_max-ecg_step)],'ycolor','b','xtick',[],'xcolor','w','FontSize',fsize-4);
118 ylabel('ECG','FontSize',fsize);
119
120 axes('position',[.1 .5 .8 .2]);
121 axis([0 10 -1.05 1.05]);

```

```

122 set(gca,'ytick',[-0.5 0.5],'yticklabel',[sprintf('%12.2e meters', accel_min+accel_step);
      sprintf('%12.2e meters', accel_max-accel_step)],'ycolor','r','xtick',[],'xcolor','w','
      FontSize',fsize-4);
123 ylabel('Accelerometer','FontSize',fsize);
124
125 axes('position',[.1 .3 .8 .2]);
126 axis([0 10 -1.05 1.05]);
127 set(gca,'ytick',[-0.5 0.5],'yticklabel',[sprintf('%12.2e Vpeak', amp_min+amp_step); sprintf('
      %12.2e Vpeak',amp_max-amp_step)],'ycolor',[0 0.5 0],'xtick',[],'xcolor','w','FontSize',
      fsize-4);
128 ylabel('Radar Amplitude','FontSize',fsize);
129
130 axes('position',[.1 .1 .8 .2]);
131 axis([0 10 -1.1 1.05]);
132 set(gca,'ytick',[-0.5 0.5],'yticklabel',[sprintf('%12.2g radians',phase_min+phase_step);
      sprintf('%12.2g radians', phase_max-phase_step)],'ycolor',[0.75 0 0.75],'Color','w','
      FontSize',fsize-4);
133 ylabel('Radar Phase','FontSize',fsize);
134 xlabel('Time (s)','FontSize',fsize);
135
136 axes('position',[.1 .1 .8 .8],'FontSize',fsize-4);
137 hold on;
138 plot(t, f_ecg_norm, 'b');
139 plot(t, f_accel_norm - 2.1, 'r');
140 plot(t, f_amp_norm - 4.2, 'Color', [0 0.5 0]);
141 plot(t, f_phase_norm - 6.3, 'Color', [0.75 0 0.75]);
142 [pks, locs] = findpeaks(f_ecg_norm(num_coef:end), 'minpeakheight', 0.5, 'minpeakdistance', 0.3
      *10000);
143 locs = locs + num_coef;
144 line([t(locs); t(locs)], [ones(1,length(locs))*-7.4; ones(1,length(locs))*1.1],'LineStyle',':
      ', 'Color','k');
145 hold off;
146
147 axis([0 10 -7.4 1.1]);
148 set(gca,'ytick',[],'xtick',[],'Color','none');
149 legend('ECG', 'Accel.', 'Radar Amp.', 'Radar Phase', 'Location', 'SouthWest');
150
151 title({'ECG, accelerometer, and radar data'; [subj_num, '#', int2str(seq_num)]},'FontSize',
      fsize, 'FontWeight', 'bold');

```

```

1  %%%%%%%%%%%%%%%%%%%%%%%%%%%%%%%%%%%%%%%%%%%%%%%%%%%%%%%%%%%%%%%%%%%%%%%%%
2  % get_data.m
3  %%%%%%%%%%%%%%%%%%%%%%%%%%%%%%%%%%%%%%%%%%%%%%%%%%%%%%%%%%%%%%%%%%%%%%%%%
4  function [acc_data, ecg_data, amp_data, phase_data, t] = get_data(subject_num, date,
    sequence_num)
5  % Parse date
6  [month, remain] = strtok(date, '/');
7  [day, remain] = strtok(remain, '/');
8  year = strtok(remain);
9
10 % Assume data is stored in folder called Subject Data in the current
11 % directory
12 file_name = ['Subject Data\', subject_num, '\JPL_', subject_num, '_', month, '_', day, '_',
    year(2:end), '_', num2str(sequence_num), '.mat'];
13
14 % Assume data has already been compressed into mat file. If not, use
15 % compress_dop.m
16 load(file_name);
17
18 % Read in data from structure
19 acc_data = data_save.acc_data;
20 ecg_data = data_save.ecg_data;
21 amp_data = data_save.amp;
22 phase_data = data_save.demod;
23 t = data_save.t;

```

```

1  %%%%%%%%%%%%%%%%%%%%%%%%%%%%%%%%%%%%%%%%%%%%%%%%%%%%%%%%%%%%%%%%%%%%%%%%%
2  % compress_dop.m
3  %%%%%%%%%%%%%%%%%%%%%%%%%%%%%%%%%%%%%%%%%%%%%%%%%%%%%%%%%%%%%%%%%%%%%%%%%
4  function [] = compress_dop(folder, subject_num, date, sequence_num, fs_eff)
5
6  % Parse date
7  [month, remain] = strtok(date, '/');
8  [day, remain] = strtok(remain, '/');
9  year = strtok(remain);
10
11 % Open ecg and accelerometer waveforms for processing
12 f_ecg = [folder, '\JPL-', subject_num, '-', month, '-', day, '-', year(2:3), '-', num2str(
    sequence_num), '_ECG.wfm'];
13 f_acc = [folder, '\JPL-', subject_num, '-', month, '-', day, '-', year(2:3), '-', num2str(
    sequence_num), '_ACC.wfm'];
14 f_save = [folder, '\JPL-', subject_num, '-', month, '-', day, '-', year(2:3), '-', num2str(
    sequence_num), '.mat'];
15
16 % Get info about waveforms
17 [info, jnk1, jnk2] = wfm_ascii_dpo(f_ecg, 1, 1);
18
19 total_length = round(info.N);
20 sample_rate = round(info.Fs);
21 rms_length = round(info.Fs / fs_eff);
22 max_read_size = 1e6;
23
24 % Initialize variables
25 data_save.ecg_data = zeros([round(total_length/rms_length) 1]);
26 data_save.acc_data = zeros([round(total_length/rms_length) 1]);
27 samples_per_read = floor(max_read_size / rms_length);
28 read_size = samples_per_read * rms_length;
29
30 % Compute phase and amplitude using FM_Demod routine
31 [data_save.amp, data_save.demod] = FM_Demod(folder, subject_num, date, sequence_num,
    rms_length, total_length, sample_rate);
32
33 % Window and compute mean of ECG and ACC waveforms
34 for i=1:ceil(total_length/read_size)
35
36     % Get large segment of data
37     [jnk1, outdata_ecg, jnk2] = wfm_ascii_dpo(f_ecg, (i-1)*read_size + 1, i*read_size);
38     [jnk1, outdata_acc, jnk2] = wfm_ascii_dpo(f_acc, (i-1)*read_size + 1, i*read_size);
39
40     % Loop over each window
41     for j=1:samples_per_read
42         % If we've reached the end, done
43         if (((i-1)*read_size + j*rms_length) > total_length)
44             break;
45         end
46
47         % For each window, compute the mean of the values in the window and
48         % make that one data point for the output
49         data_save.ecg_data((i-1)*samples_per_read + j) = mean(outdata_ecg((j-1)*rms_length +
            1:j*rms_length));
50         data_save.acc_data((i-1)*samples_per_read + j) = mean(outdata_acc((j-1)*rms_length +
            1:j*rms_length));
51     end
52
53     disp([folder, '\JPL-', subject_num, '-', month, '-', day, '-', year(2:end), '-', num2str(
        sequence_num), ' ', num2str(i), '/', num2str(ceil(total_length/read_size))]);
54 end

```

```
55
56 % Compute vector of time indices
57 data_save.t = (1:length(data_save.ecg_data))*((total_length / sample_rate) / length(
    data_save.ecg_data));
58
59 % Save data we've calculated into mat file
60 save(f_save , 'data_save');
```

```

1 %%%%%%%%%%%%%%%%%%%%%%%%%%%%%%%%%%%%%%%%%%%%%%%%%%%%%%%%%%%%%%%%%%%%%%%%%
2 % FM.Demod.m
3 %%%%%%%%%%%%%%%%%%%%%%%%%%%%%%%%%%%%%%%%%%%%%%%%%%%%%%%%%%%%%%%%%%%%%%%%%
4 function [amp, demod] = FM.Demod(folder, subject_num, date, sequence_num, avg_points,
    record_length, sample_rate)
5 % Initialize variables
6 filt_length = 1000;
7 seg_length = 1e6;
8 tot_length = seg_length + filt_length;
9 unwrap_cutoff = 0.5;
10  $\Delta$  = 5000;
11
12 % Parse date and compute string of radar waveform file
13 [month, remain] = strtok(date, '/');
14 [day, remain] = strtok(remain, '/');
15 year = strtok(remain);
16 fname = [folder, '\JPL_', subject_num, '_', month, '_', day, '_', year(2:3), '_', num2str(
    sequence_num), '_RDR.wfm'];
17
18 % Read in large segment of data and compute fft
19 [temp_data, data_fft, temp_data2] = wfm_ascii_dpo(fname, 1, 25e6);
20 data_fft = abs(fft(data_fft));
21 % Max frequency in first half of fft must be center frequency
22 [temp_data, loc] = max(data_fft(1:floor(length(data_fft)/2)));
23 RF_freq = loc * (sample_rate / length(data_fft))
24 clear data_fft
25
26 % Cutoff for lowpass filter
27 f_cutoff = max(RF_freq / 2,  $\Delta$ );
28
29 % Initialize variables
30 outdata = zeros([tot_length 1]);
31 I = zeros([tot_length 1]);
32 Q = zeros([tot_length 1]);
33 cosData = zeros([seg_length 1]);
34 sinData = zeros([seg_length 1]);
35 demod_full = zeros([seg_length 1]);
36 demod_unwrap = zeros([seg_length 1]);
37 demod = zeros([record_length / avg_points 1]);
38 amp = zeros([record_length / avg_points 1]);
39 last_demod = 0;
40 base = 0;
41
42 % Compute low pass filter coefficients
43 b = fir1(filt_length, f_cutoff/(sample_rate/2));
44 b2 = fir1(filt_length, [(RF_freq -  $\Delta$ )/(sample_rate/2) (RF_freq +  $\Delta$ )/(sample_rate/2)]);
45
46 % Break data up into large segments, read them in one by one, and compute
47 % the phase and amplitude for each point
48 for i=1:floor(record_length/seg_length)
49
50     % Read in segments from .wav file
51     [temp_data, outdata(filt_length+1:end), temp_data2] = wfm_ascii_dpo(fname, (i-1)*
        seg_length + 1, i*seg_length);
52     % filter data and store end of data segment to append to next data
53     % segment
54     outdata_f = filter(b2, 1, outdata);
55     outdata(1:filt_length) = outdata(end-filt_length+1:end);
56
57     % Multiply by sine and cosine waves
58     cosData(:,1) = cosd(RF_freq*360*((1/sample_rate)*((i-1)*seg_length+1:i*seg_length)));

```

```

59     sinData(:,1) = sind(RF_freq*360*((1/sample_rate)*((i-1)*seg_length+1:i*seg_length)));
60
61     % Low pass filter outputs of mixing
62     I(filt_length+1:tot_length) = outdata_f(filt_length+1:end) .* sinData;
63     Q(filt_length+1:tot_length) = outdata_f(filt_length+1:end) .* cosData;
64     I_f = filter(b, 1, I);
65     Q_f = filter(b, 1, Q);
66     I(1:filt_length) = I(tot_length-filt_length+1:tot_length);
67     Q(1:filt_length) = Q(tot_length-filt_length+1:tot_length);
68
69     % Compute phase by taking inverse tangent
70     demod_full(1:seg_length) = atan(Q_f(filt_length+1:tot_length) ./ I_f(filt_length+1:
        tot_length) );
71
72     % Detect a phase discontinuity between segments
73     if ((demod_full(1) - last_demod) > unwrap_cutoff)
74         base = base - pi;
75     elseif ((last_demod - demod_full(1)) > unwrap_cutoff)
76         base = base + pi;
77     end
78
79     % Add current multiple of pi from previous phase unwrapping
80     demod_unwrap(1) = demod_full(1) + base;
81
82     % Detect phase jumps by taking first and second derivatives and make
83     % sure these phase jumps are isolated from any other similar jumps
84     demod_diff = diff(demod_full);
85     demod_diff_2 = [pi; diff(demod_diff)];
86     demod_diff_3 = -[diff(demod_diff); pi];
87     cut_greater = (demod_diff > unwrap_cutoff);
88     cut_lesser = (-demod_diff > unwrap_cutoff);
89     diff2_greater = (demod_diff_2 > unwrap_cutoff);
90     diff2_lesser = (-demod_diff_2 > unwrap_cutoff);
91     diff3_greater = (demod_diff_3 > unwrap_cutoff);
92     diff3_lesser = (-demod_diff_3 > unwrap_cutoff);
93     base_minus_pi = (cut_greater & diff2_greater & diff3_greater);
94     base_plus_pi = (cut_lesser & diff2_lesser & diff3_lesser);
95     base_vector = cumsum( base_minus_pi*-pi + base_plus_pi*pi );
96     demod_unwrap(2:end) = demod_full(2:end) + base_vector + base;
97
98     % Keep track of variables for next segment
99     base = base_vector(end) + base;
100    last_demod = demod_full(length(demod_full));
101
102    % Window data and average to form output data points. Also compute and
103    % window amplitude using I,Q, and the calculated phase
104    for j=1:(seg_length / avg_points)
105        demod((i-1)*(seg_length / avg_points) + j) = mean(demod_unwrap((j-1)*avg_points + 1:j*
            avg_points));
106        amp((i-1)*(seg_length / avg_points) + j) = mean((Q_f(filt_length+(j-1)*avg_points+1:
            filt_length+j*avg_points)./sin(demod_unwrap((j-1)*avg_points + 1:j*avg_points))) +
            (I_f(filt_length+(j-1)*avg_points+1:filt_length+j*avg_points)./cos(demod_unwrap((
            j-1)*avg_points + 1:j*avg_points))));
107    end
108
109    % Print message to indicate how far into the demodulation process we are
110    sprintf( '%d/%d\n', i, floor(record_length/seg_length) )
111 end

```





## Appendix B

# COUHES Protocol

---

**To:** Julie Greenberg  
E25-518

**From:** Leigh Finn, Chair  
COUHES

**Date:** 07/18/2008

**Committee Action:** Approval

**COUHES Protocol #:** 0806002811

**Study Title:** Signal Processing Methodologies for the Remote Sensing of Vital Signs with UWB Radar

**Expiration Date:** 07/16/2009

The above-referenced protocol has been APPROVED following Full Board Review by the Committee on the Use of Humans as Experimental Subjects (COUHES).

If the research involves collaboration with another institution then the research cannot commence until COUHES receives written notification of approval from the collaborating institution's IRB.

It is the Principal Investigator's responsibility to obtain review and continued approval before the expiration date. Please allow sufficient time for continued approval. You may not continue any research activity beyond the expiration date without COUHES approval. Failure to receive approval for continuation before the expiration date will result in the automatic suspension of the approval of this protocol. Information collected following suspension is unapproved research and cannot be reported or published as research data. If you do not wish continued approval, please notify the Committee of the study termination.

**Adverse Events:** Any serious or unexpected adverse event must be reported to COUHES within 48 hours. All other adverse events should be reported in writing within 10 working days.

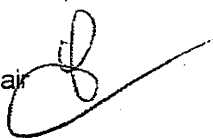
**Amendments:** Any changes to the protocol that impact human subjects, including changes in experimental design, equipment, personnel or funding, must be approved by COUHES before they can be initiated.

Prospective new study personnel must, where applicable, complete training in human subjects research and in the HIPAA Privacy Rule before participating in the study.

COUHES should be notified when your study is completed. You must maintain a research file for at least 3 years after completion of the study. This file should include all correspondence with COUHES, original signed consent forms, and study data.

---

**To:** Julie Greenberg  
E25-518

**From:** Leigh Finn, Chair  
COUHES 

**Date:** 03/04/2009

**Committee Action:** Amendment to Approved Protocol

**COUHES Protocol #:** 0806002811

**Study Title:** Signal Processing Methodologies for the Remote Sensing of Vital Signs with UWB Radar

**Expiration Date:** 07/16/2009

The amendment to the above-referenced protocol has been APPROVED following expedited review by the Committee on the Use of Humans as Experimental Subjects (COUHES).

If the research involves collaboration with another institution then the research cannot commence until COUHES receives written notification of approval from the collaborating institution's IRB.

It is the Principal Investigator's responsibility to obtain review and continued approval before the expiration date. Please allow sufficient time for continued approval. You may not continue any research activity beyond the expiration date without COUHES approval. Failure to receive approval for continuation before the expiration date will result in the automatic suspension of the approval of this protocol. Information collected following suspension is unapproved research and cannot be reported or published as research data. If you do not wish continued approval, please notify the Committee of the study termination.

**Adverse Events:** Any serious or unexpected adverse event must be reported to COUHES within 48 hours. All other adverse events should be reported in writing within 10 working days.

**Amendments:** Any changes to the protocol that impact human subjects, including changes in experimental design, equipment, personnel or funding, must be approved by COUHES before they can be initiated.

Prospective new study personnel must, where applicable, complete training in human subjects research and in the HIPAA Privacy Rule before participating in the study.

COUHES should be notified when your study is completed. You must maintain a research file for at least 3 years after completion of the study. This file should include all correspondence with COUHES, original signed consent forms, and study data.

# Protocol For Human Subject Testing

Jonathan Burnham, x8-4273

## *1. Overview of changes*

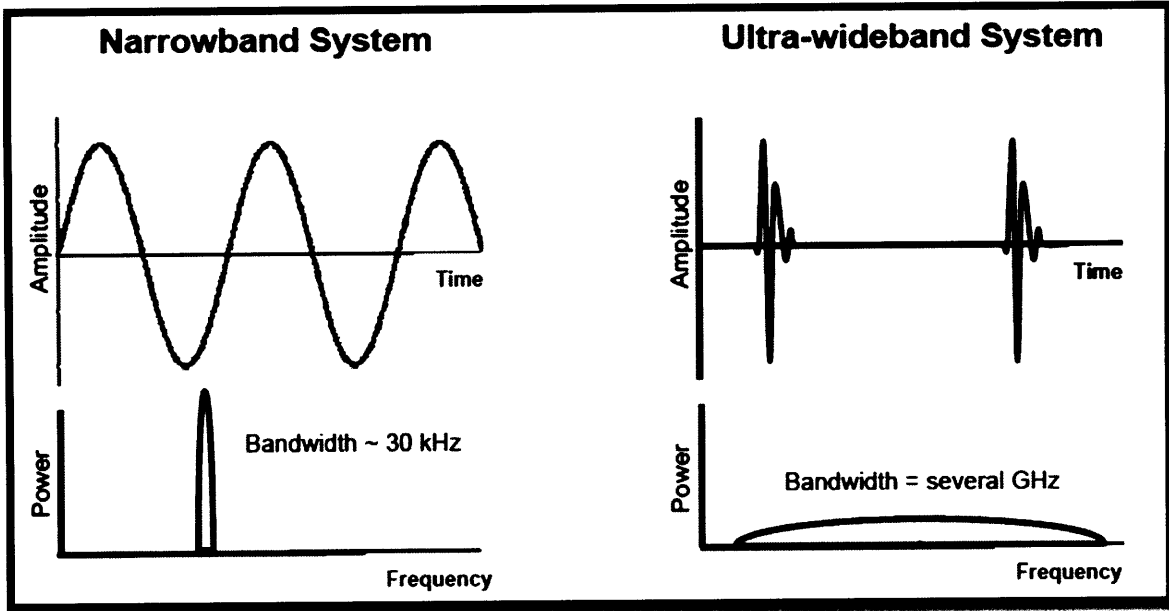
On 7/18/2008 the MIT COUHES board approved for human subject testing an Ultra-wideband radar system designed to interrogate a human subject and detect modulations caused by the subjects respiration and heart beat. In order to compare data from the previously approved UWB system with data from a more traditional radar, it is desired to collect data with human subjects using a fixed frequency transmitter and a different receiver structure. The only changes affecting the system from a human subject testing perspective is the change from an UWB transmitter to a fixed-frequency, microwave transmitter. The power levels with the fixed-frequency setup are even lower than those employed in the UWB transmitter and far well below all maximum-permissible exposure standards. Given the low impact these changes have on safety for the human subject, an expedited review is requested so that testing may begin as soon as possible.

## *2. Overview of experiment*

In order to develop the signal processing algorithms, data must first be collected. For this project, the data will consist of the electromagnetic reflections off of a human subject from an ultra-wideband radar system. Electrocardiogram (ECG) and possibly impedance cardiogram (ICG) data will also be collected from the human subject using commercial monitoring equipment. The ECG and ICG data will provide a point of comparison between the ultra-wideband radar system and "true" data.

## *3. Explanation of technology*

Ultra-wideband (UWB) radar is different from conventional Doppler radar in a number of ways. Conventional radar emits electromagnetic radiation at a fixed frequency and gathers information from the phase change caused by the targets motion. UWB radar, on the other hand, emits a very brief pulse of energy many times a second. The brief pulse translates to a very broad frequency spectrum. However, the amount of power at any one frequency in the spectrum is very low. This broad frequency spectrum gives UWB radar unique characteristics including improved penetration of a wide range of materials. Its low average power prevents it from interfering with other electrical equipment and makes it completely safe.



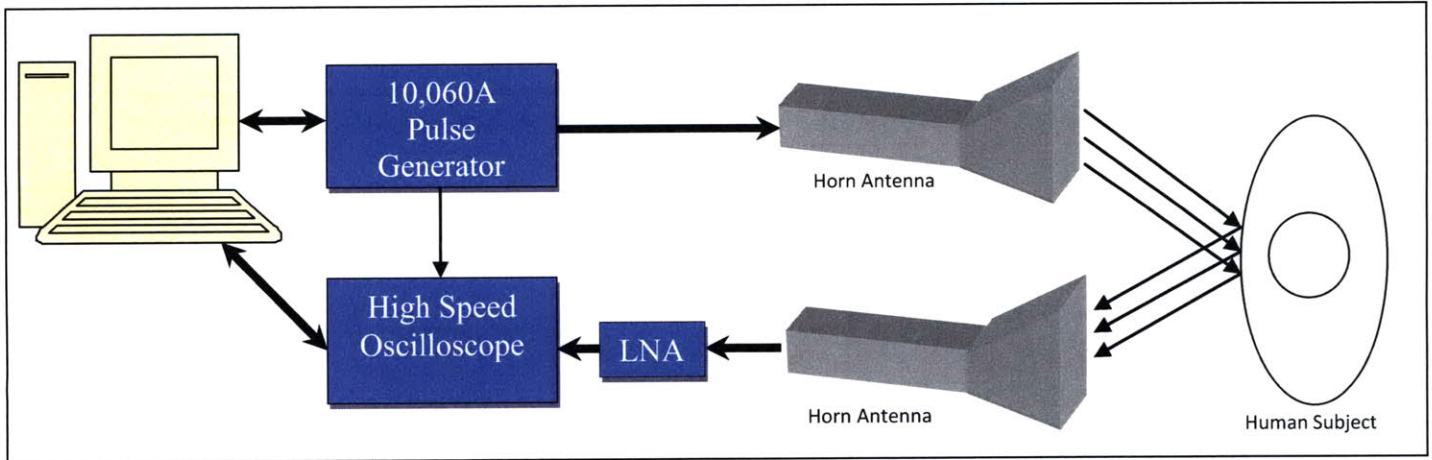
#### 4. Description of test setups

There are two test setups. One is a conventional radar, while the other is an UWB radar. There are two components to the UWB testing setup. The first is the UWB radar collection system. The second is the medical ECG and ICG monitors and the accelerometer. These monitors will be used in the conventional manner and pose no risk to the subject. Because the investigator who will be working with the human subjects (Jonathan Burnham) is a male, only male volunteers will be used in the study to avoid any issues with placing ECG electrodes on the subjects' chest.

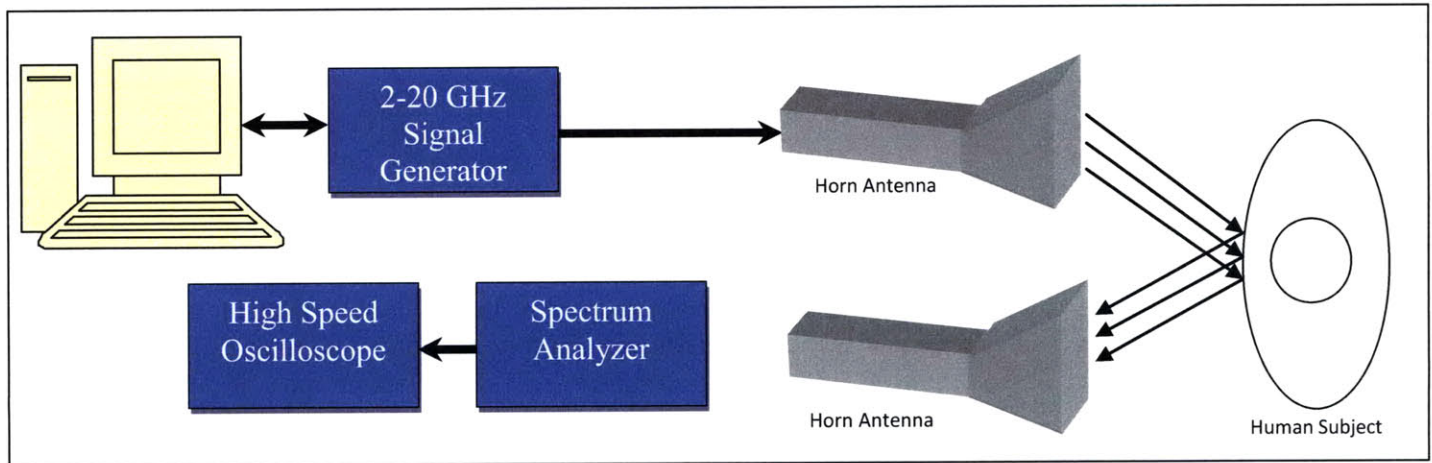
The UWB radar system consists of a transmitting and receiving section, all under the control of a computer. The transmitting section consists of the 10,060A pulse generator from Picosecond Pulse Labs connected to a high-bandwidth horn antenna. The pulses will be broadcast over the air and reflect off of the human subject. The returning pulses will be modulated by the subjects' physiological activity and picked up by a second horn antenna. The received signal will be amplified by a broadband, low-noise amplifier (LNA) and then digitized by a high-speed oscilloscope

The conventional system will use the same ECG/ICG and accelerometer, but instead of a pulse generator as the transceiver, a 2-20 GHz signal generator will be used. On the receiving section, a spectrum analyzer and external down mixing components (not shown) will be used in between the receiving horn antenna and the oscilloscope.

A diagram of both setups is shown below



**UWB Radar Setup**



**Fixed-Frequency (Conventional) Radar Setup**

## 5. Outline of experiment

- a) ECG/ICG electrodes will be mounted on chest and/or appendages of subject
- b) Accelerometer board will be mounted on chest of subject
- c) Data will be collected with UWB or fixed frequency radar system and ECG/ICG monitors for 1-3 minutes
- d) Position of subject relative to antennas will be altered
  - a. Angle of antennas to plane of chest will be varied  $\pm 180$  degrees
  - b. Distance from subject to antennas will be varied between 0-10 meters
- e) Data will again be collected with UWB or fixed frequency radar system and ECG/ICG monitors for 1-3 minutes
- f) This will be repeated until range of angles and distances is met
- g) Experiment may be repeated for other radar setup
  - a. Subject will be tested for no longer than 30 minutes in total

## 5. Analysis of risk to subject – UWB radar

The transmitting section of the UWB radar is the only portion of the test setup that presents any kind of risk to the human subject. The 10,060A Pulse Generator (data sheet attached) will be configured for different voltage settings and pulse widths, but the worse case settings are as below:

Max Amplitude: **10 V**  
Max Pulse Width: **10 ns**  
Min Rise Time: **55 ps -> (bandwidth ~ 0-18.2 GHz)**  
Max repetition rate: **100 KHz**  
Output Waveform: **Impulse**

The source impedance is 50  $\Omega$  and will be fed into a matched antenna, so the peak power output from the system is 2 W. The smallest 1-18 GHz horn antenna seen to date measures 84x80 mm at its front, so if the horn antenna were able to focus all of the available power into this aperture, the peak power density at the opening would be:

$$\frac{2 \text{ W}}{0.084 \text{ m} \times 0.080 \text{ m}} = 297.62 \text{ W/m}^2$$

The peak electric-field strength is therefore:

$$E_{peak} = \sqrt{377 \times 297.62} = 334.97 \text{ V/m}$$

The maximum energy density during any 10 ms interval is:

$$\int_0^{10 \text{ ms}} S(t) dt = 297.62 \frac{\text{W}}{\text{m}^2} \times 10 \text{ ns} \times 100 \text{ KHz} \times 10 \text{ ms} = 0.00298 \frac{\text{J}}{\text{m}^2}$$

According to the *IEEE Standard for Safety Levels with Respect to Human Exposure to Radio Frequency Electromagnetic Fields, 3 kHz to 300 GHz (C95.1-2005)*, the maximum permissible peak-electric-field strength is **100 kV/m** and the maximum permissible peak energy density for an uncontrolled environment is **720 J/m<sup>2</sup>** in the 100-400 MHz range (according to my interpretation, it is higher at other frequency ranges). As we can see, the peak electric-field strength and energy density for the proposed system falls far under the maximum permissible levels.

The above maximum permissible levels are for pulsed RF signals, however the repetition rate of the proposed system exceeds the maximum rate for the pulsed calculations. Using normal averaging time calculations, the average power density is:

$$S_{avg} = 297.62 \text{ W} \times 10 \text{ ns} \times 100 \text{ KHz} = 0.298 \frac{\text{W}}{\text{m}^2}$$

This is once again far smaller than the maximum permissible average power of  $2 \text{ W/m}^2$  in an uncontrolled environment as stated by the IEEE standard for the frequency range from 100-400 MHz (again, according to my interpretation, other frequency ranges have even higher maximum permissible average powers).

## ***6. Analysis of risk to subject – fixed-frequency radar***

The transmitting section of the radar will use an oscillator operating at 0 dBm (1 mW) with a frequency anywhere between 2-18 GHz. At 2 GHz, the IEEE maximum permissible exposure for an unregulated environment is  $1.33 \text{ mW/cm}^2$  [1]. The oscillator will connect to a horn antenna and transmit the signal toward the human subject. The horn antenna will diffuse the RF energy significantly, but even if it did not and focused all the radiation on to a single square centimeter, the setup would still be under the  $1.33 \text{ mW/cm}^2$  limit listed above. At higher frequencies the maximum permissible exposure limit is even higher.

A more substantive analysis of the emitted power of the setup would be to consider the gain of the horn antenna. The horn antenna that will be used has a maximum gain of 17 dB (measured at 1 meter) and is 15 cm deep. Antenna gain is defined as

$$\text{gain} = \frac{\text{power boresight}}{\text{power isotropic}}$$

To estimate the power per  $\text{cm}^2$  delivered to the subject standing right next to the horn, we multiply the isotropic power over  $1 \text{ cm}^2$  by the gain. Even though the user would be in the near field of the antenna and the equation above is valid only for the far field, this approach is conservative because the power in the near field can only be less than the power calculation using far field equations. [2] Using far field equations, the isotropic power from 1 mW at a distance of 15 cm is

$$\text{Isotropic Power} = \frac{1}{4\pi 15^2} \text{mW/cm}^2 = 0.354 \text{ }\mu\text{W/cm}^2$$

Multiplying this by the gain factor of the horn antenna gives:

$$\text{Absorbed Power} = 0.354 \text{ }\mu\text{W/cm}^2 * 10^{\frac{17 \text{ dB}}{10}} = 17.73 \text{ }\mu\text{W/cm}^2$$

As we can see, this is far under the exposure limits set by the IEEE or any other current standard.



#### ***4. Conclusion***

As shown above, the proposed experiment poses virtually no risk to the human subject. Based upon the low power of this system and the use of reliable commercial equipment, I request that this study be granted expedited approval for human subject testing as described.

[1] IEEE Std C95.1, 1999 Edition, IEEE Standard for Safety Levels with Respect to Human Exposure to Radio Frequency Electromagnetic Fields, 3 kHz to 300 GHz

[2] Military EW Handbook,  
<http://www.phys.hawaii.edu/~anita/web/paperwork/currently%20organizing/Military%20EW%20%20Handbook%20Excerpt/antnrfld.pdf>



# Bibliography

- [1] N. V. Rivera, S. Venkatesh, C. Anderson, and R. M. Buehrer. Multi-target estimation of heart and respiration rates using ultra wideband sensors. In *Proceedings of the 14th European Signal Processing Conference (EUSIPCO 2006)*, Florence, Italy, September 4-8, 2006.
- [2] S. L. Krachman, Gerard J. Criner, and Gilbert E. D'Alonzo. Sleep in the intensive care unit. *Chest*, 107(6):1713–1720, June 1995.
- [3] Neil S. Freedman, Natalie Kotzer, and Richard J. Schwab. Patient perception of sleep quality and etiology of sleep disruption in the intensive care unit. *American Journal of Respiratory and Critical Care Medicine*, 159(4):1155–1162, April 1, 1999.
- [4] Christine N. Paulson, John T. Chang, Carlos E. Romero, Joseph Watson, Fred J. Pearce, and Nathan Levin. Ultra-wideband radar methods and techniques of medical sensing and imaging. In *Smart Medical and Biomedical Sensor Technology III*, volume 6007 of *Society of Photo-Optical Instrumentation Engineers (SPIE) Conference Series*, pages 96–107, Boston, MA, October 24, 2005.
- [5] E.F. Greneker. Radar sensing of heartbeat and respiration at a distance with applications of the technology. In *Radar 97 (Conf. Publ. No. 449)*, pages 150–154, Edinburgh, UK, October 14-16, 1997.
- [6] O.B. Lubecke, P.-W. Ong, and V.M. Lubecke. 10 GHz Doppler radar sensing of respiration and heart movement. In *Proceedings of the IEEE 28th Annual Northeast Bioengineering Conference*, pages 55–56, Philadelphia, PA, April 20-21, 2002.
- [7] S. Azevedo and T.E. McEwan. Micropower impulse radar. *IEEE Potentials*, 16(2):15–20, April/May 1997.
- [8] S. Nag, H. Fluhler, and M. Barnes. Preliminary interferometric images of moving targets obtained using a time-modulated ultra-wide band through-wall penetration radar. In *Proceedings of the 2001 IEEE Radar Conference*, pages 64–69, Atlanta, GA, May 1-3, 2001.
- [9] Eugene F. Greneker III. Radar sensing of heartbeat and respiration at a distance with security applications. In *Radar Sensor Technology II*, volume 3066, pages 22–27, April 24, 1997.
- [10] J. C. Lin. Microwave sensing of physiological movement and volume change: a review. *Bioelectromagnetics*, 13(6):557–565, 1992.

- [11] Y. E. Moskalenko. Utilization of superhigh frequencies in biological investigations. *Biophysics (USSR)*, 3(5):619–626, 1958.
- [12] Y. E. Moskalenko. On the application of centimeter radio waves for electrodeless recordings of volume changes of biological objects. *Biophysics (USSR)*, 5(2):225–228, 1960.
- [13] C. C. Johnson and A. W. Guy. Nonionizing electromagnetic wave effects in biological materials and systems. *Proceedings of the IEEE*, 60(6):692–718, June 1972.
- [14] William P. Allen Jr. Method for measuring physiological parameter, April 25, 1978. U.S. Patent Number 4,085,740.
- [15] C. G. Caro and J. A. Bloice. Contactless apnoea detector based on radar. *Lancet*, 2(7731):959–961, Oct 30, 1971.
- [16] J. C. Lin. Noninvasive microwave measurement of respiration. *Proceedings of the IEEE*, 63(10):1530–1530, 1975.
- [17] Kun-Mu Chen, Devendra Misra, Huei Wang, Huey-Ru Chuang, and Elliot Postow. An X-band microwave life-detection system. *IEEE Transactions on Biomedical Engineering*, BME-33(7):697–701, July 1986.
- [18] J. Geisheimer. RVSM [Radar Vital Signs Monitor]. *IEEE Potentials*, 17(5):21–24, December/January 1998.
- [19] Steven M. Sharpe, Seals Joseph, Anita H. MacDonald, and Scott R. Crowgey. Non-contact vital signs monitor, September 25, 1990. U.S. Patent Number 4,958,638.
- [20] E. M. Staderini. UWB radars in medicine. *IEEE Aerospace and Electronic Systems Magazine*, 17(1):13–18, January 2002.
- [21] T. E. McEwan. Body monitoring and imaging apparatus and method, November 12, 1996. U.S. Patent Number 5,573,012.
- [22] T. E. McEwan. Ultra-wideband receiver, September 6, 1994. U.S. Patent Number 5,345,471.
- [23] T. E. McEwan. Ultra-wideband radar motion sensor, November 1, 1994. U.S. Patent Number 5,361,070.
- [24] T. E. McEwan. Body monitoring and imaging apparatus and method, June 16, 1998. U.S. Patent Number 5,766,208.
- [25] Report by the Democratic Staff, Committee on Science, U.S. House of Representatives. Technology Transfer at Department of Energy National Laboratories: The Development & Commercialization of Micropower Impulse Radar at Lawrence Livermore National Laboratory, April 9, 1999.
- [26] S. Venkatesh, C.R. Anderson, N.V. Rivera, and R.M. Buehrer. Implementation and analysis of respiration-rate estimation using impulse-based UWB. In *IEEE Military Communications Conference*, volume 5, pages 3314–3320, Atlantic City, NJ, October 17-20, 2005.

- [27] W. Hadded, J. Chang, T. Rosenbury, G. Dallum, P. Welsch, D. Scott, D. Duarte, and V. Acevedo-Bolton. Microwave hematoma detector for the rapid assessment of head injuries. Technical report, Lawrence Livermore National Laboratory, February 11, 2000.
- [28] G. Ossberger, T. Buchegger, E. Schimback, A. Stelzer, and R. Weigel. Non-invasive respiratory movement detection and monitoring of hidden humans using ultra wide-band pulse radar. In *International Workshop on Ultra Wideband Systems, Joint with Conference on Ultrawideband Systems and Technologies*, pages 395–399, May 18-21, 2004.
- [29] Carlos G. Bilich. Bio-medical sensing using ultra wideband communications and radar technology: A feasibility study. In *Pervasive Health Conference and Workshops*, pages 1–9, November 29 - December 1, 2006.
- [30] David H. Staelin. *Receivers, Antennas, and Signals in Communication and Sensing Systems*. MIT, Cambridge, MA, 2008. Class Notes for Receivers, Antennas, and Signals.
- [31] F. Mohammad-Zadeh, F. Taghibakhsh, and B. Kaminska. Contactless heart monitoring (CHM). In *Canadian Conference on Electrical and Computer Engineering*, pages 583–585, April 22-26, 2007.
- [32] D. Obeid, S. Sadek, G. Zaharia, and G. E. Zein. Noncontact heartbeat detection at 2.4, 5.8, and 60 GHz: A comparative study. *Microwave and Optical Technology Letters*, 51(3):666–669, 2009.
- [33] June Y. Lee and James C. Lin. A microprocessor-based noninvasive arterial pulse wave analyzer. *IEEE Transactions on Biomedical Engineering*, BME-32(6):451–455, June 1985.
- [34] P. Boric-Lubecke, A.D. Droitcour, V.M. Lubecke, Jenshan Lin, and G.T.A. Kovacs. Wireless IC Doppler radars for sensing of heart and respiration activity. In *6th International Conference on Telecommunications in Modern Satellite, Cable and Broadcasting Service*, volume 1, pages 337–344, October 1-3, 2003.
- [35] G. D. Clifford, F. Azuaje, and P. McSharry. *Advanced methods and tools for ECG data analysis*, chapter 1, pages 1–12. Artech House, 2006.
- [36] Teo Wee Siong. Cardiac arrhythmias. Image taken from [http://www.eguide.com.sg/contents.asp?c=200100&p=current&f=cardiac\\_arrhythmias.htm](http://www.eguide.com.sg/contents.asp?c=200100&p=current&f=cardiac_arrhythmias.htm).
- [37] Vanderbilt Instruction in Biomedical Engineering for Secondary Science. Electrocardiogram mosaic. Image taken from [www.vanth.org/vibes/electro.html](http://www.vanth.org/vibes/electro.html).
- [38] J.C. Lin, J. Kiernicki, M. Kiernicki, and P.B. Wollschlaeger. Microwave apexcardiography. *IEEE Transactions on Microwave Theory and Techniques*, 27(6):618–620, June 1979.
- [39] E. Tafur, L. S. Cohen, and H. D. Levine. The normal apex cardiogram: Its temporal relationship to electrical, acoustic, and mechanical cardiac events. *Circulation*, 30(3):381–391, 1964.

- [40] S. Gabriel, R. W. Lau, and C. Gabriel. The dielectric properties of biological tissues: II. measurements in the frequency range 10 Hz to 20 GHz. *Physics in Medicine and Biology*, 41(11):2251–2269, 1996.
- [41] C. Li, Y. Xiao, and J. Lin. Experiment and spectral analysis of a low-power Ka-band heartbeat detector measuring from four sides of a human body. *IEEE Transactions on Microwave Theory and Techniques*, 54(12 Part 2):4464–4471, December 2006.
- [42] M. Singh and G. Ramachandran. Reconstruction of sequential cardiac in-plane displacement patterns on the chest wall by laser speckle interferometry. *IEEE Transactions on Biomedical Engineering*, 38(5):483–489, May 1991.
- [43] IEEE standard for safety levels with respect to human exposure to radio frequency electromagnetic fields, 3 kHz to 300 GHz. *IEEE Std C95.1, 1999 Edition*, April 16, 1999.
- [44] Military EW handbook. <http://www.phys.hawaii.edu/~anita/web/paperwork/currently%20organizing/Military%20EW%20%20Handbook%20Excerpt/antnrfld.pdf>.
- [45] DSP FM demodulator for SSTV. <http://www.spetzler.dk/bjarke/Projects/Dsp/DSP%20FM%20Demodulator%20for%20SSTV.htm>.
- [46] Randy White. Tektronix wfm file reader, May 9, 2007. <http://www.mathworks.com/matlabcentral/fileexchange/14918>.
- [47] Bonnie Kemske. Touching the body: A ceramic possibility. *Interpreting Ceramics*, 8, 2005. Image taken from <http://www.uwic.ac.uk/icrc/issue008/articles/22images/diagram.jpg>.
- [48] D. Smardzija, O. Boric-Lubecke, A. Host-Madsen, V. M. Lubecke, T. Sizer II, A. D. Droitcour, and G. T. A. Kovacs. Applications of mimo techniques to sensing of cardiopulmonary activity, April 3-7, 2005.